

Triplet states in organic semiconductors

A. Köhler^{a,*}, H. Bässler^b

^a Department of Physics, University of Bayreuth, D-95440 Bayreuth, Germany

^b Department of Chemistry, Philipps-University of Marburg, D-35032 Marburg, Germany

ARTICLE INFO

Article history:

Available online 6 November 2009

Keywords:

Triplet
Organic semiconductors
Phosphorescence
OLEDs
Excitons

ABSTRACT

Today's technology is not possible without optoelectronic devices such as light-emitting diodes, transistors and solar cells. These basic units of modern electronic appliances may be made not only from traditional inorganic semiconductors, but also from organic semiconductors, i.e. hydrocarbon molecules that combine semiconducting properties with some mechanical properties such as easy processability and flexibility. The weak van der Waals forces that bind the molecules to a solid imply a low dielectric constant, so that coulomb and exchange interactions between electrons are significant. As a result, photoexcitation or electrical excitation results in strongly bound electron–hole pairs, so-called excitons. Depending on the relative orientation of the electron and hole spin, the exciton may be of a overall singlet or triplet spin state. While the fluorescent singlet state has been investigated intensively since the first reports of organic electroluminescence, research into the properties of the phosphorescent triplet state has intensified mainly during the last decade. In this review we give an overview on the photophysical processes associated with the formation of triplet states and their decay, as well as the energy levels and energy transfer processes of triplet states. We aim to give a careful introduction for those new to this particular research area as well as to highlight some of the current research issues and intriguing questions for those familiar with the field. The main focus of this review is on molecular assemblies and polymer films, though relevant work on molecular crystals is also included where it assists in forming a larger picture.

© 2009 Elsevier B.V. All rights reserved.

Contents

1. Introduction	72
2. Basic properties of triplet states in organic semiconductors	73
2.1. Organic semiconductors	73
2.2. Singlet and triplet excited states	73
2.2.1. Molecular films	73
2.2.2. Molecular crystals	74
2.2.3. Polymer films	75
3. The energy levels of triplet states	76
3.1. The exchange energy	76
3.1.1. Polymers and oligomers with π – π^* transitions	76
3.1.2. Polymers and oligomers with n – π^* transitions	77
3.1.3. Compounds with charge-transfer type transitions	78
3.1.4. The exchange energy in polaron pairs and excimers	78
3.2. The zero field splitting	78
3.3. Higher-lying triplet states	79
4. The generation of triplet states	81
4.1. Optical methods	81
4.1.1. Triplet state population via intersystem crossing	81
4.1.2. Triplet excitation via sensitization	83
4.1.3. Triplet generation via fission of singlet excitons	84

* Corresponding author.

E-mail address: anna.koehler@uni-bayreuth.de (A. Köhler).

4.2.	Electrical excitation	84
4.2.1.	Approaches to experimentally determine the singlet generation fraction	85
4.2.2.	Theoretical concepts	86
4.2.3.	The role of charge-transfer states	86
4.2.4.	Summary and outlook	86
5.	Processes during the lifetime of a triplet state.	87
5.1.	Triplet state diffusion	87
5.1.1.	Förster and Dexter type energy transfer	87
5.1.2.	Diffusion in molecular crystals	89
5.1.3.	Diffusion in amorphous systems	89
5.2.	Energy transfer processes in host–guest systems	91
5.3.	Formation of triplet excimers	93
6.	The decay of triplet states	94
6.1.	Phosphorescence	94
6.1.1.	Phosphorescence spectra	94
6.1.2.	Phosphorescence lifetime	96
6.1.3.	Exploitation of phosphorescence in OLEDs	97
6.2.	Delayed fluorescence and triplet–triplet annihilation	99
6.2.1.	The kinetics of delayed fluorescence via triplet–triplet annihilation	99
6.2.2.	The origin of delayed fluorescence—TTA versus polaron pair recombination	100
6.2.3.	Delayed fluorescence by sensitization	101
6.2.4.	Magnetic field effects on delayed fluorescence	102
6.3.	Non-radiative quenching of triplet states in OLED structures	103
6.4.	Exploitation of triplet states in solar cells	104
7.	Concluding remarks	105
	Acknowledgements	105
	References	107

1. Introduction

Today, organic semiconductors are used commercially in display and lighting applications as light-emitting diodes (LEDs) or transistors, and they progress to enter the solar cell market. As a result, interest in the science behind this novel class of materials has risen sharply. The optoelectronic properties of organic semiconductors differ from conventional inorganic crystalline semiconductors in many respects, and knowledge of organic semiconductor photophysics is imperative to further advances with the associated semiconductor applications. In this article, we aim to give an overview on research that contributed to our understanding of the spin triplet excited states in organic semiconductors.

While the fluorescent spin singlet excited state has been investigated intensely ever since the discovery of electroluminescence in organic materials [1–4], the spin triplet excited state remained more elusive until improvements in detection technology [5] and the use of organometallic complexes [6] made this state more easily accessible for spectroscopic investigations as well as for technological exploitation. In purely organic compounds, emission from a spin triplet state, i.e. phosphorescence, is forbidden by spin-selection rules and it is thus only very weak. When a heavy metal is incorporated in the otherwise organic structure this allows for a spin flip, so that emission becomes possible and is strong. Knowledge of electronic processes involving the triplet state is necessary not only because our understanding of the electronic structure of organic semiconductor were incomplete without it, but also because the triplet state plays a significant role in device applications. As the name suggests, there are three degenerate triplet states to one singlet state. Consequently, the recombination of charge carriers in organic LEDs creates a large number of triplet states, though there is some discussion on the value of this number (see Section 4.2.1). Unfortunately, in organic materials, the energy stored in triplet states is not available for light emission because most of the triplet states decay non-radiatively. The fraction of triplets formed thus limits the efficiency of organic LEDs [7]. However,

triplet states can be used towards light emission when organometallic compounds are employed, and beautiful examples of highly efficient LEDs with single color emission or white light emission have been demonstrated [6,8–12]. It has also been suggested that the use of triplet states may improve the efficiencies of solar cells [13–18]. As detailed in Section 6.4, this is based on the premise that the long lifetime of triplet states compared to singlet states may imply a larger diffusion length and thus a higher probability to reach a dissociation site. It remains to be seen if this assumption holds considering that the diffusion rate of triplets could well be slower than that of singlets. Furthermore, the electron–hole pair of a triplet state is strongly bound and therefore requires strong acceptors for dissociation resulting in a low open-circuit voltage. This needs to be taken into account when considering their exploitation in solar cells. Triplet states not only play a role as species actively used for device applications. They can also contribute to undesired processes that reduce device lifetime. For example, triplet states with an energy above about 1 eV are able to transfer their energy to oxygen which happens to have a triplet ground state. This creates oxygen in a singlet excited state (S_1 at 0.98 eV [19]) which is chemically aggressive and may reduce device lifetime [20,21].

These few examples illustrate that it is most useful to develop a detailed understanding of the spin triplet excited state. In this article, we aim to give an overview on the photophysical processes associated with the triplet state in organic semiconductors. After some introduction into basic properties of the triplet state we shall discuss how a triplet state may be generated, which processes it may be associated with during its lifetime, and what mechanisms lead to its decay. While we lay emphasis on processes that are of particular importance to applications, we have also included phenomena that are necessary to gain some fundamental insight and understanding. For example, today's applications typically use amorphous films of organic semiconductors where the effects of disorder can govern the physical properties. Yet the effects of disorder are difficult to appreciate and understand without some background on the physics of molecular crystals, where disorder is

mostly absent. Therefore, in order to develop a comprehensive picture of the triplet state photophysics, we consider molecular and polymeric disordered films as well as ordered molecular crystals.

For the sake of readability, we do not spell out all the chemical abbreviations for the compounds referred to in the text. A table listing the abbreviations and the chemical names is appended at the end of the article.

2. Basic properties of triplet states in organic semiconductors

2.1. Organic semiconductors

When discussing triplet states in organic semiconductors, we need to take a step back and first briefly consider the electronic structure of organic semiconductors as such. These materials are called “organic” since they consist mostly of carbon and hydrogen with a few heteroatoms such as sulfur, oxygen or nitrogen included. They show properties associated with a semiconductor such as light absorption, light emission and the conduction of charges. While absorption and emission are indeed intrinsic to these compounds, the charges conducted by organic “semiconductors” are usually created extrinsically, for example by injection from electrodes in a diode configuration or through the dissociation of a photoexcited coulombically bound electron–hole pair. Organic solids are, indeed, insulators rather than semiconductors although it became meanwhile common practice to consider them as “organic semiconductors”. Organic solids come in three varieties that are:

- (i) *molecular assemblies*: they may be deposited as an amorphous film through evaporation or spin-coating. Thin amorphous films of molecules are employed for device applications such as LEDs, and molecularly doped polymer films are used on a large technological scale in xerography [22].
- (ii) *molecular crystals*: the high degree of order in a crystal where the basis consists of molecules renders them very suitable to study the differences between the physics of organic and inorganic semiconductors. The crystals are brittle and so crystal slices require a certain minimum thickness for sample preparation and handling. This renders them of little use to LED applications as a thick film in a sandwich diode configuration needs a high driving voltage [23]. The sample thickness is not relevant for transistor applications, where the high mobilities obtainable in crystalline structures are an important desired parameter. For example, in field effect transistors made from single crystals of acenes, such as tetracene, rubrene and pentacene, hole mobilities ranging around $0.2\text{--}20\text{ cm}^2\text{ V}^{-1}\text{ s}^{-1}$ have been obtained [24,25].
- (iii) *polymer films*: they may be considered as a chain of covalently coupled molecular repeat units. Technologically, they appeal due to their solution-processability. This allows for a range of deposition techniques including simple spin-coating, ink-jet deposition or industrial reel-to-reel coating. They are also more suitable to blending than molecules since polymer blends are thermodynamically more stable and so are less susceptible to crystallization.

The semiconducting properties in all of these types of organic semiconductors arise through a conjugated system of π -electrons, though their excited states and associated photophysical properties vary slightly depending on the order and coupling in the solid. In this article it is understood that we refer to molecules and polymers with extended π -orbitals unless stated otherwise, and so we shall omit the term “conjugated” for simplicity.

2.2. Singlet and triplet excited states

2.2.1. Molecular films

Organic solids are based on molecular building blocks, and the easiest place to start with discussing excited states is therefore a molecule with its molecular orbitals. Semiconducting properties arise in organic solids when the frontier orbitals – the highest occupied molecular orbital (HOMO) and the lowest unoccupied molecular orbital (LUMO) – are π and π^* -orbitals that delocalize over the molecule. Absorption of light (optical excitation) promotes an electron from the HOMO to the LUMO, thus creating an excited state. Such an excited state can also be formed through electrical excitation that occurs in a diode configuration where the molecular film is sandwiched between two electrodes. For electrical excitation, an electron may be injected from the cathode into an empty π^* LUMO and another electron is taken out by the anode from the full π HOMO thus creating a hole. These charges migrate through the solid until both reside on the same or a neighbouring molecule and are coulombically bound. The resulting configuration is that of an intramolecular or intermolecular excited state. In contrast to optical excitation which preserves spin and thus only creates singlet excitons, electrical excitation leads to the formation of both singlet and triplet states. To clarify the terminology, we refer to a singlet (triplet) state when the spin of electron in the π^* orbital and that of the remaining electron in the π -orbital are anti-parallel (parallel) and so add up to a total spin of zero (one) in units of \hbar , and we number excited states in energetic order, i.e. S_1 , S_2 , or T_1 , T_2 , etc., for the energetically lowest or second lowest singlet or triplet excited state. The spin of a state is given by the total spin of all electrons in all orbitals, yet the electrons in filled orbitals are paired anti-parallel and so contribute zero to the total spin. Fig. 1 shows the orbital configuration for the S_0 , S_1 and T_1 state along with the resulting state diagram and a vectorial representation of the coupling between two spins.

Spin angular momentum is a vectorial quantity that couples according to the rules of quantum mechanics. The unpaired electrons in the π^* and the π orbital, that comprise the excited state, form a two particle system. From quantum mechanics we know that two particles with spin angular momentum have simultaneous eigenstates to S^2 and S_z , with eigenvalues S and M_s where S is the spin angular momentum operator, and S_z denotes its z -component. There are four such eigenstates of the two particle system. The full wavefunction of a particle can be written as the product of a spatial wavefunction, that depends only on spatial coordinates, and a spin wavefunction that is a function of the particle's spin. When α and β denote the spin wavefunctions of the one-electron states with eigenvalues $s = 1/2$, $m_s = 1/2$ and $s = -1/2$, $m_s = -1/2$, the spin wavefunctions of the four eigenstates to the two particle system can be written as

$$\begin{aligned} \alpha_1\alpha_2, & \quad \text{yielding } S = 1 \text{ and } M_s = 1, \\ \frac{1}{\sqrt{2}}\{\alpha_1\beta_2 + \beta_1\alpha_2\}, & \quad \text{yielding } S = 1 \text{ and } M_s = 0, \\ \beta_1\beta_2, & \quad \text{yielding } S = 1 \text{ and } M_s = -1, \\ \frac{1}{\sqrt{2}}\{\alpha_1\beta_2 - \beta_1\alpha_2\}, & \quad \text{yielding } S = 0 \text{ and } M_s = 1, \end{aligned}$$

The index 1 and 2 on α and β refer to electron 1 and 2. The first three spin wavefunctions with $S = 1$ only differ in the z -component of the spin which takes the eigenvalues $M_s = 1, 0, -1$. This arrangement is therefore called a triplet. The fourth wavefunction with $S = 0$ has only a single possible value of the z -component, that is $M_s = 0$ and is therefore referred to as singlet. A vectorial representation is given in Fig. 1. Note that for the triplet

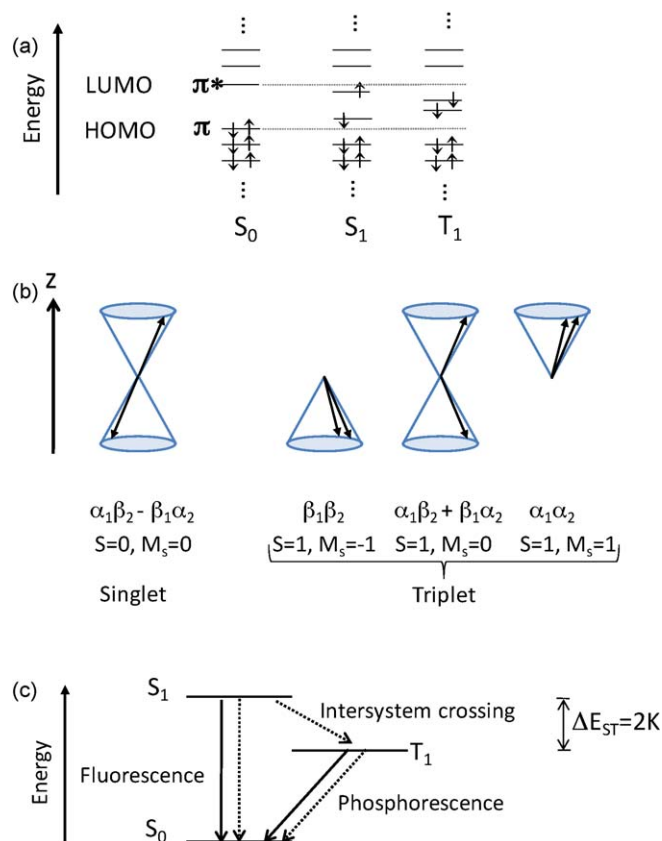


Fig. 1. (a) Singlet and triplet states in an orbital configuration scheme. The arrows indicate the electron spin, the horizontal grey line is a guide to the eye. In this representation, Coulomb and exchange energies are explicitly included in the positions of the frontier orbitals. For the triplet state, only one spin configuration is shown. (b) Vector diagram illustrating the relative orientations of the two electron spins for the singlet and the triplet state. The two spins, indicated by arrows, precess around a local magnetic field in z -direction. The anti-parallel and 180° out of phase configuration corresponds to the situation in a singlet state, while the other three in phase configurations yield a triplet state. The corresponding spin wavefunctions and the eigenvalues of S and M_s are also given. (c) Singlet and triplet states in a state diagram. Solid and dotted lines represent radiative and non-radiative decay channels.

wavefunctions, the spins are always in phase, while they are 180° out of phase for the singlet state. In order to preserve the Pauli exclusion principle, the symmetric spin wavefunctions of the triplet state are always combined with an antisymmetric spatial wavefunction, while the converse is the case for the singlet state. For a more detailed introduction to the quantum mechanical description of singlet and triplet excited states in molecules we refer the reader to common textbooks on molecular quantum mechanics such as the one by Atkins [26].

In organic semiconductors, the dielectric constant is low ($\epsilon \approx 3$), so that coulomb and exchange interactions between the electrons in the molecular orbitals are significant. The former lowers the energy of a singlet or triplet state both by the same amount, while the latter increases the singlet state energy and lowers the triplet state energy [27]. This energy difference between singlet and triplet state is the exchange energy, or, to be precise, twice the value of the exchange integral K . It results from the interaction of the electron in the HOMO with that in the LUMO. To a first order approximation, the exchange interaction scales exponentially with the overlap of the respective electron wavefunctions [28]. Usually, the wavefunctions of the electron in the HOMO and that in the LUMO overlap significantly, which results in a large exchange energy in the order of 0.7–1.0 eV [29–31]. The effect of chemical structure and extent of the excited state on the exchange energy

and the triplet state energy will be discussed in more detail in Section 3.1.

In the solid state, excited state energies are shifted with respect to the gas phase due to the polarization of the dielectric solid. In an amorphous film or glass of molecules, each molecule is embedded in a slightly different environment, with different orientations and distances of the neighboring molecules. The resulting random variation of the electronic polarization of the neighborhood leads to a random variation of the gas-to-solid shift, and therefore gives rise to a Gaussian distribution of the density of states [32]. For a triplet state, the standard deviation of this distribution is smaller than for a singlet state. This is because the excited state electron-hole wavefunction is smaller for a triplet than for a singlet configuration due to the stronger electron correlation in the triplet state [30,33–38]. As a result, the smaller triplet state is less susceptible to fluctuations in the polarization of the environment than the more extended singlet state. Experimentally, this is manifested in a smaller linewidth of the 0–0 line in phosphorescence than in fluorescence as illustrated in Fig. 2 for the case of PF2/6. While the linewidth of the emission is only a measure for the broadening of the occupied density of states (DOS), this is proportional to the overall width of the DOS.

2.2.2. Molecular crystals

This inhomogeneous broadening is avoided when the molecules are in an ordered crystalline structure. Due to the absence of disorder, molecular crystals are well suited to highlight the salient differences between organic and inorganic semiconductors and we proceed to do this here with a view to the triplet excited state. From a structural point of view, crystalline organic and inorganic semiconductors are different insofar that the former is based on molecular building blocks that are coupled by weak van der Waals interactions while the latter has a basis of atoms linked by strong covalent or ionic bonding. This results in profound electronic differences such as the width of electronic bands and the size of dielectric screening.

In inorganic semiconductors valence and conduction bands are several eV wide and the dielectric constant ϵ_r is on the order of 10. For example, in crystalline silicon and GaAs $\epsilon_r = 12$ and 13, respectively. Wide bands imply that the mean scattering length of charge carriers is much larger than the lattice parameter and exceeds considerably the coulombic capture radius r_c of an electron hole pair. r_c is defined as the distance at which the coulombic binding energy is kT , thus

$$r_c = \frac{e^2}{4\pi\epsilon_0\epsilon_r kT}. \quad (1)$$

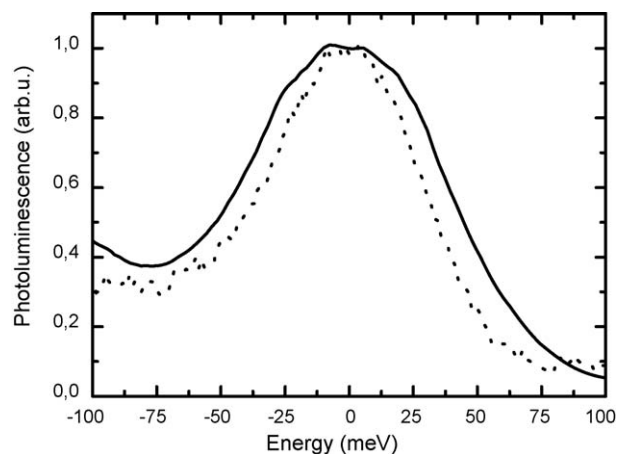


Fig. 2. Normalized fluorescence spectrum (solid line) and phosphorescence spectrum (dotted line) of PF2/6 shifted by 2.889 eV and 2.175 eV, respectively.

For example, at 295 K the capture radius is 4.6 nm in a material with $\epsilon_r = 12$. When optical excitation creates an electron–hole pair, both charge carriers can delocalize in the wide bands. Any scattering event occurs at some distance outside the coulomb capture radius, and so the created charges are not coulombically bound but free. In short, optical excitation generates a free hole in the valence band and a free electron in the conduction band. As they are independent of each other, the relative orientation of their spins is not defined, and their exchange energy is zero. At low temperature, the coulomb capture radius increases and so coulombically bound electron hole pairs, i.e. Wannier-type excitons, can exist, yet they are still weakly bound and have a large distance between electron and hole. In Si, GaAs and Ge, binding energies of Wannier excitons are 14.7 meV, 4.2 meV and 2.5 meV, respectively, and the distances between electron and hole range around 5–10 nm [39–41]. The large separation between electron and hole implies little overlap between their respective wavefunctions and consequently a low exchange energy. For bulk inorganic semiconductors, the exchange energy is usually on the order of millielectronvolts, and so the energetic distinction between singlet and triplet excitons is marginal [42].

In molecular crystals, the situation is fundamentally different. Weak intermolecular van der Waals coupling leads to much narrower valence and conduction bands with bandwidths below 0.5 eV [43]. The oscillator strength for a direct valence to conduction band transitions is very small, and the dielectric constant is typically 3–4. The low oscillator strength means direct transitions hardly occur. If they were to occur, they would result in bound electron–hole pairs for the following reason. Narrow bands imply a mean scattering length comparable to the intermolecular spacing while a low dielectric constant gives a large coulomb capture radius. For $T = 295$ K and $\epsilon_r = 3$, the coulombic capture radius is about 19 nm. So, any directly excited electron and hole were scattered within their mutually attractive potential and so relax to a bound state. Due to the low oscillator strength of band-to-band transitions, this consideration of crystal states is hypothetical. Instead, the optical absorption creates predominantly an excited states on an individual molecule. Due to the translational invariance of the crystal, this excited state may equally likely reside on any neighboring molecule. It can therefore move through the crystal, and may be treated as a quasiparticle, the exciton. While strictly valid only in the symmetric environment of a crystal, the term exciton has been generally adopted to denote any mobile excited state.

In a molecular crystal, the electron and hole associated with an excited state may reside on the same molecule (Frenkel exciton) or adjacent molecules (charge-transfer exciton). An electron hole pair localized on adjacent molecules with an intermolecular separation of 0.6 nm, characteristic of molecular crystals, has a Coulombic binding energy as large as 0.65 eV. The exchange energy of Frenkel excitons in molecular crystals is about 1 eV or slightly larger – in an anthracene crystal it is 1.3 eV [44] – and is essentially determined by the parent molecule.

In summary, the strong difference between the small $S_1 - T_1$ splitting in an inorganic semiconductor compared to the large value the $S_1 - T_1$ gap takes in an organic semiconductor results from the different polarizabilities, as expressed by the dielectric constants. The large polarizability in the inorganic semiconductor implies that the interactions between electrons can be largely neglected. In organic solids, however, coulomb and exchange interactions are large and so become central to the photophysical processes.

2.2.3. Polymer films

Among the three types of organic semiconductors, conjugated polymers are the electronically most complex species, which

renders them the scientifically most interesting category. The complexity arises since, in a polymer, repeating molecular units are linked through covalent bonds. In contrast to an amorphous or crystalline molecular solid where the molecules comprising the solid are only coupled through van der Waals forces and where the excited state is confined to a molecule or a molecule and its neighbor, in a polymer the excited state wavefunction can extend over several molecular units. The eventual extent of the excited state on the polymer chain depends on a number of factors. On one hand the coulomb interaction acts to reduce the electron hole distance. On the other hand, the energy associated with the distortion of the molecular bond and the electronic energy decrease when the size of the excited state increases. Somewhere between these parameters, an equilibrium distance settles.

The exchange energy, i.e. the $S_1 - T_1$ energy difference, depends on the interaction between the charges involved and thus on the overlap of their respective wavefunctions. After all, electron and hole are no point-like objects but they have delocalized, exponentially decaying wavefunctions, that overlap to some extent. Clearly, their mutual distance affects this wavefunction overlap. The mean electron–hole distance $\langle r_{eh} \rangle$ is often taken as a measure for the size of an exciton. In π -conjugated polymers such as poly(*p*-phenylene vinylene)s, poly(*p*-phenylene)s, poly(*p*-ethynylene)s, and polythiophenes calculations and experiment have given values below 1 nm for $\langle r_{eh} \rangle$ in the singlet state and some 30% less for the triplet state [30,36–38]. The chain segment over which the centre of gravity of the electron–hole pair moves in a coherent fashion is the conjugation length. One may adopt the picture of an electron–hole pair separated by a fixed distance that moves coherently within the conjugation length. Sometimes, one may consider the part of the chain over which there is a significant distortion of the σ -bonded backbone in the excited state geometry compared to the ground state geometry as a measure for the spread of the exciton with its associated lattice distortion.

So far we have considered an excited state that resides on one polymer chain, the intra-chain exciton. An excited state may also spread over two adjacent chains to form an inter-chain exciton. In this case, the overall excited state wavefunction has covalent and ionic contributions and may be represented in the general form as

$$\psi = c_1 \psi(A^+ B) + c_2 \psi(AB^+) + c_3 \psi(A^- B^-) + c_4 \psi(A^+ B^-), \quad (2)$$

where A and B refer to different polymers or molecules, the symbols $^+$, $+$ and $-$ indicate the excited or charged state, and c denotes a constant. In the literature, different usages of the terms inter-chain exciton, excimer/excplex, charge-transfer exciton and polaron pair occur, so we briefly clarify the terminology we adopt here. Intra-chain exciton and inter-chain exciton we already have defined above. An excimer or excplex is an excited state extending over two adjacent molecules or polymers with the wavefunction given in Eq. (2), yet our general understanding is that the covalent terms dominate ($c_1, c_2 \gg c_3, c_4$). For an excimer, the two molecules are the same ($A = B$), while they differ for an excplex. When the ionic terms dominate in Eq. (2) ($c_3, c_4 \gg c_1, c_2$), we call the excited state a charge-transfer exciton. In fact the large intermolecular separation in molecular crystals of about 0.6 nm usually implies zero contribution from a covalent part and a fully ionic character of the excited state, while there is some covalent contribution in amorphous films where locally intermolecular distances may be shorter. In LED operation, excited states are formed through the recombination of two injected charges. When the positive and negative charge on two completely ionic chains or molecules are bound by coulomb interactions, we talk about a geminate polaron pair. While not strictly correct, we often use the terms geminate polaron pair and charge-transfer state in a synonymous manner or omit the term geminate when the

coulomb interaction is already implied by the context. (The distinction between geminate and non-geminate, i.e. non-bound, electron-hole pairs is of more relevance to inorganic semiconductors.)

3. The energy levels of triplet states

Within the manifold of triplet states T_1 , T_2 , T_3 and so on, excited triplet state usually relax to the energetically lowest of them, T_1 , from which most of the triplet photophysics takes place. For energy transfer processes and phosphorescent applications, the energy of T_1 and the structural parameters that control it are therefore of some concern. While it is usually not possible to predict the T_1 energy relative to the molecular ground state S_0 , one can give estimates for the size of the exchange energy based upon the chemical structure of the molecule, and so one may come to general conclusions about the T_1 energy relative to S_1 . Since the energy of S_1 is easily obtained through an absorption spectrum, one can arrive at the T_1 energy through this “detour”.

3.1. The exchange energy

3.1.1. Polymers and oligomers with π - π^* transitions

For conjugated polymers where the first excited state is of a $\pi\pi^*$ character, i.e. formed by one electron in a π -orbital and one in a π^* -orbital, the $S_1 - T_1$ gap is experimentally found to be about 0.7 eV, virtually independent of chemical structure (Fig. 3). This result has been derived by comparing the phosphorescence spectra of organic and Pt-containing poly(phenylene ethynylene)s with different spacers in the repeat unit [29], and for various derivatives of the poly(*p*-phenylene) family such as MeLPPP, PF or PIF [45]. Energy transfer measurements have corroborated this for derivatives of the poly(phenylene vinylene) and the poly(thiophene) families [31]. When comparing literature values it is of course necessary to derive the $S_1 - T_1$ gap in a consistent manner. We take the 0–0 peak in fluorescence and phosphorescence to identify the S_1 and T_1 energy, respectively.

In Section 2.2, we mentioned that first the exchange energy is controlled by wavefunction overlap and that second the extent of the excited state in a π -conjugated polymer is only weakly

dependent on the variation of the effective conjugation length of a polymer chain. This is in contrast to oligomers, in which confinement effects become more important as the oligomer length decreases. Quantum-chemical calculations indicate that for polymers with a $\pi\pi^*$ first excited state, the electron-hole distance and, concomitantly, the exchange energy is virtually independent of chemical structure [30]. When the size of the excited state is confined, for example by strong torsion in the chain or by a reduction of the oligomer length, the electron-hole wavefunction overlap and thus coulomb and exchange energy increase. Since the singlet exciton is more extended than the triplet exciton, any confinement increases the singlet state energy more than the triplet state energy. This is well observed by Hertel and co-workers for the emission spectra of the poly(*p*-phenylene) family, where the degree of intra-chain torsion increases in the order MeLPPP, PIF, PF2/6, DDO-PPP for the polymers (Fig. 4) [45]. This oligomer length effect is well known and well established for the S_1 and T_1 states, for example for MeLPPP oligomers or oligothiophenes [46]. There have been attempts to quantify the different evolution with chain length for singlet and triplet states according to $E(n) = E_\infty + \text{const}(1/n)$ [31,45]. It is noteworthy that the transition energies for the polymer exceed the value determined by extrapolating those energies to $n \rightarrow \infty$. Usually this is considered as a signature of finite conjugation length L_{eff} because of chain distortion. Empirically, L_{eff} is determined from the extrapolated $E(n) = E_\infty + \text{const}(1/n)$ dependence. While this may be qualitatively correct, quantitative assessment is problematic because, according to recent theories, there is a theoretically predicted deviation from the $1/n$ law at large chain lengths [37,47]. This effect has been substantiated by fluorescence spectroscopy on oligomers of ladder-type phenylenes [48] and explained in terms of an old model derived for polyenes by Kuhn [49]. A recent summary of relevant data including quantum-chemical analysis has recently been published by Gierschner et al. [50].

The dependence of the exchange interaction on the extent of the π -system is also borne out by the spectroscopy of 2D rather than 1D π -conjugated chromophores. In the series of the disc-like molecules benzene, triphenylene, coronene and hexa-peri-hexabenzocoronene (HBC) the $S_1 - T_1$ energy splitting decreases from 0.9 eV (benzene), 0.75 eV (triphenylene) to 0.55 eV (coronene)

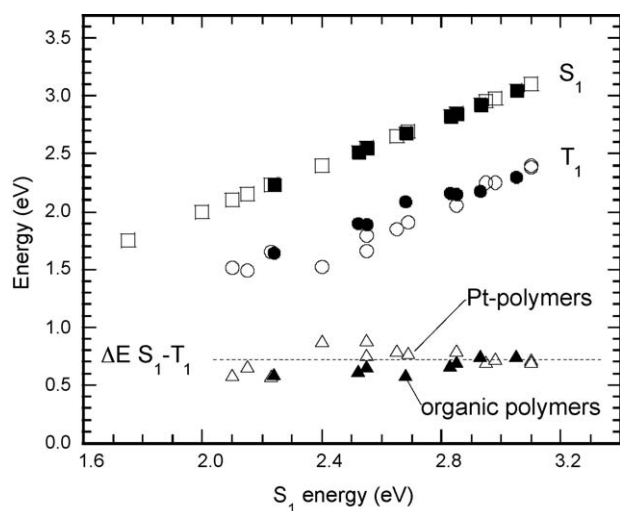


Fig. 3. The energies of S_1 and T_1 for a series of Pt-containing phenylene ethynlenes (open symbols), analogous organic phenylene ethynlenes (closed symbols) and poly(*p*-phenylene) derivatives (closed symbols). The $S_1 - T_1$ energy difference ΔE is also indicated. The dashed line represents a linear fit to the data. Reproduced with permission from Ref. [30], copyright Wiley-VCH Verlag GmbH & Co. KGaA.

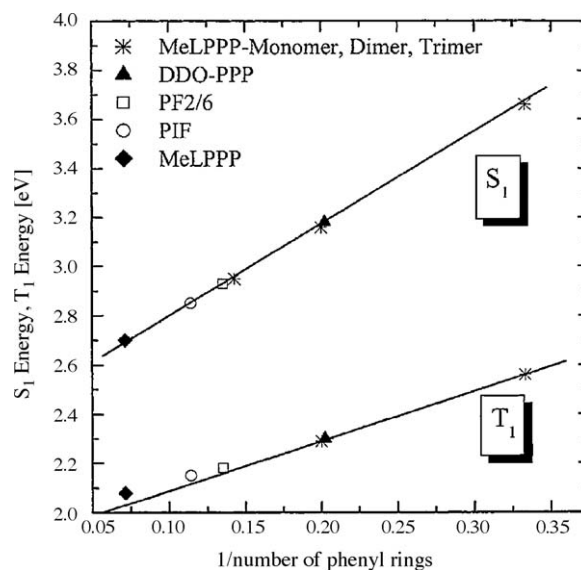


Fig. 4. The S_1 and T_1 energies as function of the inverse number of phenyl rings in the chemical structure for the MeLPPP monomer, dimer and trimer and for the poly(*p*-phenylene) polymers DDO-PPP, PF2/6, PIF, MeLPPP. For the polymers, the degree of planarity increases in this order. Reproduced with permission from Ref. [45], copyright Wiley-VCH Verlag GmbH & Co. KGaA.

[19]. No further decrease is observed for HBC [51]. This $S_1 - T_1$ energy splitting is difficult to measure accurately, since the 0–0 transition of the singlet and triplet transitions can be symmetry-forbidden to different degrees. Except for HBC both the $S_1 \rightarrow S_0$ and the $T_1 \rightarrow S_0$ transitions in these molecules are symmetry forbidden and acquire finite oscillator strength only by vibronic coupling. Therefore the $S_1 \rightarrow S_0$ 0–0 and $T_1 \rightarrow S_0$ 0–0 transitions are barely detectable. Interestingly, high resolution absorption, fluorescence and phosphorescence spectra of coronene in a triphenylene matrix at 4.2 K as compared to spectra measured in *n*-paraffin solid matrix indicate that there can be some symmetry breaking imposed by the molecular environment so that the selection rules are relaxed [52]. It appears that a related phenomenon occurs in HCB. While the $S_1 \rightarrow S_0$ 0–0 transitions remains to be symmetry forbidden, the $T_1 \rightarrow S_0$ 0–0 transition at 2.16 eV has acquired a finite oscillator strength. Although the 1.98 eV feature is still the dominant transition in the phosphorescence spectrum, the $T_1 \rightarrow S_0$ 0–0 transition has a much greater fractional intensity than the $S_1 \rightarrow S_0$ 0–0 transition in the fluorescence spectrum. This suggests that the relaxation of the symmetry selection rule is more efficient in the triplet state as compared to the S_1 state when the size of the π -electron system increases. This trend further enhanced when HBC is mono-substituted by platinum-acetylide [53]. Whereas the $S_1 \rightarrow S_0$ transition is symmetry-forbidden as evidenced by the very weak oscillator strength of the $S_1 \rightarrow S_0$ 0–0 transition and the long singlet lifetime (45 ns), the $T_1 \rightarrow S_0$ 0–0 transition – with a $S_1 - T_1$ gap of 0.6 eV – is the strongest feature in phosphorescence (with lifetime of 20 μ s). A similar situation is encountered on doubly substituted HBC carrying phenylene-ethynyl-Pt moieties in para-position [51].

3.1.2. Polymers and oligomers with $n-\pi^*$ transitions

So far we have illustrated that for polymers with $\pi\pi^*$ transition, the exchange energy is minimized to around 0.7 eV when the polymer is mostly planar, with a long conjugation length. Sometimes, a smaller exchange energy is desired, for example to obtain a high $T_1 \rightarrow S_0$ transition energy in host materials or emitters for blue phosphorescence while at the same time, a low HOMO–LUMO gap is required to facilitate good charge injection from the electrodes. Furthermore, perturbation theory predicts that the radiative decay rate of the $T_1 \rightarrow S_0$ transition scales approximately inversely with the square of the $S_1 - T_1$ gap (see Section 4.1.1 and chapter one of [28]). There are different ways to achieve the necessary reduction in electron–hole wavefunction overlap. One approach is to use polymers or molecules where the optical transition involves either orbitals that have a different orientation in space, such as some $n-\pi^*$ transitions, or orbitals that are localized at different parts of the molecular unit, such as donor–acceptor-type compounds, or a combination of both effects. The effect of wavefunction overlap on the exchange integral is illustrated in Fig. 5 for an $\pi\pi^*$ transition and a $n\pi^*$ transition.

Benzophenone, for example, despite being a small molecule compared to an oligomer or polymer, has an exchange energy as small as 0.22 eV since the overlap between the charge in the n -orbital at the carbonyl group and the countercharge in the π^* orbital in the aromatic system is small (Page 13 in Ref. [28]). Carbazole-containing compounds are also known to have $n\pi^*$ transitions. This explains why Brunner, Van Dijken and co-workers at Phillips in Eindhoven reported exchange energies as low as 0.4 eV in polymers and molecules for various carbazole-containing compounds [54,55]. In their phosphorescence measurements they noticed that the low exchange energies were realized in particular when monomer units are linked in the meta-position of adjacent phenyl rings, while higher values concur with connections through the para-position. The emission spectra of such a carbazole polymer are shown in Fig. 6. Phosphorescence studies on

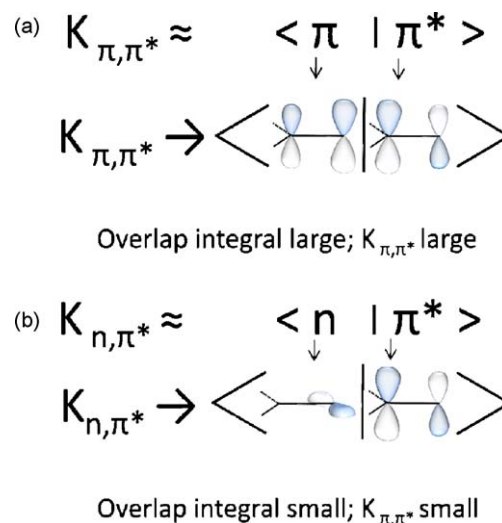


Fig. 5. Visualization of the wavefunction overlap between (a) a $\pi\pi^*$ transition and (b) a $n\pi^*$ transition. In this oversimplified illustration, the exchange integral K is taken to scale with the size of the wavefunction overlap. After [27], Chapter 2.

Pt-polymers with carbazole units as a spacer between ethynylenes indicated that this difference arises since in compounds with para-connected phenyl rings, the hole may delocalize through the π -orbital of the para-connected rings resulting in significant

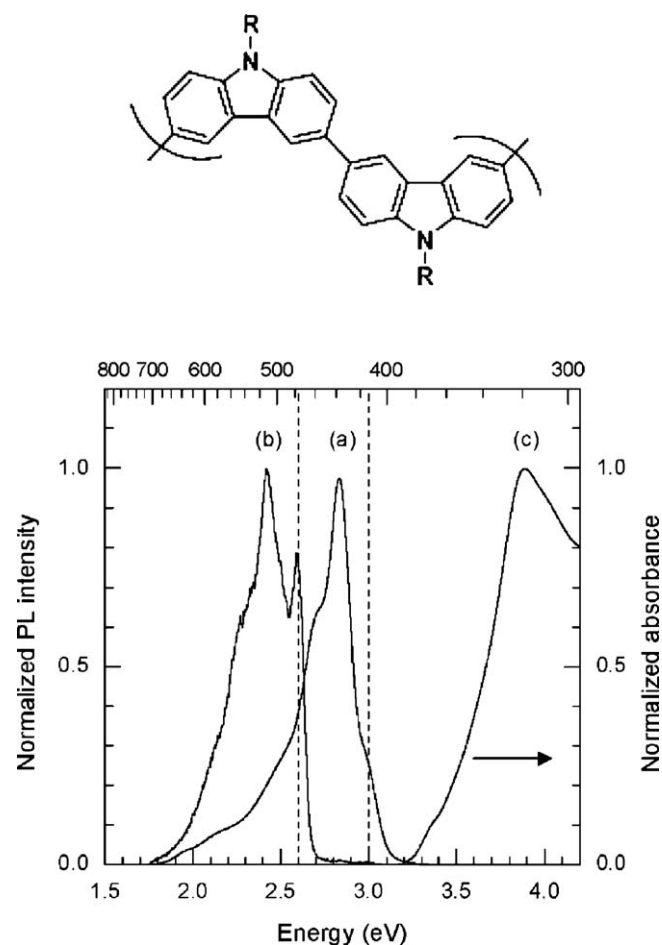


Fig. 6. The 20 K fluorescence (a) and phosphorescence (b) spectra for the carbazole polymer shown above, along with the room temperature absorption spectrum. The vertical dashed lines indicate the position of the 0–0 transition. Reprinted with permission from [54], copyright 2004 American Chemical Society.

overlap with the electron in the π^* orbital, while a meta-linkage forces a stronger localization of the hole on the carbazole atom and its non-bonding orbital [56]. In a more sophisticated manner, quantum-chemical calculations by Avilov et al. show that connecting carbazole monomers through their meta-position localised the triplet exciton to two about 2 phenyl rings and thus results in a high triplet state energy, while interconnecting monomers in the para-position leads to the triplet being delocalised over about 4 phenyl rings and so lowers the energy of the triplet state [57].

3.1.3. Compounds with charge-transfer type transitions

As outlined above, the exchange interaction among a pair of electron and hole that form an excited triplet state depends exponentially on the intra-pair distance. The $S_1 - T_1$ energy gap Δ_{ST} must therefore decrease substantially if these charges are localized on different molecules such as to form a charge-transfer (CT) state. By definition, metal-to-ligand charge-transfer transitions (MLCT)s yield a localization of hole and electron at different parts of the molecule, and thus a small exchange energy in the order of 0.2–0.3 eV [58–60]. MLCTs are common in complexes that consist of a central metal, often a transition metal such as platinum or iridium, and organic ligands, for example ppy, tpy, btp (see Table 1 in Appendix A for structural formulae) [28]. In the charge-transfer transition, an electron is removed from the central metal d-orbital and placed in the ligand π^* orbital. Often, transitions do not have a pure MLCT character, but they may have admixtures from the $\pi-\pi^*$ HOMO–LUMO transition on the ligand, and this can increase the exchange energy [30,58,59]. Furthermore, it is possible that a ligand–metal complex has efficient MLCT and, concomitantly, a small exchange energy, yet there is an additional $\pi\pi^*$ transition on the ligand that produces a singlet state above the MLCT singlet and a triplet state below the MLCT triplet, because the $\pi\pi^*$ transition is associated with a larger exchange interaction. If this ligand centered $\pi\pi^*$ transition does not have sufficient spin–orbit coupling from the central metal, it can reduce the overall phosphorescence yield. Finally, one needs to keep in mind that while a high degree of electron–hole separation gives the desired low exchange energy, by Fermi's Golden rule it also results in a low oscillator strength of the transition. Sometimes, a compromise between emission color and emission yield needs to be considered. Strong red and green phosphorescence have been reported while blue phosphorescence of good color quality and efficient yield has remained somewhat more elusive. Organometallic complexes have been pioneered chemically by Thompson and from a device-oriented view by Forrest [6,9,58,59,61,62]. There are a number of detailed and high-quality studies available on the triplet state in such organometallic phosphorescent complexes. A good overview can be obtained in a book recently edited by Yersin [28].

In purely organic compounds, reports of strongly electron-accepting or electron-donating moieties that give small exchange energies are less common. One reason for this is fact that compounds with strong donor–acceptor interaction have low transition energies, and low-lying triplet states are difficult to detect since the non-radiative decay rate of the triplet state increases exponentially with the $T_1 \rightarrow S_0$ energy (vide infra) [40,63–66]. Another reason is that many donor–acceptor compounds are based on $\pi-\pi^*$ transitions that still have some non-negligible overlap.

3.1.4. The exchange energy in polaron pairs and excimers

Information on Δ_{ST} of polaron pairs in for instance adjacent conjugated polymer chains was inferred from thermally stimulated luminescence on films of conventional as well as nano-structured ladder-type MeLPPP [67]. In this technique, one excites the sample optically. After a delay time of up to 1000 s, an

afterglow is measured as a function time either at constant temperature (4.2 K) or upon controlled heating. It turns out that at 4.2 K only phosphorescence can be detected, while higher temperatures are needed in order to observe fluorescence. The intensity of the emission signal varies with temperature such that “glow peaks” are recorded upon heating the sample. The essential result is that fluorescence peaks appear at higher temperatures than phosphorescence peaks. This indicates that all eh-pairs generated at 4.2 K relax to their triplet state. Fluorescence-type afterglow requires thermal activation of the eh-pair from the triplet to the singlet state. An analysis of the activation energy needed to produce the fluorescence signal yields Δ_{ST} values of 3 meV and 6 meV for untreated and nano-structured MeLPPP, respectively. The larger value for the nano-structured sample is attributed to improved inter-chain ordering with concomitantly shorter inter-chain separation. Quantum-chemical calculations using test structures obtained via molecular mechanics calculations yield Δ_{ST} gaps reaching from 2.5 meV to 10 meV for inter-chain spacings between 0.38 nm and 4.8 nm, consistent with the experiment [67]. Evidently, the Δ_{ST} gap is morphology dependent, yet the magnitude of Δ_{ST} for polaron pairs is similar. This implies that at 295 K, $\Delta_{ST}/kT \ll 1$, i.e. it is sufficiently small so that singlet–triplet interconversion is essentially barrierless for polaron pairs. In a subsequent quantum-chemical study, Difley et al. [68] found that Δ_{ST} of organic dyes and oligomers depends sensitively on both the material and the relative orientation of the donor–acceptor pair. Furthermore, in contrast with the commonly accepted notion, they find that the singlet CT state can, and very often does lie below the triplet state. This is attributed to a strong kinetic exchange component in closely spaced systems that favors the singlet state. A lower energy of the singlet CT state than the triplet CT state has been inferred experimentally from the temperature dependence of the photoluminescence efficiency in Alq₃. Segal and co-workers report Δ_{ST} gaps of about –7 meV, consistent in sign but not in magnitude with their theoretical calculations of –70 meV and –25 meV for δ -Alq₃ and α -Alq₃ [69].

3.2. The zero field splitting

So far we have considered how the exchange energy affects the $T_1 \rightarrow S_0$ energy, and this is appropriate since the exchange interaction contributes a large value to the triplet energy. Smaller energetic contributions add to this from spin–spin interactions of the two unpaired electrons in the triplet state. This spin–spin interaction splits the triplet state into three substrates. Since this interaction depends on the orientation of the triplet state relative to the molecular coordinates it is a tensorial quantity. This is revealed in level splitting in phosphorescence excitation spectroscopy [70] and in ESR experiments [71,72]. Because the level splitting occurs at zero magnetic field, it is referred to as zero-field splitting (ZSF) [73]. In hydrocarbon-type molecular crystals, the splitting is of the order of 0.1 cm^{–1}, i.e. 10 μ eV. The splitting can increase by up to a factor of 10–100 when charge transfer between ligand and metal atom occurs, so that the heavy metal orbitals contribute to the transition. Fig. 7 shows the emission of the three T_1 substrates for Ir(btp)₂acac, along with an excitation spectrum and an energy level diagram [74]. The magnitude of ZSF is important when considering the radiative transition from the triplet state of metal–ligand CT complexes such as Ir(ppy)₃ because the spin–orbit coupling is different for the different sublevels. The radiative decay rate depends on the values of the matrix elements for the spin–orbit interactions of the respective triplet substrate with higher-lying singlet states, and on the allowedness of the interacting $S_n \leftarrow S_0$ transitions (vide infra). However, since the level splitting is mostly on the order of 1 meV or less for organometallic complexes, all sublevels will equally be populated at 295 K. This

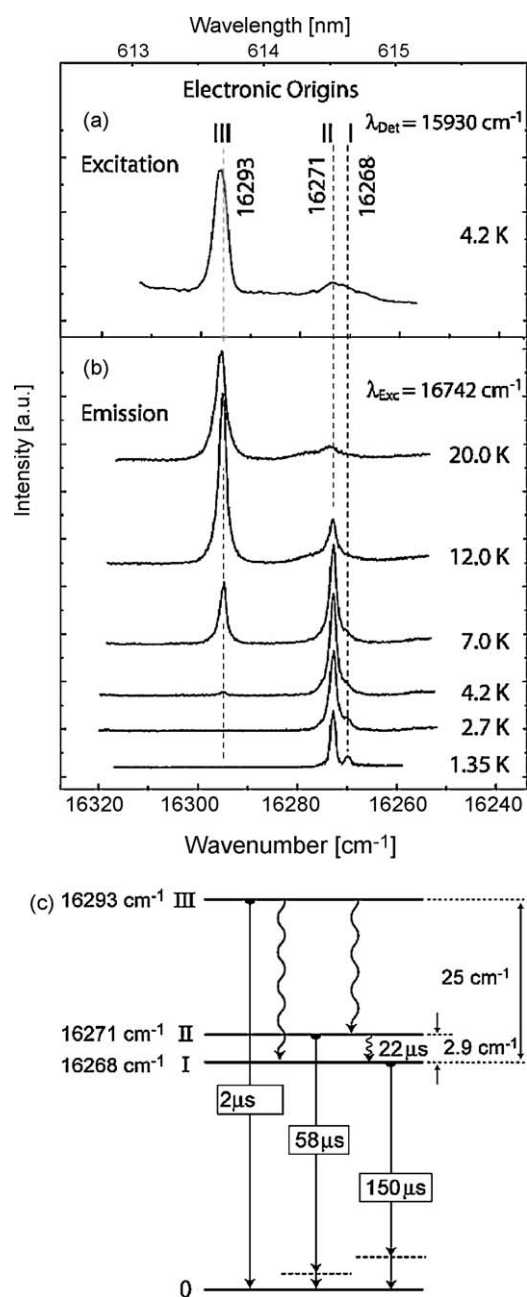


Fig. 7. The zero field splitting in $\text{Ir}(\text{btp})_2(\text{acac})$. (a) Excitation spectrum recorded at 4.2 K with the emission detected on a vibrational satellite of the $\text{II} \rightarrow 0$ transition at $15,930 \text{ cm}^{-1}$. (b) Emission spectra at different temperatures with excitation into a vibrational satellite of the $\text{III} \leftarrow 0$ transition at $16,742 \text{ cm}^{-1}$. (c) Energy level diagram for the lowest triplet state T_1 . After excitation into the highest energy substate III, fast relaxation into the lower energy substates II and I occurs. Relaxation from II to I is slow. The lifetimes of the different substates are also indicated. Reprinted with permission from Ref. [74], copyright 2007 American Chemical Society.

implies that phosphorescence from LEDs doped with metal complexes will always occur from the level that has the highest oscillator strength. This is no longer granted at low temperatures. If the active sublevel is not the lowest state of the complex, phosphorescence will be frozen out once the level splitting is large compared to kT . For a level splitting of 1 meV this is the case when $T < 10 \text{ K}$ [28]. For an $\text{Ir}(\text{ppy})_3$ -cored dendrimer Ribierre et al. [75] found a large ZFS energy of $7 \pm 1 \text{ meV}$. Site selective high resolution spectroscopy on Flrpic isolated in solid CH_2Cl_2 and THF matrices indicated that the magnitude of ZFS depends on the nature of the molecular cage in which the chromophore is embedded [76]. For

instance, in a poly-crystalline CH_2Cl_2 host, two discrete sites have been identified with zero field splittings of 4.9 meV and 9.5 meV while in amorphous THF the splittings are spread out over a range of 5.1–8.2 meV.

3.3. Higher-lying triplet states

There are many excited spin triplet states at higher energies than T_1 . Most of them are not accessible through absorption from T_1 as their wavefunction has the wrong symmetry for optical transitions with T_1 or S_0 . These dark triplet states play a role in the intersystem crossing process from the S_1 state into the triplet manifold. Intersystem crossing (ISC) from singlet to triplet states depends on spin-orbit coupling and on the vibrational overlap between the singlet and triplet states involved. This overlap increases significantly when singlet and triplet states are energetically close [63–65]. As a result, ISC into a dark higher-lying triplet state followed by internal conversion to T_1 can sometimes occur efficiently, even when ISC into T_1 itself is not effective. Beljonne and co-workers have shown that for bithiophene and terthiophene, efficient ISC occurs into a T_4 triplet state that lies just little below the S_1 state, and this accounts for the unusually low fluorescence quantum yield of these short oligothiophenes. As shown in Fig. 8, the order between S_1 and T_4 reverses for longer oligomers, so ISC becomes less efficient and the fluorescence quantum yield increases with oligomer length [35,33]. A similar effect is known in anthracene crystals. Whereas for isolated anthracene molecules, efficient ISC from S_1 to a higher triplet state reduces the fluorescence, a change in the relative order of the singlet and higher triplet state reduces the ISC rate by two orders of magnitude because in the anthracene crystal the T_2 state is 900 cm^{-1} (73 meV) above the S_1 state and requires thermal activation for reaching it [44]. Direct ISC from the S_1 state to the T_1 in the anthracene crystal is inefficient since the excess energy (1.3 eV) has to be dissipated non-radiatively (vide infra).

The first higher-lying triplet state after T_1 that is optically accessible is usually referred to as T_n , since the exact number of dark triplet states separating it from T_1 is not known. The $T_n \leftarrow T_1$ transition can be probed using steady state or time-resolved photoinduced absorption measurements (PiA). In this experiment, a white light probe beam is first used to measure the absorption of the sample in the ground state. Then a pump beam is employed to populate the T_1 state via $S_1 \leftarrow S_0$ absorption followed by $S_1 \rightarrow T_1$ ISC, as illustrated in Fig. 9. Finally the absorption in the presence of the pump beam is measured again with the white light probe, and the fractional change of transmission, $\Delta T/T$ is displayed. Ideally, the spectrum shows the reduction of the ground state absorption and

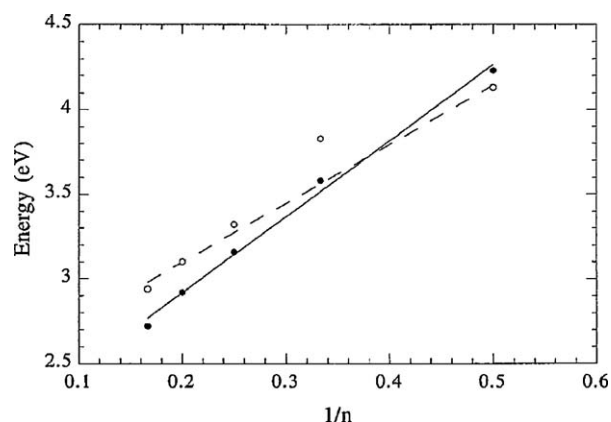


Fig. 8. The INDO/MRD-CI calculated S_1 and T_1 energies for oligothiophenes as function of the inverse number of thiophene rings. Reprinted with permission from [35], copyright 1996 American Chemical Society.

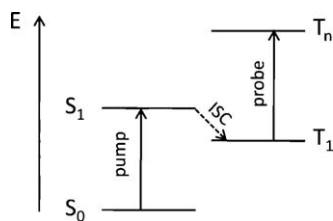


Fig. 9. Schematic of the transitions involved in the $T_n \leftarrow T_1$ photoinduced absorption.

the occurrence of the $T_n \leftarrow T_1$ absorption, usually somewhere in the red spectral range. On timescales in the ns–s range, the time dependence of the $T_n \leftarrow T_1$ absorption is determined by the lifetime of the T_1 state from which the absorption occurs. On very short timescales such as fs–ns, the temporal evolution of the $T_n \leftarrow T_1$ absorption is determined by the ISC yield, i.e. the rate with which the T_1 state is populated. In *solid films*, the triplet state absorption spectrum is often characterized by a broad spectrum, while measurements in *frozen solution* yield narrow spectra with a dominant, narrow 0–0 peak and very low intensity of any vibrational side peaks, as was shown by Peeters et al. for oligophenylenevinyls and by Wasserberg et al. for oligofluorines [77,78]. The broadness of many solid-state spectra, in particular in polymers, arises since often the triplet state absorption merges with another nearby absorption that may be due to polarons or interchain interactions. These features can be differentiated by their dependence on time and temperature. As already mentioned, the lifetime of the triplet absorption matches the lifetime of the underlying triplet state. Furthermore, in polymers, the population of triplet states is high at low temperature and decreases at room temperature due to diffusion to quenching sites. In contrast, polaronic and other absorption features are still prevailing at room temperature. The narrow absorption spectra observed for polymers of about 70 meV FWHM in frozen solutions and low intensity of the vibrational sidepeaks suggest the T_n state to delocalize over several repeat units. This is further supported by the strong dependence of the $T_n \leftarrow T_1$ transition energy on oligomer length [77,78]. Both effects, the narrowing of the transition and the redshift with oligomer length, are illustrated in Fig. 10. From the similar evolution with chain length for $T_n \leftarrow T_1$ than for $S_1 \leftarrow S_0$ one can conclude that T_n is similarly extended than S_1 [48,77,78]. The $T_n \leftarrow T_1$ absorption is a convenient way to monitor the dynamics of triplet excitations in systems that have low radiative $T_1 \rightarrow S_0$ transition rates and therefore phosphoresce only weakly [79].

Finally, we draw attention to the fact that in conjugated polymers with $\pi\pi^*$ excited states, the energy of the $T_n \leftarrow T_1$ transition appears to be approximately 1.5 eV, with little dependence on the chemical structure. This is illustrated in Fig. 11, where the $T_n \leftarrow T_1$ transition energies of the PPP, PPV and PPE-type polymers listed in Table 2 of Appendix A are summarized. Even though the energies of the $S_1 \leftarrow S_0$ vary by more than 1 eV, the values of the triplet state absorption are centred around 1.47 eV with a standard deviation of 0.11 eV. The quantum-chemical origin for this is not fully understood. We conjecture that the constancy of this transition energy may in some way reflect a electron–hole wavefunction overlap that varies only little with chemical structure for the T_n state, in a similar fashion as there is little variation for the electron hole wavefunction overlap for T_1 [30]. In any case, a useful rule of thumb for experimentalists is that in polymers with $\pi\pi^*$ excited states, the T_1 state is about 0.7 eV below S_1 and the T_n state is located roughly 0.7 eV above S_1 . When reducing the conjugation length, for example by using oligomers, T_1 increases little in energy while S_1 and T_n increase much.

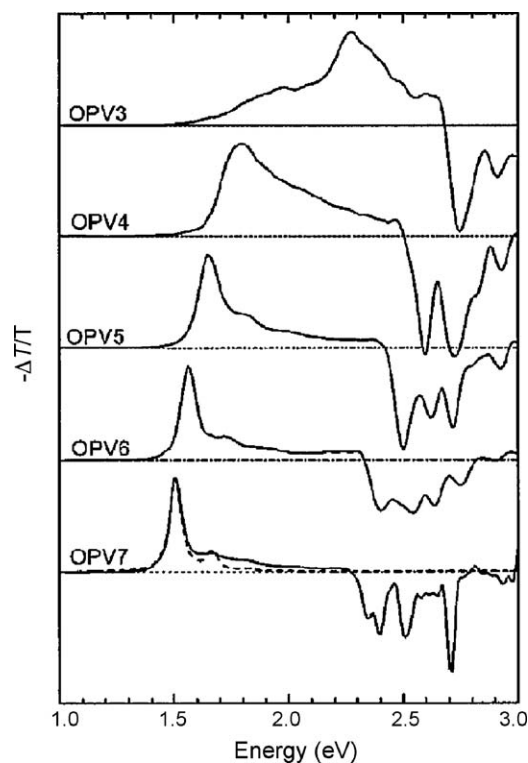


Fig. 10. Photoinduced absorption spectra for a series of phenylenevinylene oligomers OPV $_n$, where n denotes the number of repeat units, recorded at 100 K in MeTHF. Reprinted with permission from [77], copyright 2000 American Institute of Physics.

In addition to the energetic position of the $T_n \leftarrow T_1$ absorption, the oscillator strength of this transition can be of interest. This value is required for example in order to determine whether the recombination rate of electrons and holes depends on the relative orientation of their spins (see Section 4.2.1). Methods to determine the triplet absorption cross-section include monitoring the bleaching of the singlet ground state or using a triplet

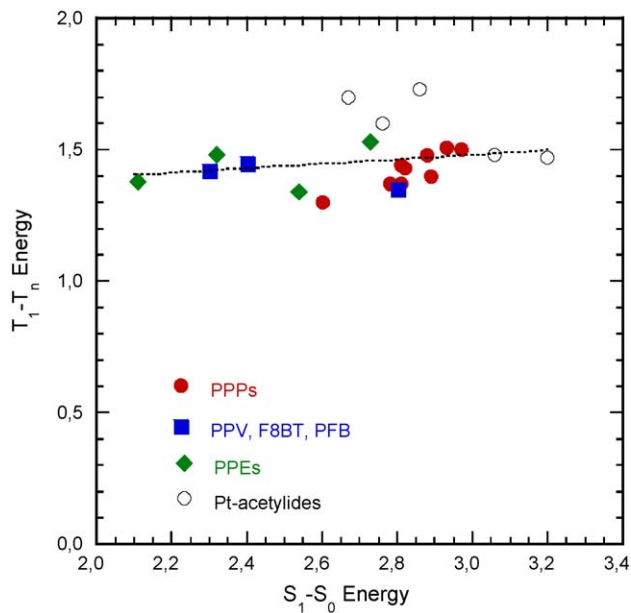


Fig. 11. The $T_1 \leftarrow T_n$ transition energies plotted against the $S_1 \leftarrow S_0$ energy for a variety of polymers. The dotted line indicates a linear fit to all values. A list of the polymers considered and the associated references can be found in Table 2 in Appendix A.

sensitization technique [80–82]. A thorough compilation of techniques and values can be found in the two review articles by Carmichael and co-workers [80,81]. In the singlet depletion technique the ground state bleaching of the $T_n \leftarrow T_1$ absorbance spectrum is compared to a ground state molar extinction spectrum. The two molar extinction spectra are correlated via

$$^3\varepsilon_0(\lambda) = ^1\varepsilon_0(\lambda) + \frac{\Delta A_0(\lambda)}{[^3O^*]l}, \quad (3)$$

where $^3\varepsilon_0(\lambda)$ and $^1\varepsilon_0(\lambda)$ are the respective molar extinction coefficients, $\Delta A_0(\lambda)$ is the difference in the absorption and the ground state absorption at a particular wavelength, l is the path length and $[^3O^*]$ is the triplet excited-state concentration at the time correlating with $\Delta A_0(\lambda)$. In the triplet sensitization technique, the $T_n \leftarrow T_1$ molar extinction coefficient of the investigated molecule, $\Delta\varepsilon_M$, is determined by comparison against a sensitizer with known triplet state extinction coefficient $\Delta\varepsilon_S$, according to

$$\frac{\Delta A_S}{\Delta A_M} = \frac{\Delta\varepsilon_S}{\Delta\varepsilon_M} \frac{k_{obs}}{k_{obs} - k_d}, \quad (4)$$

where ΔA_S and ΔA_M are the differential $T_n \leftarrow T_1$ absorbance change in the sensitizer and the molecule of interest, respectively, k_{obs} is the observed rate constant in the presence of the sensitizer and k_d is the triplet decay constant of the molecule without the sensitizer. Typically, β -carotene is used due to its large excited state molar absorption coefficient around $17 \times 10^4 \text{ M}^{-1} \text{ cm}^{-1}$ [80–82]. For platinum phenylene ethynylene oligomers, strong $T_n \leftarrow T_1$ molar extinction coefficients were determined in the range of $2 \times 10^4 \text{ M}^{-1} \text{ cm}^{-1}$ to $7.5 \times 10^4 \text{ M}^{-1} \text{ cm}^{-1}$, depending on the chemical structure and wavelength [82–84].

Recently, Greenham et al. employed the technique of pump-probe saturation spectroscopy to determine the $T_n \leftarrow T_1$ absorption cross-section in a thin film of a conjugated polymer [85]. They generated a population of T_1 states of F8BT by a continuous wave pump laser and excited the T_1 states to the T_n state with an intense fs probe pulse. As long as the number of T_1 states promoted to the T_n state is much less than the total number T_1 states generated by the pump beam, the fractional transition intensity is independent of the pump intensity. Observing a decrease of $\Delta T/T$ with increasing pump intensity is a signature that saturation is occurring because a significant fraction of T_1 excitations are promoted to the T_n level. One can also monitor the recovery of the T_1 population by a second probe pulse of low intensity after a variable delay time. The experiment yields a $T_n \leftarrow T_1$ cross-section of $\sigma = 2.0 \times 10^{-16} \text{ cm}^2$ at a photon energy of 1.47 eV which corresponds to the maximum of the $T_n \leftarrow T_1$ transition. This is in excellent agreement with the value predicted by DFT calculations but is by a factor of about 5 less than that for members of the poly-phenylenevinylene family [86]. For comparison, it is useful to convert the molecular absorption cross-section σ into the decadic absorption coefficient ε . 1ε measured in $\text{M}^{-1} \text{ cm}^{-1}$ units corresponds to $3.81 \times 10^{-19} \sigma$ in cm^2 units, since $\sigma = (10^3 \ln 10/N_A)\varepsilon$, with N_A being Avogadro's number. This yields an absorption coefficient of $0.05 \times 10^4 \text{ M}^{-1} \text{ cm}^{-1}$ for F8BT. Not all of the T_n states excited actually return the T_1 state from which they were promoted. The recovery experiments on the triplet excitations in F8BT [85] demonstrate that only 80% the T_n states relax back to T_1 state with a decay time of 300 fs via internal conversion and the rest dissociate to longer lived coulombically bound electron–holes pairs. This is reminiscent to autoionization of higher Franck-Condon states in molecular crystals [87].

Triplet state absorption can be employed for optical power limiting applications using the mechanism of reverse saturable absorption (RSA). RSA requires an excited-state absorption cross-section that exceeds the ground state absorption at the same

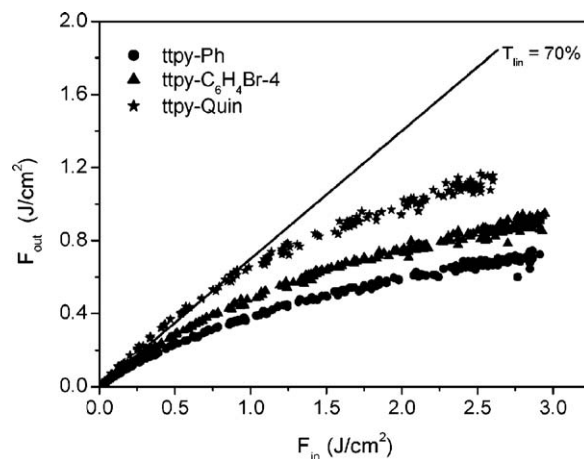


Fig. 12. Transmitted fluence as a function of incident fluence from a 4.1 ns laser pulse for three platinum(II)4'-tolylterpyridyl arylacetylide complexes in acetonitrile in a 2-mm cell. The linear transmission for each solution is 70%. Reprinted with permission from [88], copyright 2005 American Chemical Society.

wavelength, and it results in a reduced transmittance when the incident intensity is higher than the limiting threshold. A weak $T_1 \leftarrow S_0$ absorption in combination with a moderate or high $T_n \leftarrow T_1$ transition may be realized, for example, in organometallic complexes such as Pt(II) acetylides [88,89]. The resulting optical limiting is shown in Fig. 12 for three Pt(II) acetylide complexes.

4. The generation of triplet states

4.1. Optical methods

4.1.1. Triplet state population via intersystem crossing

When light is absorbed and creates a singlet S_1 state, the triplet T_1 state can become populated through intersystem crossing. The ISC rate can be written as [90]:

$$k_{ISC} = \frac{2\pi}{\hbar} \langle ^1\psi^0 | H_{SO} | ^3\psi^0 \rangle [FCWD], \quad (5)$$

where $^1\psi^0$ and $^3\psi^0$ refer to the unperturbed singlet and triplet state wavefunctions, and FCWD is the Franck-Condon weighted density of states, i.e. the density of vibrational states in the triplet times the Franck-Condon vibrational overlap. In other words, the ISC rate depends on two factors, the strength of the spin–orbit coupling and the vibrational overlap between the wavefunctions of the S_1 and triplet state involved. The vibrational overlap factor controls many non-radiative processes and is discussed in more detail in Section 6.1.2. It depends exponentially on the energy difference between the two states involved [63,91]. Consequently, ISC from S_1 into a nearby high-energy triplet state followed by internal conversion to T_1 can be more efficient than direct ISC from S_1 to T_1 .

The effect of spin–orbit coupling on an originally unperturbed triplet state T_1 is to mix it with one or more singlet states. The resulting state is usually referred to as a nominal triplet state T'_1 . In a simplified manner this can be written as [27,92]:

$$|T'_1\rangle = |T_1\rangle + \sum_k \frac{\langle S_k | H_{SO} | T_1 \rangle}{E(T_1) - E(S_k)} |S_k\rangle \quad (6)$$

where $|T'_1\rangle$, $|T_1\rangle$, $|S_k\rangle$ denote the wavefunction of the perturbed first triplet excited state, the unperturbed first triplet excited state and the unperturbed k th singlet state. This equation applies to each triplet substate separately, so that they can differ on the composition of higher-lying singlet state admixtures. The same equation also applies to the singlet ground state, which will

acquire some triplet admixture, albeit very small due to the large energy gap between S_0 and the triplet manifold, so that $S'_0 \approx S_0$. The observed phosphorescence takes its intensity from the allowed transitions between S_0 and the singlets mixed into the triplet state, and to a lesser extent, from the allowed transitions between the triplet excited state and the triplets mixed into S_0 [92,19]. Spin-orbit coupling is the most general mechanism that enables intersystem crossing. For a many-electron central field case such as a hydrogen-like atom, the spin-orbit coupling operator $H_{SO} \propto Z^4/n^3(l+1)(l+0.5)l$, where n , l are quantum numbers and Z is atomic charge, i.e. it increases strongly for heavy atoms and decreases with the distance of the electron from the nucleus.

Spin-orbit coupling implies that a momentum change due to a change in spin momentum can be balanced by a change in orbital momentum, since only the sum of spin and orbital momentum needs to be conserved. This is the case, for example, when for an electron in a p -orbital a spin flip is accompanied by a change of the associated angular momentum from l_y to l_x [27]. In aromatic hydrocarbon molecules such as polyacenes, the T_1 state results from a $\pi\pi^*$ transition. The singlet states allowing for the possibility of a jump between p_x and p_y orbitals, that is necessary for the spin flip associated with a $T_1 - S_0$ transition, are $\sigma\pi^*$ states. Since the σ and π orbitals are orthogonal in planar molecules and the energy gap between $\sigma\pi^*$ and $\pi\pi^*$ states is large, the associated matrix element should be zero. It is argued that the matrix element obtains a finite value when the molecule undergoes vibrations that destroy the planar symmetry of the molecule and mix the σ and π orbitals, such as out-of-plane C–H vibrations [19,27,92]. Further, the vibrational structure of the phosphorescence spectrum is supposed to be dominated by the vibrations that allow the transition to occur [27]. By phosphorescence excitation spectroscopy on glassy benzophenone at 6 K it has been concluded that coupling to a torsional mode of the phenyl rings increases spin-orbit coupling in the $^3n\pi^*$ state by up to two orders of magnitude [93]. Similarly, for dibenzothiophene-fluorene oligomers a strongly increased intersystem crossing rate in certain solvents was attributed to solvent-induced twisting of the oligomer conformation, while no such increase was observed for analogous polymers [94]. For polymers, rotations of the phenyl ring or rotations of an ethynylene bond may be particularly suited to enhance spin-orbit coupling [90]. We note, however, that we are not aware of an extended systematic experimental study on the effect of vibrations on spin-orbit coupling in hydrocarbons, while phosphorescence is reported in fully planar compounds with extended π -systems that would be difficult to distort such as MeLPPP at 10 K or crystalline anthracene at 2 K, where most vibrations and rotations are frozen out [70,79].

The most effective way, however, to obtain a strong spin-orbit coupling and thus a strong intersystem crossing is with the help of heavy atoms, for example by incorporating them into the chemical structure (internal heavy atom effect). Consequently, the use of organometallic complexes has become common practice for phosphorescent LEDs. Comparison between phenylene ethynyls with and without platinum atoms in the chain backbone has shown that very little mixing with the metal wavefunction is sufficient for spin-orbit coupling to become significant [29,82,95]. In solutions of organic molecules, it is well known that detection of phosphorescence is easier in solvents with bromine or iodine, and that the occasional collision with the solvent molecule suffice to induce the necessary spin-orbit coupling (external heavy atom effect). Minaev et al. [96] explained this external heavy atom effect in terms of back-charge-transfer from the heavy atom next to the sensor molecule. In solid state, phosphorescence measurements on MeLPPP have been attributed to the effect of residual platinum atoms in the film [97]. Similar experiments have been reported by Monkman and co-workers [98]. They found that by doping a

solution of polyspirobifluorene with iridium complexes the intersystem crossing rate in the polymer host to be enhanced by more than one order of magnitude. They explained their results in terms of spectrally favorable Förster virtual exchange between the Ir-complex ground state and the polymer singlet excited state combined with Dexter-type virtual exchange between the polymer ground state and the excited state of the complex.

The efficiency of intersystem crossing is given by $\Phi_{ISC} = k_{ISC}/(k_{ISC} + k_r + k_{nr})$. It can range from less than 1% for rigid organic polymers such as MeLPPP up to nearly 100% for organic molecules with lone pairs states such as benzophenone or quinoxaline. For MeLPPP, Φ_{ISC} can be estimated using a typical intersystem crossing rate for organic hydrocarbons in the order of 10^7 s^{-1} , and a lifetime of the singlet S_1 state in MeLPPP on the order of 300 ps [37]. Assuming there are no other significant non-radiative decay channels, this implies a radiative decay rate around $3 \times 10^9 \text{ s}^{-1}$ and suggests an efficiency of 0.2% for intersystem crossing in MeLPPP. This is in agreement with experiment [99]. For benzophenone, the intersystem crossing rate itself is very high due to efficient vibrational coupling via the non-bonding orbital in combination with a small $S_1 - T_1$ energy gap of only 0.22 eV [27]. This reduces the lifetime of the S_1 state to 100 ps [100]. A similar situation is encountered in quinoxaline [101]. In consequence, the intersystem crossing yield in both compounds is near 100%. In many organometallic compounds, the intersystem crossing yield is also near 100% due to the very high metal-induced spin-orbit coupling. For example, for *trans*-Pt(II)-complexes with phenyl ethynyl ligands, Rogers and co-workers determined the intersystem crossing yield to range between 60% and 92%, depending on length and nature of the organic ligand [82]. For these and other Pt-acetylides, the intersystem crossing rate has been determined to be $\geq 10^{12} \text{ s}^{-1}$ [82,102]. Typical intersystem crossing rates for organic hydrocarbon molecules are $1.0 \times 10^7 \text{ s}^{-1}$ for triphenylene, $1.5 \times 10^7 \text{ s}^{-1}$ for chrysene, and $0.88 \times 10^7 \text{ s}^{-1}$ for benzene. Non-deuterated and deuterated anthracene have relatively high ISC rate of about $11 \times 10^7 \text{ s}^{-1}$ and $9 \times 10^7 \text{ s}^{-1}$, respectively, while naphthalene and pyrene have unusually low values of $0.02 \times 10^7 \text{ s}^{-1}$ and $0.003 \times 10^7 \text{ s}^{-1}$ [19]. The low value in naphthalene may be due to the fact that the $S_1 - T_1$ gap in naphthalene is as large as 1.4 eV, while the T_2 state is energetically above S_1 , so that the radiationless ISC transition becomes very inefficient. (A similar energetic ordering causes a low ISC rate in an anthracene crystal.) In pyrene, the situation is likely to be similar. In contrast, in the anthracene molecule, the T_2 state is just below S_1 , rendering ISC nearly isoenergetic and thus fast [44].

There is also intersystem crossing in excitations that are spread out over a pair of chromophores, for instance in charge-transfer states. The ISC rate was measured for a polymer blend (F8BT:PFB) in which the primary optical excitations relax to an polaron pair at the internal interface [103]. The initial excitations are S_1 excitons that form polaron pairs on a 100 ps time scale. On this short time scale, the polaron pairs retain their spin memory, i.e. the pairs are also in the S_1 state (in contrast to the experiment by Kadashchuk, where the polaron pairs all relaxed to the T_1 state on the long time scale measured). Ford et al. employed time-resolved $T_n \leftarrow T_1$ absorption measurements to monitor the appearance of the F8BT triplet states that are generated via ISC crossing within the eh-pair. Data analysis yields a lower bound of the ISC rate constant of $2 \times 10^6 \text{ s}^{-1}$ for the polaron pairs at the (F8BT:PFB) interface. Similar experiments have been reported on blends of MDMO-PPV with different cyano-containing acceptors [104] in which the initial S_1 state of the MDMO-PPV donor rapidly forms a pair radical cation and anions.

It can occur that in an excited state of a pair of chromophores ISC is enhanced relative to that in the corresponding single molecular chromophore. An example is perylenediimide (PDI). In

PDI, the triplet yields is as low as less than 1%. The likely reason is related to the large $S_1 - T_1$ gap of the parent perylene molecules. If there is no higher-lying triplet level close S_1 , the radiationless decay from the S_1 to the T_1 state is very inefficient. Surprisingly, in a cofacially stacked PDI-dimer with a xanthene linker, in which the singlet state excitation forms an excimer, up to 50% of all initial excitations end up as T_1 states on one of the PDI units. The fact that the T_1 yield depends on the polarity of the solvent supports the notion that the transition from the (singlet) excimer state of the PDI-dimer to the T_1 state of the monomer is promoted by an intermediate CT pair state whose energetic position varies with solvent polarity. Although the CT state is above that of the excimer, its energetic proximity increases the rate of the excimer to T_1 transition. In addition, the longer lifetime of the singlet state in the excimer may also contribute to the larger intersystem crossing yield. A similar enhancement of triplet formation has been observed in F8BT:PFB complexes in which the triplet yields in the parent compounds are only 1.9% (F8BT) and 3.4% (PFB) as compared to a maximum yield of 24% in the F8BT:PFB 5:1 blend [86].

In order to determine the rate constant for ISC, k_{ISC} , one has to measure both the lifetime of the singlet state from which ISC proceeds and either the quantum efficiency of ISC or the absorption cross-section of the $T_n \leftarrow T_1$ absorption. This is obvious from the rate equations for ISC:

$$\frac{d[S_1]}{dt} = G - (k_r + k_{nr} + k_{ISC})[S_1] \quad (7)$$

$$\frac{d[T_1]}{dt} = k_{ISC}[S_1] - k_T[T_1] \quad (8)$$

where G is the number of S_1 excitations generated by a short laser pulse, the square brackets denote the concentration, $k_r + k_{nr}$ is the sum of radiative and non-radiative decay constants of the S_1 state, i.e. $(k_r + k_{nr} + k_{ISC})^{-1} = \tau_S$ where τ_S is the singlet exciton lifetime, and k_T is the reciprocal triplet lifetime (Fig. 13). Since $k_{ISC}[S_1] \gg k_T[T_1]$, Eqs. (7) and (8) yield the fraction of triplets generated by the laser pulse,

$$[T_1] = G \frac{k_{ISC}}{k_r + k_{nr} + k_{ISC}} (1 - e^{-t/\tau_S}) \quad (9)$$

For $\tau_S \ll t \ll \tau_T^{-1}$, it follows that $[T_1] = Gk_{ISC}\tau_S$. In this way, King et al. [105] determined $k_{ISC} = 5 \times 10^6 \text{ s}^{-1}$ for polyspirofluorene chains in dilute solution where $\tau_S = 2.3 \text{ ns}$ and the triplet yield is 1.2%. This value is comparable with values calculated from the singlet lifetime and the fluorescence and phosphorescence yields [19]. For compounds with strong spin orbit coupling, $k_{ISC} \gg k_r + k_{nr}$ so that $\tau_S = (k_{ISC})^{-1}$, i.e. the singlet lifetime is entirely determined by the intersystem crossing rate. From Eq. (9) it follows that the build-up of the T_1 population that can be observed in a time-resolved $T_n \leftarrow T_1$ absorption experiment then maps the intersystem crossing rate k_{ISC} .

Recently, Hedley et al. [106] succeeded to measure directly ISC in a phosphorescent metal complex $\text{Ir}(\text{piq})_3$. Upon exciting the

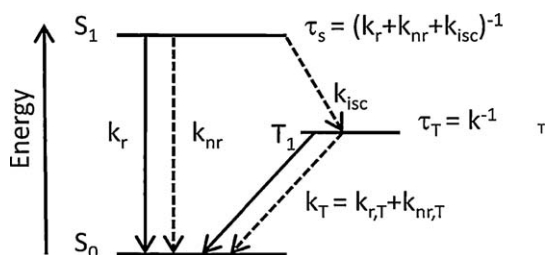


Fig. 13. Energy level diagram with rate constants concerning the triplet state generation and decay.

$^1\text{MLCT}$ state by 100 fs pulses from a Ti:sapphire oscillator they measured the decay of the emission from the $^1\text{MLCT}$ state and the simultaneous rise of phosphorescence emitted from the $^3\text{MLCT}$ state and found that ISC occurs with a decay/rise time of $70 \pm 10 \text{ fs}$. By monitoring the recovery of hot phosphorescence emitted from Franck-Condon states located 140 meV above the T_1 level, the vibrational cooling time is found to be 95 fs.

Spin-orbit coupling can also cause the triplet state to have a polarization that is different from the singlet state. For molecules such as the planar acenes, fluorene, coronene, chrysene anthracene and picene, the polarization of the triplet state emission was found to have two components: a dominant one (about 70% of the total emission intensity) out of the molecular plane and the other one parallel to the long molecular axis. This has been attributed to the fact that the spin-orbit coupling operator mixes singlet and triplet states of the same parity (u or g), but of different symmetry. Since the different admixtures change the symmetry of the wave function, different polarizations of the $T_1 \rightarrow S_0$ emission become possible, depending on the particular symmetries of the admixed singlet states. For some molecules it has been possible to attribute the observed in-plane and out-of-plane components of the phosphorescence to admixtures of particular singlets according to their symmetry [92,19].

For conjugated polymers, the orientation of the transition dipole moment in S_1 , T_1 and T_n was determined through steady state measurements of $S_1 \rightarrow S_0$ and $T_1 \rightarrow S_0$ emission and $S_1 \leftarrow S_0$ and $T_n \leftarrow T_1$ absorption for an oriented Pt-polymer that contained MEH-substituted phenyl ring. While the $S_1 - S_0$ and $T_n - T_1$ transitions were found to be polarized entirely parallel to the chain, the $T_1 - S_0$ transition has components both parallel and perpendicular to the polymer chain, with the latter contributing about 70% to the emission [107]. Using the gated detection technique for emission measurements, a similar result has been reported subsequently for the purely organic, aligned PF2/6 [108]. This confirms the general notion and illustrates that the difference in polarization is not induced by the heavy metal. It is possible that, like for the planar acenes, spin-orbit-induced mixing of the singlet and triplet states may also account for the difference in S_1 and T_1 polarization in conjugated polymers, though detailed quantum-chemical calculations are required to confirm this and to reveal which particular singlet states are mixed with the triplet.

The fact that T_1 has more than half of its emission polarized orthogonal to the chain axis might be exploited to obtain gain in microcavities based on phosphorescent emitters. Gain is often limited by reabsorption of the emitted light by charges. Since the charge-induced absorption is usually along the chain and a large fraction of the phosphorescence is perpendicular to the chain axis, this orthogonality should reduce the problematic reabsorption.

4.1.2. Triplet excitation via sensitization

In hydrocarbons with weak spin-orbit coupling, intersystem crossing from the S_1 state to the T_1 state is weak and, concomitantly, phosphorescence is difficult to detect. This is a frequently encountered problem, and can be circumvented by using triplet sensitizers. They cause a high population of the triplet state and thus ensure a measureable phosphorescence intensity. The requirement for successful sensitization is that (i) the singlet and triplet states of the sensitizer are below those of the triplet emitter and (ii) the sensitizer has a high intersystem crossing yield. The basic idea is that the singlet state of a sensitizer is excited either directly or via energy transfer from the S_1 state of the hydrocarbon molecule of interest. This is followed by efficient intersystem crossing on the sensitizer and subsequent energy transfer from the triplet state of the sensitizer to the triplet energy level of the hydrocarbon molecule one wishes to investigate. In Fig. 14, different methods to employ sensitizer are illustrated.

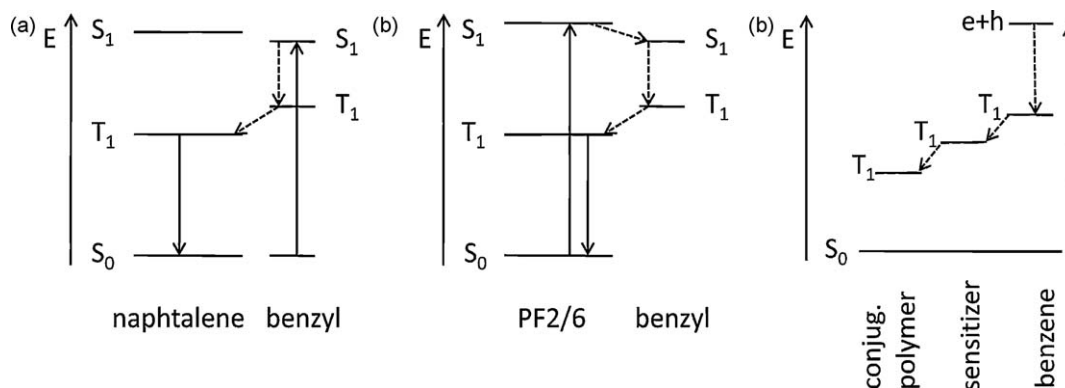


Fig. 14. Energy level diagram for triplet sensitization schemes. (a) after Terenin and Ermolaev [109], (b) after Bagnich et al. [110] and (c) after Monkman et al. [111].

In 1956, Terenin and Ermolaev [109] pioneered this method to observe phosphorescence of hydrocarbons such as naphthalene and diphenyl in inert solution sensitized by compounds containing carbonyl groups like benzyl, diacetyl, benzaldehyde *et cetera*. In these carbonyl containing systems the $S_1 - T_1$ gap is small, typically on the order of 0.2–0.3 eV, and intersystem crossing yields are close to 100%. In more recent times, Bagnich et al. [110] used this technique to measure phosphorescence of a polyfluorene (PF2/6) film doped with benzyl. Since the S_1 state of benzyl is 0.28 eV below that of PF2/6 and the benzyl triplet is 0.17 eV above of the T_1 state of PF2/6, benzyl acts as sort of a catalyst. Upon exciting the PF host rapid energy transfer populates the benzyl S_1 state followed by rapid ISC to the benzyl T_1 state and efficient triplet transfer to the T_1 state of PF2/6 and phosphorescence can be observed.

Monkman et al. [111] adapted Terenin and Ermolaev's technique to determine the T_1 levels of a series of conjugated polymers in benzene solution. They populated the T_1 state of benzene via the recombination of electrons and holes generated by a 100 ns pulse of 10 MeV electrons from a linear accelerator. The benzene solution was doped by a series of triplet sensitizers and the polymer. The triplet state from the benzene was transferred onto the sensitizer and from there to the polymer. (Of course, the recombination of electrons and holes also results in singlet states, but these, too, lead to a sensitizer triplet state eventually.) A series of sensitizers were employed in order to scan a range of T_1 levels and the induced $T_n \leftarrow T_1$ absorption of the polymer was measured. Vanishing triplet absorption of the polymer was taken as an indicator that its T_1 level is above the T_1 level of the sensitizer. This technique is particularly useful in liquid solution in which triplet states are inevitably quenched by triplet scavengers such as oxygen.

4.1.3. Triplet generation via fission of singlet excitons

An unconventional and rare way to generate triplet excitations is via the fission of a singlet state into a pair of triplets that are localized on adjacent chromophores. The condition for this process to occur is that the S_1 state and a pair of triplets are energetically close. This can be observed for example in condensed phases of tetracene and pentacene. In pentacene, $E_{S_1} > 2E_{T_1}$, and so fluorescence is completely quenched through singlet fission. For tetracene, the energy of the T_1 state is about 0.15 eV above that of the S_1 exciton. As a result, singlet fission and the associated fluorescence quenching becomes thermally activated [112]. Recently, singlet fission has been studied for bis-(tetracene)s in solution in which the tetracene units are linked together covalently with a phenylene spacer [113,114]. Singlet fission was observed for a para-linkage, yet not for a meta-linkage. In contrast to a tetracene crystal, the two triplets are confined to the bis-tetracene and form a metastable pair that can return to the S_1 state and emit delayed

fluorescence. Quantum-chemical calculations indicate that electronic coupling between the two tetracene units is primarily through bond. They provide an explanation why fission rates depend on the type of linkage between the tetracene units. Hypothetically one can think of exploiting S_1 fission into a pair of lower energy excitations in an appropriately designed photovoltaic cell.

4.2. Electrical excitation

Excited states may be formed by optical or electrical excitation. The excitation and decay pathways are illustrated in Fig. 15. Since optical transitions between the singlet ground state and the triplet excited state are forbidden, optical excitations of organic semiconductors initially creates only singlet excited states. Some triplet states may then be formed as a result of intersystem crossing from the singlet excited state. In contrast to optical excitation, the process of electrical excitation by charge injection from the electrodes involves placing electrons on or removing them from the polymer chain. Electron and hole diffuse through the semiconductor film until they are attracted by their mutual coulomb force and recombine on a chromophore to form either singlet S_1 or triplet T_1 excited states. This process is likely to occur through intermediate charge-transfer states with singlet or triplet character 1CT and 3CT as shown schematically in Fig. 16. If singlet and triplet states were formed with equal cross-sections, then by statistical arguments, initially 75% of the excited states would be in the triplet spin state while only 25% would be in the singlet state. In addition, intersystem crossing from singlet to triplet states can still occur. These formation ratios place a constraint on the ultimate efficiency with which light can be generated in a organic semiconductor LED. For singlet states, the externally measured

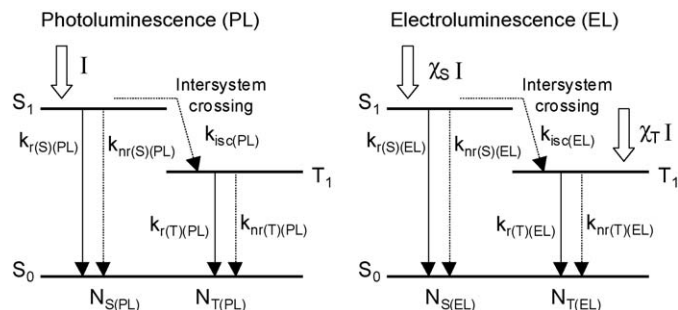


Fig. 15. A simple model for the emission spectra in photoluminescence (a) and electroluminescence (b). I represents an initial number of excitons. k_{nr} , k_r and k_{ISC} represent non-radiative, radiative and intersystem crossing rates, respectively, and N_S and N_T represent the number of singlet and triplet photons that would be expected to be emitted. χ_S and χ_T are the singlet and triplet generation fractions, respectively. S_0 is the singlet ground state. Reprinted from [122].

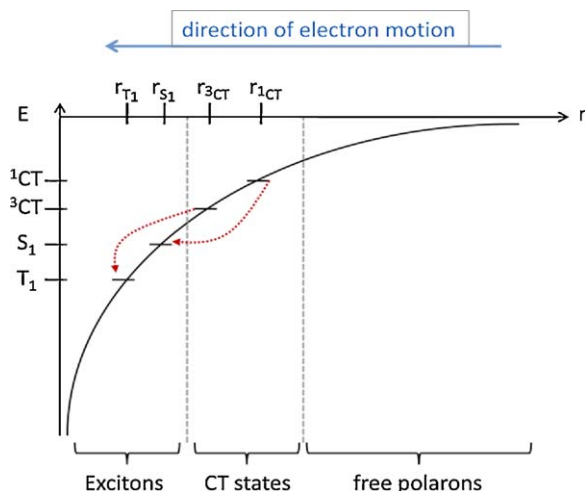


Fig. 16. Schematic for the electron hole recombination process in the reference frame of the hole. In this very simple model the recombination occurs into S_1 and T_1 states via intermediate charge-transfer states of either singlet or triplet character, 1CT and 3CT , respectively. After [137].

electroluminescence quantum yield η_{EL} is lower than the fluorescence quantum yield, η_{PL} , in the device structure, since only a fraction γ of the injected electrons and holes recombine to form excitons, only a fraction χ_S of these are in the singlet state, and only a fraction η_{out} of the light is able to couple out of the device. As a result, $\eta_{EL} = \eta_{PL}\gamma\chi_S\eta_{out}$. Fluorescence yield, charge recombination and outcoupling can all be optimized to maximum values by suitable design of materials and device architecture [115], so that the singlet generation fraction χ_S becomes the major efficiency limiting factor for organic LEDs. Moreover, understanding what controls the spin of the excited state implies understanding of the recombination process *per se*, which is fundamental to electroluminescence in organic semiconductors. For both reasons, much experimental and theoretical effort has been dedicated to this issue. In this section, we will give a brief overview on the different experimental approaches to this issue, the theoretical understanding that has developed, the role of charge-transfer states in this process and an outlook on future perspectives. A detailed discussion is beyond the scope of the current manuscript. For a more in-depth introduction we refer the reader to two dedicated review articles [116,117].

4.2.1. Approaches to experimentally determine the singlet generation fraction

The first indications that more than 25% of the excited states may be in a singlet spin state came from comparison of the *absolute* quantum yield of electroluminescence and fluorescence, either in an integrating sphere or in combination with careful calculations of the light outcoupling [118–120]. Values around 35–50% were reported for polymer materials used in a single-layer device. Recently, using this approach with an integrating sphere measurement, a singlet generation ratio of about 50% was reported for a small molecule device based on a hole-transporting layer, an emissive layer, and an electron-transporting layer. It is conceivable that interfacial processes may play a role in this multilayer device which suggest a higher singlet generation ratio at variance with related work on small molecule devices (*vide infra*) [121].

Difficulties naturally associated with absolute measurements can be avoided when only the *relative* intensity of electroluminescence and photoluminescence are compared, since many factors cancel out. Using this approach, singlet generation fractions were reported to be around 50% for a Pt-acetylide polymer yet around 25% for its associated monomer [122] and 22% for Alq₃ [123]. This

technique requires the simultaneous detection of singlet and triplet state luminescence, in both EL and PL, and is therefore restrained to compounds with strong spin orbit coupling. When the triplet $T_1 - T_n$ absorption is monitored instead of the phosphorescence, this method can be adopted to purely organic compounds, as was beautifully demonstrated by Rothe et al. [124] They found χ_S to be 44% for a spiro-polyfluorene-type polymer.

Both absolute and relative measurements of EL and PL efficiencies are carried out in an operating light-emitting diode. The singlet generation fraction may also be determined by purely optical measurements on films, when photoluminescence and photoinduced absorption measurements are combined with optically detected magnetic resonance. In this case, the cross-sections for singlet and triplet formation, σ_S and σ_T are determined and the singlet generation ratio is given by $\chi_S = \sigma_S/(\sigma_S + \sigma_T)$. In these measurements, polaron absorption peaks are monitored. An applied magnetic field splits the spin up and spin down sublevels, which recombine with different rates depending on whether they form spin parallel or anti-parallel polaron pairs. A microwave absorption signal is used to pump the system to back equilibrium between the spin up and spin down sublevels, and from the intensity of this absorption signal δt , the cross-section for singlet and triplet state formation is derived [116,125–127]. Singlet generation ratios for a number of compounds have been determined that are in good agreement with values otherwise determined. In particular, a clear increase of the singlet generation fraction with conjugation length was observed [126,127]. The use of this technique to determine singlet generation fractions has been questioned, though [128,129]. It was suggested that an apparent higher singlet formation rate may be due to an enhanced annihilation of triplet excitons by polarons. This is refuted by Yang and co-workers, and the discussion on this seems to be ongoing [130–133].

Less controversial is the determination of the singlet generation fraction from the rate of singlet and triplet formation, g_S and g_T , respectively, according to $\chi_S = g_S/(g_S + g_T)$ [134,135]. The rate of singlet formation is determined through measurements of the absolute EL and PL quantum yield and calculation of the light outcoupling from the device. The rate of triplet formation can be derived if lifetime, intensity and cross-section of the $T_1 - T_n$ absorption are known. Measurement of the former two is trivial, while determination of the triplet absorption cross-section requires some skill. Using triplet absorption cross-sections that are based on quantum-chemical calculations or pulse radiolysis measurements, singlet generation fractions up to 80% have been reported for PPV, PFO and F8BT derivatives, independent of drive voltage [134,135]. The calculated values for F8BT of $2 \times 10^{-16} \text{ cm}^2$ [86] has recently been confirmed experimentally to be $3 \times 10^{-16} \text{ cm}^2$ [136].

A different approach to deriving the singlet generation ratio χ_S consists in measuring the photoluminescence quenching that results from the application of an electric field. Segal and co-workers deduced that a field-induced change in PL and concomitant appearance of photocurrent be proportional to the product of light outcoupling and photoluminescence efficiencies $\eta_{PL}\eta_{out}$, so that the singlet generation fraction can be deduced according to $\eta_{EL} = \eta_{PL}\gamma\chi_S\eta_{out}$, provided the EL quantum yield is measured as well and γ is estimated. Segal et al. find singlet generation fractions of 20% for both, Alq₃ and MEH-PPV [137]. Similarly, Reufer and co-workers consider the recombination of geminate polaron pairs that result from field-induced quenching of fluorescence and phosphorescence [138]. When the field is turned off, the singlet emission recovers much more strongly than the triplet emission. From this it is concluded that virtually no additional triplets are generated, and that therefore the total spin of the polaron pair state remains unchanged on typical timescales

of carrier capture and recombination under electrical injection. Reufer and colleagues do not consider the possibility that a triplet polaron pair be converted into a singlet polaron pair, maybe because they consider the triplet polaron pair to be energetically below the singlet polaron pair [67]. Recent calculations on a number of compounds have however shown that the singlet charge-transfer state can be energetically below the triplet charge-transfer state [68]. If interconversion to a singlet state were, in principle, possible, it would be consistent with the experimental results by Reufer.

The experimental results may be summarized as follows. With the exception of the multi-layer small molecule OLED by Okumoto et al. [121], all measurements agree on a singlet generation fraction of $\leq 25\%$ for small molecules. For polymers, singlet-triplet ratios ranging from over 25% up to 80%, implying spin-dependent carrier recombination, are reported in organic and organometallic compounds, based on absolute EL and PL measurements [118–120], relative EL and PL measurements [122,124], magnetic resonance measurements [126] and measurements of the triplet absorption cross-section [86,134,135]. This conjugation length dependence of the singlet generation fractions is questioned and spin independent recombination is suggested on the basis of a different interpretation of magnetic resonance experiments [128,129] and through field dependent PL quenching experiments [137,138]. Particularly illuminating in this context is the recent work by Segal and colleagues, where the organometallic compound PtOEP is added as a dopant to the emissive Alq₃ film. This was found to result in a singlet generation fraction χ_s of 84%, while this is below 25% when only the organic OEP is added as dopant [69]. An additional electrofluorescence was also observed when the organometallic FIrpic was used as an additional layer next to the red emitter DCM₂, compared to a device where the FIrpic was separated from the DCM₂ by 100 Å of BCP. This important work points to the role of spin interconversion in the charge-transfer states that precedes the final recombination step and depends on the intermolecular architecture. Several attempts have been made to illuminate the spin dependence of the recombination process from a theoretical point of view.

4.2.2. Theoretical concepts

The recombination of electron and hole can only depend on their mutual spin orientation when two requirements are fulfilled. The first is that there must be different rate for forming the singlet and triplet states. The second is that there must be a mechanism that randomizes the spins of an electron and hole that are in close proximity to one another, but that have not yet formed an excited state. Without spin-randomizing, the singlet and triplet formation may occur with different rates but they would still lead to the same final populations. Spin-randomizing mechanisms include for example intersystem crossing in the intermediate charge-transfer state, or dissociation of an intermediate charge-transfer state. The number of singlet and triplet states formed then depends on the relative size of the singlet formation rate, the triplet formation rate, and the spin randomization rate.

A number of reasons have been put forward to account for the different formation rates. One view is that the vibrational relaxation from the initial polaron states to the final singlet and triplet states controls the singlet formation ratio [139–142]. These Marcus-type argument are formulated in different ways, with or without intermediate states [141,143]. Alternatively, one may take into account the energy levels and the ionic or covalent character of the initial polaron pair states and the final exciton states as a rate determining factor [144–146]. A comparative discussion of these contributions can be found in Refs. [116,117]. Recent theoretical and experimental work, however, also points to a significant role of intermediate charge-transfer states in the exciton formation

process. Note that we take the term “CT state” here as a generic expression to include any related species.

4.2.3. The role of charge-transfer states

The importance of CT states to the singlet formation cross-sections was first highlighted in a number of theoretical papers [141,145,147,148]. A possible formation pathway for singlet and triplet S_1 and T_1 excitons involving CT states is outlined by Beljonne and co-workers. It is considered that the charges first form bound charge-transfer 1CT and 3CT pairs. These geminate pairs allow for the intersystem crossing or dissociation process that is required for spin-dependent recombination. They may then recombine with spin-dependent rates into S_n and T_n exciton states. The rates may be affected by electronic couplings and spectral overlaps. Finally, internal conversion takes place down the singlet and triplet manifolds into S_1 or T_1 . The different theoretical considerations pertain to which of these steps is rate-limiting and what controls the rate of the steps, yet it seems undisputed that intermediate charge-transfer states play some role.

Experimental evidence for the role of CT states in affecting the number of singlets and triplets formed comes from the two Cambridge groups in the UK and the US [69,86,149]. Ford et al. compared the intensity and lifetime of the $T_n \leftarrow T_1$ absorption signal in the polymers F8BT and PFB alone, and in blends between them made with different ratios. They observed a roughly 10 times higher intensity of the triplet absorption signal in the blend compared to either component alone. Using a calculated triplet absorption cross-section of $2 \times 10^{-16} \text{ cm}^2$ for F8BT at 1.3 eV, the intersystem crossing efficiency γ could be derived. For a 1:1 blend, $\gamma = 20\%$, compared to values of about 2% and 3% for F8BT and PFB alone. This enhanced ISC was considered to take place in the charge separated states at the heterojunction that are a precursor to exciton formation in the blend. This demonstrates that coulombically bound charge pairs may enable spin randomization, which is necessary for a high singlet generation fraction. In a subsequent publication, the rate with which the charge pair at the F8BT:PFB interface recombines into a triplet exciton was determined to be $2.6 \times 10^7 \text{ s}^{-1}$, very similar to the rate of triplet formation from singlet excitons in pristine F8BT, which is $1.2 \times 10^7 \text{ s}^{-1}$ [149]. This result makes clear that the increased triplet population in blends has to be due to a long lifetime of the CT state, rather than an increased intersystem crossing rate. It is reminiscent of the increased ISC efficiency in PDI aggregates that was discussed in Section 4.1.1. A different and rather original route to highlight the influence of CT states was taken by Segal et al. [69], who increased the singlet generation fraction χ_s in the small molecule Alq₃ from below 25% to 84% by adding organometallic compounds either as a blend or as a separate layer. As mentioned above, this was attributed to the singlet CT state in Alq₃ being below the triplet CT state, and an increase in ISC in the CT state due to an external heavy atom effect, induced by the presence of the organometallic compounds.

4.2.4. Summary and outlook

The research so far may be summarized by noting that there is widespread, though not undisputed evidence that, in general, the recombination process of electron and hole takes place in a spin-dependent manner, with a higher number of singlet states formed as the conjugation length in a compound increases. This spin-dependent recombination requires different recombination rates for singlets and triplets as well as some spin-randomizing process. The relative number of singlets formed seem to depend on the intersystem crossing efficiency in the CT states (which implicitly increases with a long CT lifetime) as well as the energetic position of such CT states relative to other exciton states. From recent theoretical work it has become evident that the energetic splitting

between singlet and triplet CT states as well as intersystem crossing between them depends on the material considered, and, in addition, on the relative orientation of the individual chromophores to each other. Further work on the physics of electron–hole recombination is therefore likely to concentrate on the morphology dependence of CT states energetics and kinetics, both in pure films as well as at heterojunctions.

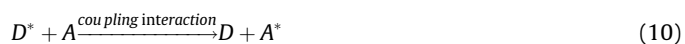
As far as the exploitation of luminescence in light-emitting devices is concerned, possible avenues comprise collecting of all excitons into the triplet state through the use of organometallic emitters [6], a combined use of singlet and triplet emission [9,61], or an engineering of an increased singlet yield [69]. Alternatively, one may attempt to alter the singlet generation fraction by controlling the spin of the injected charge carriers. Recently, Wu and co-workers reported an increase in the electroluminescence efficiency at 77 K of about 20% in MEH-PPV in a layer structure of ITO/MEH-PPV/Co(clusters)/Al when a magnetic field was applied and when the diode was operated in reverse bias [150]. This effect was not observed when the cobalt clusters were replaced by gold, or when the device was operated in forward bias. From this, Wu and colleagues concluded that the magnetic field-induced enhancement can be attributed to an increased singlet formation ratio through spin-polarized hole injection from the cobalt nanoscale clusters. Possible electrode materials for spin-polarized injection are ferromagnetic materials including Co nanoclusters or half-metallic materials such as $\text{La}_{0.7}\text{Sr}_{0.3}\text{MnO}_3$, though we note that care has to be taken to ensure suitable interfacial properties between the organic semiconductor and the spin-polarized electrode [151].

5. Processes during the lifetime of a triplet state

5.1. Triplet state diffusion

5.1.1. Förster and Dexter type energy transfer

An excited state moves through an organic semiconductor by transferring its energy non-radiatively from one site to another. Commonly, this energy transfer is treated as a one-step process where the excited state donor molecule D^* is deexcited while the ground state acceptor molecule A becomes excited through a coupling interaction:



The rate constant for this is given by

$$k = \frac{2\pi}{\hbar} \beta^2 \varrho_E \quad (11)$$

where the density of states ϱ_E is related to the spectral overlap J between the donor emission and acceptor absorption. The total coupling integral $\beta = \langle \psi_f | \hat{H} | \psi_i \rangle$ may be written as the sum of a coulomb and an exchange term $\beta = \beta^C - \beta^E = \int \psi_{D^*}(1) \psi_A(2) \hat{H} \psi_D(1) \psi_{A^*}(2) d\tau_1 d\tau_2 - \int \psi_{D^*}(1) \psi_A(2) \hat{H} \psi_D(2) \psi_{A^*}(1) d\tau_1 d\tau_2$. Förster [152] and Dexter [153] used such expressions to derive the transfer rate for the Coulomb and exchange mechanism, respectively, as

$$k^C \sim \frac{f_D f_A}{R^6 \bar{v}^2} J \quad \text{and} \quad k^E \sim e^{2R/L} J \quad (12)$$

where f denotes the oscillator strength of donor and acceptor, R is their separation, and L corresponds to an effective average orbital radius of the donor and acceptor states. This derivation can be found in many textbooks on photophysics or photochemistry of organic molecules, such as the one by Klessinger and Michl [154].

There are a few salient features to keep in mind when considering triplet state energy transfer in organic semiconductors.

- (i) The transfer rate scales with the oscillator strength f of the donor emission and acceptor absorption for the Coulomb mechanism, yet not for the exchange mechanism.
- (ii) For *both* types of mechanisms, the transfer rate further depends on the spectral overlap J between the donor emission I_D and acceptor absorption ε_A . $J = \int_0^\infty I_D \varepsilon_A d\bar{v}$ with $\int_0^\infty I_D d\bar{v} = \int_0^\infty \varepsilon_A d\bar{v} = 1$. The use of normalised spectral intensities implies that J is *not* connected to the oscillator strength of the transitions involved, and it is therefore as important to Dexter type transfer as it is for Förster type transfer. This fact is sometimes overlooked yet it may be of relevance to host–guest energy transfer processes [154].
- (iii) Further, the transition from a triplet excited state to the singlet ground state is a spin-forbidden process and therefore carries no appreciable oscillator strength, so the Coulomb term vanishes for triplets in the absence of spin–orbit coupling. For strongly phosphorescent compounds, however, there clearly is some appreciable oscillator strength, and so both terms can contribute. Exchange coupling requires wavefunction overlap and is therefore most effective at short distances, as is evident by the exponential distance dependence, while Coulomb coupling prevails at larger distances due to the R^{-6} dependence. A typical cross-over distance between both mechanism is at around 1 nm [155].
- (iv) Care must be taken when estimating the transfer radius of an excitation. Classic Förster theory implies that donor–acceptor energy transfer is a single step process. However, in condensed phases energy transfer is often a multistep process involving a random walk among a manifold of donor chromophores followed by final donor–acceptor transition. The random walk takes place through Förster energy transfer between different donor chromophores. This is of paramount importance for energy transfer in deliberately or inadvertently doped conjugated polymers in which inter-donor exciton transport can enhance the rate of the overall energy transfer process [156]. As a consequence, a transfer radius may be derived for the overall energy transfer of the excitation that far exceeds the single step Förster radius.
- (v) In the above section, only the Dexter exchange integral has been considered for resonant triplet–triplet energy transfer, which describes the simultaneous transfer of two electrons ($|D^*A\rangle \rightarrow |DA^*\rangle$). Scholes and co-workers have pointed out, though, that the total triplet–triplet coupling also includes a “through-bond” one-electron transfer contribution that appears when accounting for ionic, charge transfer like configurations such as D^+A^- and D^-A^+ [157–159]. This through-bond resonance interaction is associated with two equivalent one-electron transfer processes that are mediated via the ionic bridging configuration, i.e. $|D^*A\rangle \rightarrow |D^+A^- \rangle \rightarrow |DA^*\rangle$ and $|D^*A\rangle \rightarrow |D^-A^+ \rangle \rightarrow |DA^*\rangle$. The total matrix element for triplet–triplet coupling is then given by the approximate expression $V^{T-T} \approx (2\beta_{ET}\beta_{HT})/{}^3A - Z$, where β_{ET} is the electron transfer matrix element between donor and acceptor, β_{HT} is the corresponding hole transfer matrix element, 3A is the energy gap between the charge-separated (D^+A^-) and locally excited (D^*A) configurations, and Z is the two-electron (i.e. Dexter) exchange integral. Since β_{ET} , β_{HT} and Z are all exponentially attenuated with distance, the overall triplet–triplet coupling can often be expressed as $V^{T-T} \propto \exp(-2\alpha R)$, with R being the centre-to-centre separation of the overlapping orbitals, and α ranging around $1\text{--}2 \text{ \AA}^{-1}$. The through-bond term becomes significant at short separations ($<6 \text{ \AA}$) while the Dexter term dominates at larger separations or for heavy atoms. For details and references to experimental evidence we direct the reader to a review article on resonant energy transfer by Scholes [157] as well as to the original works by Scholes and co-workers [158,159].

Triplet diffusion by exchange mechanism in crystalline and amorphous organic semiconductors is well documented and can be seen, for example, through the observation of triplet–triplet annihilation [40]. Similarly, Dexter-type triplet transfer between chemically different donor and acceptor molecules is well established [28,155]. In contrast, reports on the diffusion of triplet excitons by dipole coupling are rare and more recent, and usually refer to organometallic compounds. For example, Adachi and co-workers observed a R^{-6} dependence in the rate constant for concentration quenching in the organometallic dyes Ir(ppy)₃, Btp₂Ir(acac) and Flrpic doped into the host materials CBP or mCP (Fig. 17) [160]. This was attributed to Förster-type energy transfer, and Förster radii R_0 in the order of about 1 nm have been derived, much shorter than the 5 nm that are common to singlet transfer in organic films. The shorter Förster radii reflect the dependence of the Förster transfer rate on the oscillator strength of the transition. Similarly, Kadashchuk and co-workers investigated the phosphorescent dye Btp₂Ir(acac). They dispersed the dye at 10 wt.% into inert, transparent polystyrene to form a solid-state solution and realized that at this concentration, triplet excitons were mobile. Evidence was provided by spectral diffusion of the phosphorescence in addition to a reduced lifetime of the 10% blend compared to a 1% blend. A concentration of 10 wt.% implies an average distance of 2.2 nm between the dye molecules. At such a large distance, wavefunction overlap cannot occur and so the transfer mechanism between the organometallic complexes is attributed to Coulomb coupling. We note that these two papers report dipole–coupling between triplet states, which is not to be confused with Förster transfer from a host singlet to a guest singlet followed by intersystem crossing into the guest triplet state [161].

Further evidence that Förster-type dipole–dipole coupling can, in fact, be important in triplet energy transfer is reported in the recent work of Wasserberg et al. [162]. They studied triplet energy transfer from a green emitting iridium complex (Ir(tBu-ppy)₃) to either the red emitting Ir(btp)₂(acac) complex or to terthiophene. It turned out that in semidilute chlorobenzene solution triplet transfer to both acceptors occurs via a diffusion-controlled

reaction with a common rate constant of $3.8 \times 10^9 \text{ L mole}^{-1} \text{ s}^{-1}$, while in solid-state polymer matrix only triplet transfer to Ir(btp)₂(acac) is observed. The reason is that – owing to weak spin–orbit coupling – in terthiophene the oscillator strength of the transition from the S_0 ground state to the $^3\pi\pi^*$ state is virtually zero whereas in Ir(btp)₂(acac) the transition to the ligand-based $^3\pi\pi^*$ state has a finite oscillator strength. Therefore transfer to terthiophene is inhibited because in a dilute system short range Dexter-type exchange interaction cannot occur while long-range resonant, i.e. Förster-type triplet transfer to Ir(btp)₂(acac) is feasible. The experimentally observed Förster radius (3.02 nm) is in quantitative agreement with Förster theory assuming a random distribution of acceptors in a rigid matrix.

When considering the exchange mechanism, it is interesting to compare the transfer of a triplet state to that of a charge. Transfer of a triplet excitation from the donor to the acceptor molecule requires the simultaneous exchange of two electrons at the respective HOMO and LUMO levels. This process is analogous to exchange of a single electron or hole between a pair of molecules except that the matrix element for the concerted exchange of the pair charges comprising the triplet state is much smaller than that for charge exchange between a radical ion and a neutral molecule. In this respect it is instructive to compare the diffusion coefficients for the transfer of charges with those for the transfer of singlet or triplet excitons in a molecular crystal. Based upon the Einstein ratio $eD = \mu kT$ between mobility μ and diffusion coefficient D of a charge in a typical molecular crystal, a mobility of $2 \text{ cm}^2 \text{ V}^{-1} \text{ s}^{-1}$ at 295 K translates into a diffusion coefficient of $0.015 \text{ cm}^2 \text{ s}^{-1}$, while the diffusion coefficient for triplet excitons are on the order $10^{-5} \text{ cm}^2 \text{ s}^{-1}$ to $10^{-4} \text{ cm}^2 \text{ s}^{-1}$. This is confirmed by experiments probing the diffusivity of triplets, D_T [163], and charge carriers, D_{CC} [164], in CBP. The triplet diffusivity was determined to be $1.4 \times 10^{-8} \text{ cm}^2 \text{ s}^{-1}$ using an equivalent of the time-of-flight technique (see Section 5.1.3). From a trap-free electron mobility of about $10^{-3} \text{ cm}^2 \text{ V}^{-1} \text{ s}^{-1}$ in CBP, measured by the time-of-flight technique, $D_{CC} = (kT/e)\mu \approx 3 \times 10^{-5} \text{ cm}^2 \text{ s}^{-1}$ is calculated. This indeed implies $D_T/D_{CC} = 5 \times 10^{-4}$. The diffusion coefficient for singlet excitons in a molecular crystal such as anthracene is on the order of $10^{-3} \text{ cm}^2 \text{ V}^{-1} \text{ s}^{-1}$ [40]. This confirms the notion that the dipole coupling is more efficient than exchange interaction, and that the exchange of a single charge proceeds faster than the simultaneous exchange of two charges.

In molecules with extended π -conjugated systems such as semiconducting polymers, Förster and Dexter type energy transfer can be anisotropic. This is particularly relevant when considering energy transfer between chromophores along a polymer chain. For Förster transfer, the point-dipole approximation used in the derivation of the transfer rate is not appropriate to describe transfer in extended π -systems at short distances and short timescales [157,165]. As a result of the extended charge distribution, singlet excitons move faster between polymer chains than along a polymer chain [166,167]. This is reminiscent of a Hertzian dipole radiating more strongly orthogonal to its axis than along it. For Dexter-type transfer, the effect is opposite. Wavefunction overlap between chromophores along a polymer chain is larger than between chains, given the typical inter-chain separation of 0.4 nm, and so triplets transfer at higher rate along a polymer than between them [168,169]. The anisotropy of energy transfer in polymer chains becomes relevant when designing host–guest systems with a polymer host and a phosphorescent guest. For example, the system of a polyfluorene host with an Ir-complex as guest shows a stronger endothermic triplet back transfer when the Ir-complex is covalently linked into the polyfluorene backbone as compared to the case where the Ir-complex is tethered to the polyfluorene by an alkyl side-chain [170,171]. For singlets, on-chain motion of the exciton can be enforced when embedding the

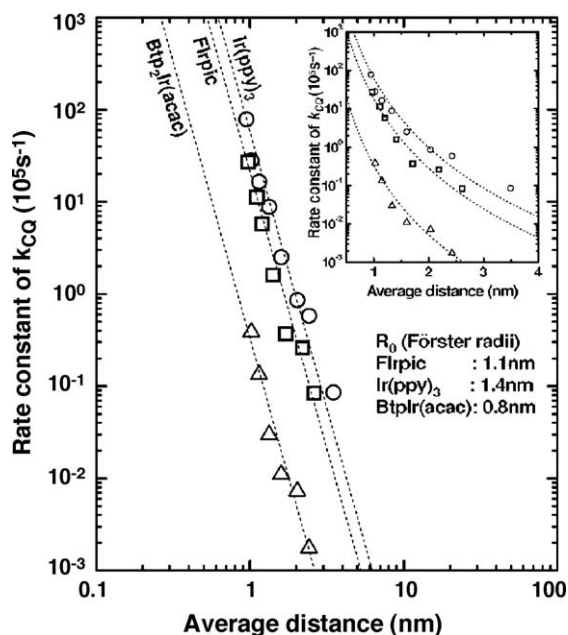


Fig. 17. Dependence of the concentration-quenching rate constants k_{CQ} on the average distance for three complexes plotted on a double logarithmic scale and, as inset, on a semi-logarithmic scale. The resulting Förster radii R_0 are also listed. Reprinted with permission from Ref. [160], copyright American Physical Society.

polymer chains in nanopores or -layers, so that the individual chains are well separated [156].

5.1.2. Diffusion in molecular crystals

Quantitative work on triplet state diffusion started in the mid-sixties of the last century when clean molecular crystals became available. Early on it was recognized that delayed fluorescence (DF) originates from the annihilation of two mobile triplet excitons. The decay time of the DF has been taken as a measure of the triplet exciton lifetime. Avakian and Merrifield went one step further and measured the diffusion length (L_d) of triplets employing the method of spatially periodic excitation to the ab-plane of a molecular crystal [172,173]. In this method, parts of the crystal are masked so that triplet excitons, generated by intersystem crossing from the singlet state generated in the unmasked, irradiated part of the crystal, can diffuse into the shadow zones underneath the mask. The idea was that delayed fluorescence, being a bimolecular rate process, depends on the square of the concentration. As a result of triplet diffusion into the shadow zones underneath the masks, the average triplet concentration decreases, and so does the DF intensity. The temporal decay of DF from the unmasked parts was recorded as a function of the spacing between the irradiated zones, and from this, L_d has been determined. From the exciton lifetime τ_T , L_d for triplet diffusion within the ab-plane of the anthracene crystal has been determined. The experimental values are $L_d \cong 20 \mu\text{m}$ and $\tau_T \cong 20 \text{ ms}$. Based upon $L_d = \sqrt{D\tau_T}$ this yields $D_T = 2 \times 10^{-4} \text{ cm}^2 \text{ s}^{-1}$. Since the electronic coupling is much stronger within the ab crystal plane where the molecules are arranged cofacially than between ab-planes, triplet diffusion should be highly anisotropic. This has been confirmed by experiments monitoring the annihilation of triplet excitons injected from a dye layer deposited on top of the ab-plane of an anthracene crystal. It turned out that the coefficient for triplet diffusion perpendicular to the ab-plane is $5 \times 10^{-7} \text{ cm}^2 \text{ s}^{-1}$ [174], i.e. more than two orders of magnitude less than in-plane motion. This confirms that exchange interaction and, concomitantly, triplet transfer is highly sensitive to wavefunction overlap among donating and accepting moieties.

It is worth noting that the lifetime of triplet excitons in molecular crystals like anthracene and naphthalene is less than the lifetime of a molecule excited to the triplet state immobilized in an inert rigid matrix. For the latter, values are 0.1 s (anthracene) and 2.6 s (naphthalene). In the crystal, τ_T is highly sensitive to purity. In the case of anthracene, the maximum value reported is 25 ms [175]. The effect of purity on the triplet lifetime is easily explained in terms of triplet exciton quenching. For incoherent two-dimensional motion within the ab-plane, $D_T = (1/4)a^2\nu_T$ where a is the lattice parameter and ν_T the exciton jump rate. For $a = 0.6 \text{ nm}$ and $D_T = 2 \times 10^{-4} \text{ cm}^2 \text{ s}^{-1}$, $\nu_T = 2 \times 10^{10} \text{ s}^{-1}$ is estimated, i.e. the exciton jump time is on the order of 50 ps. This implies that during a lifetime 20 ms a triplet exciton can visit 5×10^8 molecules provided that there is no trapping or quenching. Conversely, this means that a 20 ms lifetime can only be obtained if the relative concentration of quenching sites is less than 2×10^{-9} .

Information on the temperature dependence of triplet exciton motion is sparse since measurements require a high-quality crystal devoid of quenching sites. By zero-order reasoning there should be no temperature dependence of the diffusion coefficient because the electronic intermolecular coupling is virtually temperature-independent. However, exciting a molecule to the triplet state implies some modification of intramolecular bond lengths to occur. Intramolecular transfer of a triplet state should, therefore, be accompanied by concomitant transfer of the molecular distortion, i.e. the motion should have polaronic character. This would imply thermally activated diffusion. Although the experimentally measured diffusion coefficient increases by a factor of 5

upon raising the temperature from 130 K to 450 K, that increase is weaker than anticipated on the basis of classic Marcus theory. Munn and Siebrand conjectured that this is due to an exciton-phonon interaction that is quadratic rather than linear in the phonon coordinates [176].

5.1.3. Diffusion in amorphous systems

5.1.3.1. The influence of disorder. A distinguishing feature of disorder in organic solids is the inhomogeneously broadened absorption profile. When going from a molecular crystal to a random structure, the narrow triplet exciton band of the crystal, whose bandwidth is less than 1 meV, splits into a distribution of localized states. The reason is that the excited state dipole of the chromophore interacts with both induced dipole moments and randomly oriented permanent dipoles in the surrounding molecules. Since that energy depends on the large number of variables, each varying randomly, the distribution of states (DOS) is of Gaussian shape, $g(\varepsilon) = ((1/\sqrt{2\pi\sigma}) \exp(-(\varepsilon^2/2\sigma^2)))$. In the case of conjugated polymers, there is a superimposed distribution of the energies of the conjugation length, that is, by itself, a distributed quantity. For excitonic transitions, the Gaussian width σ is on the order of 70 meV for the S_1 state in PF2/6 films [177] and 40 for the T_1 state [79,171]. In contrast, for charges, the width of the Gaussian DOS is about 100 meV.

Once a molecule in a neat organic glass or a conjugated polymer is excited randomly within the DOS, the excitation executes an incoherent random walk. In its course, it tends to relax towards the tail states of the DOS. Consequently, the number of acceptor chromophores that it can jump to decreases with time. Finally, if the time necessary for the next jump exceeds the intrinsic decay time, the excitation will decay radiatively or non-radiatively to the ground state. Therefore, there is a fundamental difference between excitation transport in a random organic solid as compared to a crystal insofar, that in the former (i) the diffusion “constant” is no longer a constant in the strict sense but it is time dependent, (ii) there is “spectral relaxation” during hopping of the excitation, and (iii) under site selective excitation, exciton motion depends on the initial start energy implying a freezing effect if excitation occurs below a certain demarcation energy at the tail of the DOS. There is another freezing effect occurring at low temperatures. While hopping an excitation may find an acceptor site at lower energy if it executes a temperature-activated detour. At low temperatures this effect is frozen out and subsequent relaxation is slowed down, i.e. the relaxation becomes frustrated. However, this effect is only observable if the hopping motion is confined to nearest neighbor sites coupled by exchange interaction. Therefore, it is restricted to charge carrier and triplet motion rather than to long-range singlet transport [178–180].

A special case of frustration has been observed for triplet excitations in Pt-acetylide polymers [84]. The triplet excitations are localized on a chromophore consisting approximately of a single repeat unit. The energies depend on ground state conformers that differ in the torsional orientation of the 1,2 phenylene units with the planar structure being stabilized by 3 kcal/mol (0.13 eV) relative to the twisted structure. This energy difference is enough to prevent motion of triplet excitations below 150 K. This localization effect is documented by the observation of dual phosphorescence emission from both the planar and twisted oligomers.

A disordered material on which the transport of triplet excitation was studied early is a benzophenone glass that can be easily prepared by quenching the melt [100]. Owing to efficient intersystem crossing from the first excited singlet state, practically all excitations are converted to T_1 states that decay radiatively featuring bright phosphorescence within an intrinsic lifetime of

5.6 ms. The phosphorescence spectrum reveals a bathochromic shift as a function of delay time after excitation. This is a signature of spectral relaxation. At low temperatures spectral relaxation is slower because of frustrated relaxation of the excitations. The experimental results can be rationalized in terms of hopping theory, the only input parameter being the Gaussian width of the DOS assuming that (i) hopping rates are described by Miller-Abrahams hopping theory that rests on the notion of single phonon events being dominant and (ii) the Gaussian width of the DOS is 33 meV (260 cm^{-1}). It suggests that in this system the temperature dependence of triplet transport is mostly dominated by disorder and the polaronic character of triplet transport is less important here.

Another, more recent example of triplet motion in a disordered material is the work of Rothe and Monkman on π -conjugated polyfluorene (PF2/6) [181]. They excited a PF2/6 film by 150 ps pulses from a frequency doubled Nd laser at 355 nm (3.5 eV) and detected both the phosphorescence as well as the delayed fluorescence. The time evolution of the phosphorescence spectra testifies on the occurrence of spectral diffusion. Data analysis is consistent with Movaghar et al.'s concept of frustrated triplet motion within a Gaussian DOS with variance 41 meV. It is worth noting that the actual $T_1 \rightarrow S_0$ 0–0 phosphorescence features is narrower than the width of the DOS inferred from the analysis of the spectral diffusion data. This is a manifestation of the frustration in the transfer dynamics that precludes the establishment of quasi-equilibrium.

The above results demonstrate that in non-crystalline systems disorder has a profound effect on triplet motion. Exciting a chromophore to the triplet state is, however, also associated with a change of its configurational structure. Transfer of an excitation from an excited to an unexcited chromophore must, therefore, be accompanied by a simultaneous change of the molecular configurations quantified in terms of electron phonon coupling. Therefore excitation transport should have both a polaronic character as well as a disorder controlled component. The difference between purely polaronic transfer and purely disorder controlled transfer is exemplified for the case of charge transport in Fig. 18. The central question in describing triplet transport concerns the relative contribution of both effects.

The strong effect *disorder* has on the diffusion of triplet states in disordered solids has been illustrated in the two examples mentioned above, yet examples where the *polaronic* contribution is dominant are rare. For crystalline systems it appears that in anthracene the polaronic character is, indeed, important at moderate temperatures although classic Marcus theory fails to explain the results [176]. An amorphous model system with a dominant polaronic character of the triplet diffusion is given by

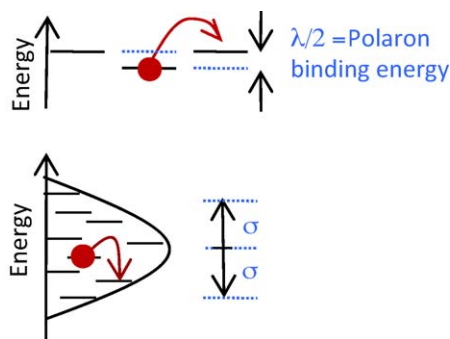


Fig. 18. Schematic of polaronic and disorder controlled charge transport. (a) The polaron binding energy $\lambda/2$ reduces the energy of an excited state. For transport, this energy difference to the unoccupied state needs to be supplied. (b) Energetic disorder causes a Gaussian distribution of site energies. The energy difference to neighbouring sites needs to be supplied.

platinum polyynes [168]. In these conjugated organometallic polymers, strong spin-orbit coupling guarantees efficient phosphorescence and the narrow linewidth of the $T_1 \rightarrow S_0$ 0–0 transition testifies on an unusually low degree of energetic disorder. In order to probe the diffusion of triplet excitations the time integrated phosphorescence spectra and the triplet lifetimes were measured in films of polymers and monomers between 10 K and 295 K. It turns out that both phosphorescence intensity and triplet lifetime decrease as the temperature increases because of temperature dependent triplet diffusion to quenching sites. Arrhenius plots bear out an activated behavior down to 80 K (polymer) and 250 K (monomer) with activation energies of 60 meV (polymer) and about 100 meV (monomer). Simply activated behavior in conjunction with very weak spectral diffusion and narrow phosphorescence linewidths indicates that in this case the temperature dependence of triplet motion is not due to disorder but to coupling of the triplet excitation to molecular distortion, i.e. to a polaron–exciton. The coupling can be quantified via a Franck–Condon analysis of the vibronic progression of the $T_1 \rightarrow S_0$ spectrum. The relaxation energy associated with a vibrational normal mode j , ω_j , is given by the energy of the mode times its Huang–Rhys parameter S_j . The total relaxation energy E_{rel} of an optical transition is obtained by summing up the individual contributions $E_{rel} = \sum_j \hbar \omega_j S_j$. E_{rel} values for polymer and monomer are 100 meV and 180 meV, respectively. This translates into a reorganization energy $\lambda = 2E_{rel}$ in terms of Marcus theory and an activation energy for triplet motion of $E_a = \lambda/2$, i.e. 50 meV (polymer) and 90 meV (monomer). The consistency with the measured activation energies confirms the polaronic character of triplet motion. Below a certain transition temperature tunneling prevails. Since the measured activation energies exceed considerably the expected zero field splittings (ZFS) in the Pt-polymer and monomer, thermally induced transitions among the triplet sublevels cannot play a significant role to triplet transport. A related work confirming the efficient intra-chain triplet transport in Pt-polymers was reported by Schanze et al. [182].

It is obvious that depending on the degree of disorder there should be a transition from polaronic to disorder controlled triplet transport. Recently a theory has been developed that considers the interplay between polaronic distortion of the excited state and disorder treated in terms of effective medium theory employing either Marcus-type or Miller-Abrahams type jump rates [183]. The former are appropriate for polaronic motion, which is a multi-phonon process, while the latter are applicable for disorder controlled transport in which single phonon jumps prevail. The essential parameters in the theory are the electronic coupling J , the reorganization energy λ that determines the activation energy E_a for polaron motion, and the variance σ of a Gaussian density of states distribution that controls inherent hopping motion. For weak electronic coupling, i.e. J a few meV only, triplet motion is non-adiabatic. In this case the excitation jumps from the lower to the upper energetic surface at the origin site and then relaxes to the energy minimum of the acceptor site. The essence of the results is shown in Fig. 19. There are two temperature regimes. Above a certain demarcation temperature transport is thermally activated. For a completely ordered system ($\sigma = 0$) the activation energy is entirely determined by λ . Upon turning on disorder, the T -dependence becomes steeper and finally approaches a $\ln D(T) \propto T^{-2}$ law characteristic of hopping motion within a Gaussian DOS. At low temperatures and $\sigma = 0$, transport occurs by temperature-independent tunneling. As σ increases, the diffusivity becomes temperature dependent. For $\sigma/E_a > 0.3$, i.e. $\sigma/\lambda > 0.075$, both regimes can no longer be distinguished. For many conjugated polymers, σ and E_{rel} are in the order of 50 meV and 200–300 meV, respectively, i.e. the disorder term controls the diffusion characteristics. The experimental results are in good

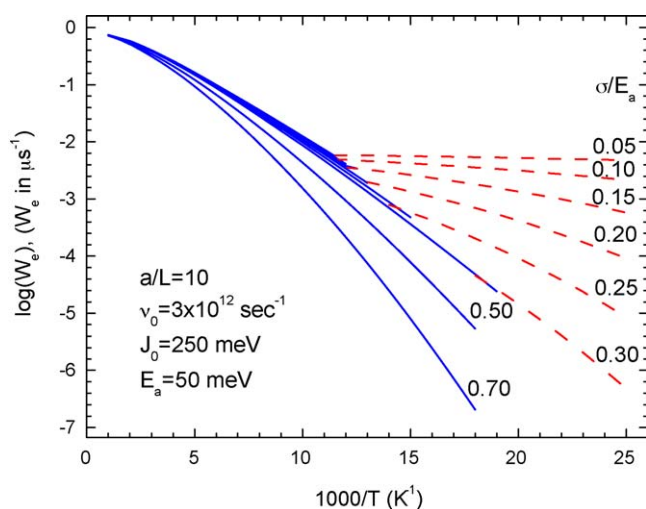


Fig. 19. Temperature dependence of the triplet transfer rate parametric in the ratio between disorder parameter σ and activation energy E_a . Reprinted with permission from [183], copyright American Physical Society.

agreements with theory (Fig. 20). When analyzing the low temperature branch of $D(T)$ one should however keep in mind that this theory is based upon the establishment of quasi-equilibrium and, thus, ignores the fact that at very low temperature relaxation of excitations becomes frustrated. Therefore it overestimates the T -dependence of the diffusivity at low T .

5.1.3.2. The triplet diffusion length. The distance over which a triplet state may migrate is a central issue for the design of LEDs and solar cells that make use of the T_1 state. Few values have been measured directly, such as 140 nm for CBP [163] and 18 nm for PtOEP [184]. The triplet diffusion length increases with the lifetime of the triplet state and the strength of the electronic coupling between adjacent chromophores, and this may account for the higher value in the organic CBP compared to the organometallic PtOEP.

The triplet diffusion length in CBP was measured by the Forrest group in the context of their work on OLEDs doped with triplet emitters aimed at harvesting triplets generated via electron–hole recombination. They deposited CBP films with different thicknesses on top of a CBP film doped with a phosphorescent triplet acceptor. After excitation with a laser pulse they measured the

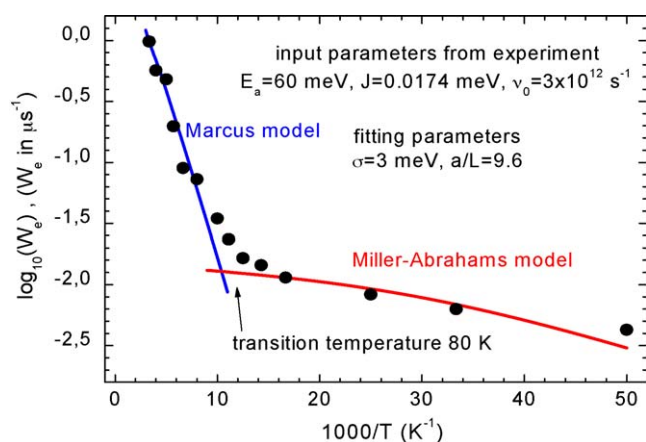


Fig. 20. Comparison between the experimental and theoretical values for the triplet transfer rate in a Pt-polymer. Solid blue line: high temperature regime with transfer by multiphonon hopping. Dashed red line: low temperature regime with transfer by single-phonon assisted tunneling. Reprinted with permission from [183], copyright American Physical Society.

arrival time of the triplet excitons at the acceptor layer as function of the transport layer thickness and of the light intensity. From this, they calculated the diffusion coefficient D_T and the diffusion length for triplet excitons by solving the diffusion equation. At higher light intensities triplet–triplet annihilation reduced the triplet lifetime and allowed to calculate the bimolecular rate constant γ_{TT} for TTA. The experimental values are $D_T = (1.4 \pm 0.3) \times 10^{-8} \text{ cm}^2 \text{ s}^{-1}$, a triplet lifetime of $(14 \pm 8) \text{ ms}$ (measured at low light intensities), a triplet diffusion length of 140 nm and $\gamma_{TT} = (1.6 \pm 0.4) \times 10^{-14} \text{ cm}^3 \text{ s}^{-1}$. If we assume an isotropic diffusion, where D_T is related to the intermolecular separation a and the triplet hopping rate ν_T via $D_T = (1/6)a^2\nu_T$, we obtain $\nu_T = 8 \times 10^6 \text{ s}^{-1}$ for the triplet hopping rate at $a = 1 \text{ nm}$. This is in good agreement with the rate for donor–acceptor energy transfer that has been measured to be $(8 \pm 4) \times 10^6 \text{ s}^{-1}$. Based upon the Smoluchowski equation of the encounter of two mobile excitations with a reaction distance of $\langle R \rangle$, $\gamma_{TT} = 8\pi\langle R \rangle D_T$, we calculate $\langle R \rangle = 0.5 \text{ nm}$. This is comparable with the intramolecular separation and indicates that in this system TTA is a diffusion-controlled reaction.

In order to determine the length of triplet diffusion in PtOEP, the Forrest group extended the technique for inferring the diffusion length of excitons from luminescence quenching at the surface in a thin sample in the absence of bimolecular exciton annihilation. It is based upon the pioneering work of Mulder published in 1967 [185] who measured the fluorescence quenching efficiency at the surface of an anthracene crystal carrying an exciton quenching layer as a function of the penetration length of the incident light. The shorter the penetration length, the more singlet excitons are quenched at a surface at which excitons decay non-radiatively. By extending the theory such as to include the angle dependence of the incident light and time dependence, Lunt and co-workers measured the diffusion length for excitons in several vapor-deposited polycrystalline organic layers. Since their lifetime was recorded simultaneously, the diffusion coefficients were determined concomitantly. This technique can be adapted to triplet diffusion provided that the incident photons generate exclusively triplets via efficient ISC. In this way Lunt and co-workers measured the diffusion length in a 30 nm thick layer of PtOEP. It turns out that the diffusion length for the monomer-type of triplet excitons is $18.0 \pm 0.6 \text{ nm}$ implying a diffusion coefficient of $4.0 \times 10^{-6} \text{ cm}^2 \text{ s}^{-1}$ and a triplet lifetime of 800 ns. The diffusion length is shorter and, correspondingly the diffusion coefficient is lower for dimer-type triplet state because a dimer site acts as a triplet trap. The diffusion length derived by Lunt is in agreement with the rough estimate of a 30 nm diffusion length in PtOEP that Yang and co-workers derive on the basis of the thickness dependence of double-layer solar cells made from PtOEP and C60 [17].

Piok and co-workers endeavored to determine the triplet diffusion length indirectly from the rate constant of the bimolecular triplet–triplet annihilation γ_{TT} for MeLPPP [99]. This requires a number of assumptions that are uncertain, and the derived value of 76 nm may be an overestimation.

5.2. Energy transfer processes in host–guest systems

Triplet state energy transfer not only controls the process of triplet diffusion within an organic semiconductor material. It is also an important route to harvest the triplet state energy in host–guest systems. Under electrical excitation, for example in a light-emitting diode structure, a large number of triplet states are formed in addition to the emissive singlet states. Triplet states can be used towards light emission when they are gathered on phosphorescent sites such as organometallic dyes or metal-containing polymers. Usually, one does not prepare a film consisting of only organometallic phosphorescent semiconductor since the close proximity of triplet states favors concentration

quenching effects such as triplet–triplet annihilation. Instead, phosphorescent guests are used at low concentration, at most a few percent, in a polymer or molecular host material. There are then different ways how the triplet state may finally be created on the phosphorescent guest.

- (i) Electron and hole are transported through the host material and recombine on the guest. This process is often assisted by charge trapping on the guest when the guest HOMO lies above the host HOMO (or converse for the LUMOs).
- (ii) Förster transfer of singlet excitons from the host to the guest followed by intersystem crossing on the guest is frequent.
- (iii) Dexter transfer of triplet states from host to guest is observed less often since Förster transfer tends to prevail.

The simultaneous use of singlet and triplet excitons towards light emission is desirable since a 100% usage of the created excited states will yield most efficient OLEDs. Systems where both Förster and Dexter transfer have been observed to take place concurrently under electrical excitation (possibly in addition to electron–hole recombination on the host) include the polymer PNP doped with the platinum porphyrin PtEOP [161] or the molecule Alq3 doped with PtEOP [6]. Simultaneous Förster and Dexter transfer have also been reported earlier for a DNA donor and porphyrin acceptor [186,187]. In the experiment by Cleave and co-workers, the evidence for the simultaneous Förster and Dexter type transfer was taken from time-resolved phosphorescence spectrum of the guest. The signal instantly observed after excitation of the host was attributed to Förster type singlet transfer. It decays with the 50 μ s lifetime of the PtOEP guest and is superimposed by a component rising on a timescale of 10 μ s that is attributed to the slower population of the guest triplet by Dexter transfer from the host triplet state. In the work by Baldo and co-workers, the participation of both singlet and triplet states in the energy transfer process is concluded from efficiency calculations. The collection of both singlet and triplet excitons on the phosphor has resulted in OLEDs with close to 100% internal efficiencies [62]. Due to non-optimized outcoupling of light from the device, this gives external quantum efficiencies (EQE) around 20%.

A different way to use both Förster and Dexter transfer in a OLED device has been demonstrated by Forrest, Thompson and co-workers with the intention to fabricate efficient white light-emitting OLEDs [9]. While Cleave et al. and Baldo et al. employed both transfer mechanisms to harvest all excited states onto one phosphorescent emitter, in 2006 Forrest moves the host triplet exciton onto red and green emitting phosphorescent dyes (PQIr and Ir(ppy)₃, respectively) by Dexter transfer while he uses the Förster mechanism to transfer the host singlet onto a blue fluorescent guest (BCzVBi) (Fig. 21). The host used for all three emitter is CBP. The use of a fluorescent emitter for the blue spectral range avoids parasitic energy losses and is furthermore of advantage to device lifetime and stability. Such selective energy transfer requires a careful device architecture. The basic idea of Forrest's design is that triplets will diffuse a long distance through the host CBP. To avoid them transferring onto the blue emitting fluorophor, one needs to keep the fluorophor concentration low (5 wt.% doping level), so that the chance of them meeting one is negligible. In addition, he spatially separates the materials into a thin 5 nm layer of host with blue emitting fluorophor and a larger 20 nm layer of host with green and red emitting phosphor. Due to the long triplet diffusion length in the CBP host, the triplets will still reach the lower energy triplet states of the green and red emitting phosphors where they are then immobilized. Undesired Förster

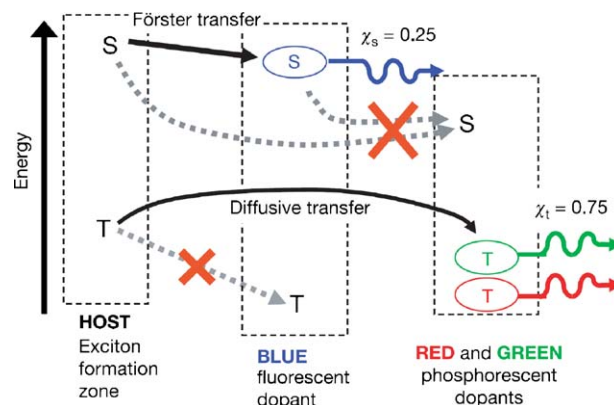


Fig. 21. Energy transfer scheme used for white light emission that uses blue fluorescence together with green and red phosphorescence. Reprinted by permission from Macmillan Publishers, LTD: from [9] copyright 2006.

transfer from the blue emitting fluorophor to the red and green emitting phosphor is avoided by inserting an undoped host spacer layer with a thickness larger than the Förster radius (3 nm) between them. Between the emissive layers and the anode (cathode), a further hole (electron) transport layer is used. This complex architecture yields white light emission with efficiency values that exceed the common incandescent lamp. In forward direction at 500 cd m^{-2} , the external quantum efficiency is 11%, and the power conversion efficiency is $\eta = 22 \text{ lm/W}$. The total maximum efficiencies are EQE = 19% and $\eta = 38 \text{ lm/W}$.

The fabrication of such an elaborate device architecture consisting of many layers is usually realized by successive thermal evaporation of the molecules involved. One alternative to the time-consuming and expensive evaporation process is the development of organic vapor-jet deposition techniques, where a jet stream of hot nitrogen gas takes up the organic semiconductor and allows for continuous deposition through a nozzle [188]. A different approach is the use of host–guest systems that can be processed from solution thus permitting simple deposition techniques such as spin-coating, doctor-blading, ink-jet printing or reel-to-reel coating. When depositing host and guest from the same solution, an undesired degree of phase separation can be an issue. This is avoided when host and guest are tethered together. Different designs of tethered host–guest systems have been reported. For example, a conjugated polymer backbone such as polyfluorene [170] or a fluorene-carbazole copolymer [189] may be used as host material with phosphorescent dyes such as Ir-complexes attached via side-chains as guest. It is also possible to add a charge transport moiety, for example the hole-transporter carbazole, as a second side-chain-attached group in addition to the phosphorescent dye [190]. A chemically very versatile approach is to use a non-conjugated polymer with good film-forming properties and such as polystyrene as a host to which then hole-transporter, electron-transporter and emitter are tethered through the side-chains [191,192]. With this method, Suzuki and co-workers obtained EQEs of about 12% and 39 lm/W at 0.02 mA/cm^2 . The multiple layer approach in device architecture and the all-in-one side-chain polymer represent two extremes of optimizing host–guest systems. This is discussed in more detail in Section 6.1.3. The use of multiple layers by thermal evaporation results in highest efficiencies while requiring sophisticated device structures. In contrast, the all-in-one side-chain polymer enables most simple device fabrication with still respectable and acceptable efficiencies.

When designing any type of host–guest systems one needs to make sure not only that the triplet state gets populated, but rather that it also stays populated until the emission (or non-radiative decay) takes place. In contrast to the energy transfer from host to

guest, which can occur via the singlet or the triplet channel, the reverse transfer of energy from the triplet state in the phosphor to the non-emissive triplet state in the organic host can only take place by Dexter type energy transfer. This requires wavefunction overlap of the donor and acceptor orbitals and is therefore sensitive to the specific conformational arrangements between host and guest. In 2003, Sudhakar et al. drew attention to this when they investigated the energy transfer from a series of Ir-complexes with triplet state energies ranging from 2.0 eV to 2.6 eV onto a fluorene trimer with a triplet energy around 2.2 eV [193]. They measured the phosphorescence lifetime of the complexes in solution as a function of the concentration of fluorene trimer. From the resulting Stern–Volmer plot, Stern–Volmer quenching rates in the range from $10^6 \text{ M}^{-1} \text{ s}^{-1}$ to $10^9 \text{ M}^{-1} \text{ s}^{-1}$ were determined, where the low rates characterize endothermic transfer while the high rates are associated with exothermic transfer. At room temperature, where most LEDs are operated, a high rate of endothermic transfer from a triplet emitter to a non-emissive host is a serious limitation to device efficiency. Sudhakar noticed that phosphorescence efficiencies in films made from fluorene trimer and the Ir-complexes were much higher than predicted on the basis of the Stern–Volmer quenching rates. He attributed this difference in the quenching behaviors between solution and film mostly to the rigid nature of the film. First, in solution, a fluorene trimer in a configuration that gives poor Dexter transfer can reorient to a configuration appropriate for efficient energy transfer. This is not possible in the film, where wavefunction overlap between adjacent molecules is either present or not. Second, in solution, the fluorene trimer and the phosphor may separate physically after the energy transfer, thus preventing a back transfer. In film, this is also precluded. Diffusion of the triplet away from the donor–acceptor interface competes with back transfer. Since both, wavefunction overlap and energy transfer away from the interface are reduced in the film compared to a solution, the guest–host triplet transfer rate is also diminished.

Wavefunction overlap enhancing endothermic host–guest energy transfer needs to be taken into account in particular for the design of host–guest systems that are chemically connected. Evans and co-workers compared the efficiencies of OLEDs made with a polyfluorene host and the organometallic guest $\text{Ir}(\text{btp})_2(\text{a-cac})$ as a function of the connection type. When the Ir-complex was incorporated into the polyfluorene chain through a covalent connection of the conjugated ligand, the electroluminescence efficiency was only half that of a device where the Ir-complex was attached through an octyl tether to the polymer. An analysis of the phosphorescence lifetimes showed that the covalent linkage and concomitant donor–acceptor orbital overlap leads to an increased endothermic energy transfer from the red emitting phosphor to the polyfluorene triplet. Further studies demonstrated that a long tether such as an octyl chain reduced endothermic guest–host transfer more than a short tether [170,171]. The incorporation of a $-(\text{CH}_2)_8-$ chain between the polymer host and phosphorescent guest is thus an important design principle for achieving higher efficiencies in those electrophosphorescent organic light-emitting diodes for which the triplet energy levels of the host and guest are similar. Finally, undesired triplet energy transfer may not only occur between a guest and its host, but also between phosphors with different triplet energies. This is a challenge for the design of white light-emitting diodes based on multiple emitters. Since triplet transfer requires spatial overlap, it can be effectively prevented by steric shielding [192,194].

One way to avoid triplet energy transfer by steric shielding consists in the use of appropriately designed dendrimers in which the core serves as a shielded phosphorescent emitter while the dendrons control charge injection and transport and the peripheral pendent groups ensure that the active layer can simply be cast

from solution. Surveys of materials with appropriate spectral properties and photoluminescence yields are listed in refs [195,196]. Well studied materials are first and second-generation $\text{Ir}(\text{ppy})_3$ -cored dendrimers with phenylene-based dendrons and 2-ethylhexyloxy surface groups whose phosphorescence yield is 80% [75]. Photoluminescence experiments indicated, however, that phosphorescence quenching does occur at higher light intensities. The authors attribute this to both surprisingly efficient triplet–triplet annihilation and Förster-type energy transfer to non-radiative defects.

At times triplet quenching is a desirable process. A prominent example is the elimination of detrimental $T_n \leftarrow T_1$ absorption that overlaps with the stimulated emission in dye lasers. To circumvent this problem 1,3,5,7 cyclotetraene (COT) can be used as triplet scavenger. COT is a flexible molecule with S_1 and T_1 states at 4.39 eV and 2.56 eV, respectively. Upon planarization the T_1 level is lowered to 0.8 eV. The large exchange energy of COT renders it an ideal molecule for triplet scavenging. When a COT molecule in fluid solution occasionally adopts a planar conformation triplet quenching can occur even if the energy of the triplet level of the donor is below 2.56 eV. Recently Scholes et al. found that this process is feasible even in a solid film as evidenced by the observation of quenching of both phosphorescence and delayed fluorescence in a PF2/6 film in which the triplet energy is 2.1 eV [197].

5.3. Formation of triplet excimers

Formation and stabilization of triplet excimers has been a heavily debated issue in the past. It had been argued that a low-energy feature in the emission of solutions of aromatic hydrocarbons and cyclophanes, such as di- α -naphthylalkanes, is due to an intermolecular triplet excimer of naphthalene [198,199]. In such systems the naphthalene moieties are forced into a sandwich structure by the alkane linkages as evidenced by the observation of a singlet-type excimer emission with a lifetime in excess of 100 ns. An additional spectrally broad emission has been detected and assigned to a triplet excimer. Later on, Nickel and Prieto have shown, though, that this emission is due to an impurity [200]. In retrospect the absence of genuine emission from triplet excimers of the acene-type of chromophores is easily understood in terms of the expected energy levels of excited singlet and triplet states of monomers and dimers of such chromophores. In monomeric oligomers with $\pi\pi^*$ transitions such as acenes, the exchange energy, i.e. the S_1 – T_1 energy difference, is > 1.0 eV while the stabilization energy of the first singlet state in a pair of parallel chromophores, i.e. the difference between the S_1 state of the monomer and the singlet state of the excimer, is typically around 0.5–0.7 eV. Meanwhile it has been recognized that the exchange energy in an electron–hole pair, localized in a pair of chromophores about 0.4 nm apart, is of the order of 10 meV only [67,68]. Even if the resonance contribution to the wavefunction in an excimer as compared to that of an anion/cation pair may increase the exchange interaction, that order of magnitude will be preserved. Therefore the lowest excited state of the system will be that of the T_1 state of the monomer as shown in Fig. 22. This implies that a hypothetical triplet excimer state would be rapidly relax to the T_1 state of the monomer. Unfortunately, the same argument would be valid for conjugated polymers with $\pi\pi^*$ transitions because the exchange energy is about 0.7 eV. This would play a detrimental role in OLEDs because triplet harvesting from excimers would not be feasible [201].

In order to observe emission from triplet excimers, its energy has to be lower than the T_1 level of the isolated oligomer/polymer. This situation is realized when the excimer binding energy exceeds the exchange energy, for instance in phosphorescent complexes having metal-to-ligand charge-transfer transitions (MLCT, see Section 3.3) whose S_1 – T_1 exchange energy is about 0.2 eV.

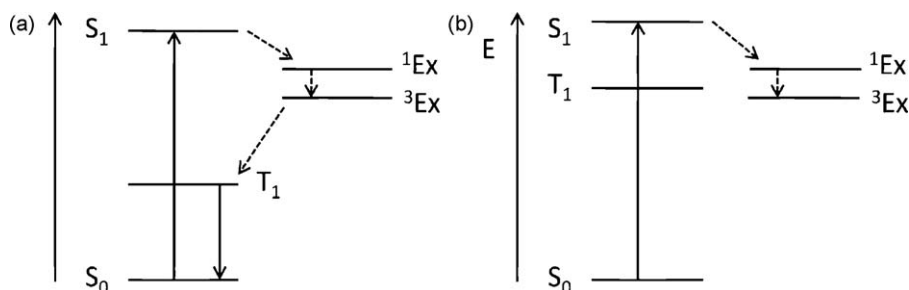


Fig. 22. Energy level diagram illustrating the relative position of monomeric and excimeric singlet and triplet states (a) for the case where the triplet on the monomer is lowest and (b) for the case where the excimer triplet is lowest.

Examples are platinum or iridium complexes with strong spin-orbit coupling. They are commonly used as phosphorescent emitters in OLEDs. In an endeavor to harvest the triplet excitations generated in an OLED and to improve the emission spectrum in white OLEDs by making advantage of triplet excimers the Forrest group conducted an in-depth study of triplet excimers. D'Andrade and Forrest [202] investigated (i) the photoluminescence (PL) of a neat F_{Pt1}-film and a film of mCP doped with F_{Pt1} and (ii) electroluminescence (EL) from an organic heterostructure in which F_{Pt1} is excited via the recombination of electrons and holes injected from the respective charge transport layers. F_{Pt1} has a square planar structure with propensity for sandwich pair formation. The PL experiments reveal monomeric phosphorescence with a T_1 - S_0 0-0 transition at 2.63 eV and an intrinsic lifetime of 8.7 μ s. Furthermore, the spectrum shows a broad feature with a maximum at 2.07 eV that is assigned to a triplet excimer. Upon cooling the sample from 295 K to 5 K the monomer emission increases at the expense of the excimer emission featuring a transport related activation energy of 35 ± 4 meV. The intrinsic lifetime of the triplet excimer is 1.6 ± 0.3 μ s. In EL, only a broad emission band centered at 1.83 eV is observed with a lifetime of 800 ± 80 ns and an emission efficiency of 14%.

The authors argue that the 2.07 eV feature is due to a triplet excimer ${}^3E_0^*$ while the 1.83 eV feature originates from an excited dimer ${}^3D^*$ with increased pair stabilization relative to that of the ${}^3E_0^*$ excimer (Fig. 23). In contrast we consider that the more stabilized state is likely to have a stronger excimer-like character.

The different intensity between ${}^3E_0^*$ and ${}^3D^*$ states in PL and EL is a signature of the different likelihood for finding a respective precursor state. An initially photoexcited triplet state in a manifold of disordered F_{Pt1} monomers can make only very few jumps during its lifetime. Therefore it cannot explore the entire distribution of states that can act as precursors for excimer or dimer emission. In contrast, an injected electron or hole can execute an efficient random walk and thus easily find a sandwich pair of F_{Pt1} molecules that can act as first shallow traps for either holes or electrons and second as a precursor for excimer or dimer formation. The site finally forms an excimer or dimer when a countercharge enters the coulombic capture radius. This is another illustration of the fact that a given defect acting as a trap in a transport system will have a greater effect on the charge transport associated with electroluminescence as compared to photoluminescence [203]. Concerning the lifetime of triplet excimers, there is no reason to expect that their lifetime be longer than that of the monomer, as it is in the case of the singlet excimer, because its transition probability is restricted by spin-selection rules rather than by the vibronic coupling. In fact, the tenfold decrease of the lifetime of F_{Pt1} 1.83 eV triplet excimer relative to that of the monomer T_1 can be fully accounted for by the increase by the non-radiative decay channel at lower transition energies. By now, the exploitation to excimer phosphorescence for the fabrication of organic white light-emitting diodes is well on its way [204–206].

Triplet excimers have also been identified in Pt-polymers. While they were conjectured early on the basis of photoluminescence lifetime measurements [207], a clear assignment was provided by Slagle et al. through nanosecond transient absorption measurements carried out as a function of concentration [208]. The authors derived rate constants for the formation of the triplet excimer of $4.7 \times 10^6 \text{ M}^{-1} \text{ s}^{-1}$.

6. The decay of triplet states

6.1. Phosphorescence

6.1.1. Phosphorescence spectra

Phosphorescence, i.e. radiative decay of the triplet excited state to the singlet ground state, is notoriously difficult to detect unless the emitter contains heavy atoms that enhance spin-orbit coupling. The latter ensures first that any primarily generated singlet states convert to triplets, and, more importantly, that the spin-forbidden $T_1 \rightarrow S_0$ transition becomes partially allowed and so acquires intensity. In the early times of molecular crystal work intrinsic phosphorescence was hardly observed although the existence of triplet excitons was proven by via delayed fluorescence measurements [40,173]. The reasons were:

- (i) In many hydrocarbon systems rate constants for intersystem crossing are about 10^7 s^{-1} . For a singlet lifetime below 1 ns this implies the yield triplet is less than 1%. Higher triplet yields are

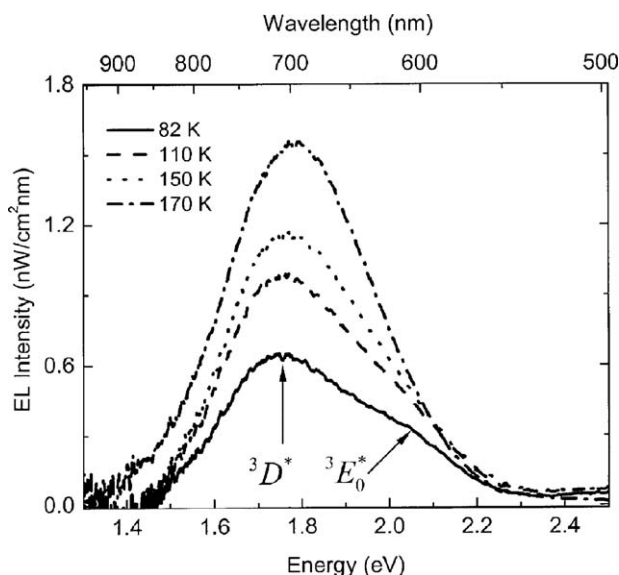


Fig. 23. The temperature dependence electroluminescence spectrum of F_{Pt1}. The peaks are assigned to the excimer and dimer triplet states, referred to as ${}^3E_0^*$ and ${}^3D^*$, respectively. Reproduced from [202].

however possible when the singlet lifetime is longer and when ISC is facilitated by an energetically close T_n state slightly above the S_1 state. An example for this is the anthracene molecule in solution (in contrast to an anthracene crystal, where S_1 is slightly below T_n).

- (ii) In a clean molecular crystal bimolecular annihilation of triplet-triplet states limits the build-up of a sufficient triplet population. This triplet-triplet annihilation is particularly important for crystals in contrast to amorphous films due to the high triplet diffusivity caused by the crystal structure.
- (iii) In the presence of impurities, triplet excitations are trapped and contribute to defect luminescence instead of intrinsic phosphorescence. As for (ii), this process is diffusion-controlled and therefore more prominent in the case of crystals.
- (iv) In time-resolved experiments, the notoriously weak phosphorescence signal is obscured by intense fluorescence.

In amorphous films, triplet diffusion is low, and so the decay routes listed as (ii) and (iii) are less effective. The technical challenge listed in (iv) can today be eliminated by using a gatable optical multichannel analyzer in the detection unit. Romanovskii et al. used the latter technique to detect phosphorescence from the conjugated polymer MeLPPP [5,209]. Later on, the principle of gated detection was applied to other organic conjugated polymers, such as such as oligomers of MeLPPP, a substituted poly(*p*-phenylene) (DDO-PPP), polyfluorene (PF2/6), polyindeno[1,2-b]fluorene (PIF), PhLPPP [45,181,210] organic poly(*p*-phenylene ethynylene)s [29], and oligothiophenes [46].

In conjugated polymers where the optical gap is shifted further to the red such as poly(*p*-phenylene vinylene)s or polythiophenes, phosphorescence is more difficult to observe. A lower S_1 state and the constant S_1 – T_1 gap in π -conjugated polymers imply a low-lying T_1 state. Since the intrinsic non-radiative decay from T_1 increases exponentially with decreasing triplet energy (see Section 6.1.2), it soon exceeds the radiative decay by orders of magnitude. The combination of a low intersystem crossing rate in organic semiconductors implying a low population of the triplet state, a low radiative rate and a high non-radiative decay rate results in an extremely low phosphorescence yield for polymers that normally fluoresce in the green or red spectral range. To overcome this problem Laquai et al. [211] doped a PhPPV film with a phosphorescent Pt-porphyrin (PtOEP) as a sensitizer with high ISC rate. Provided that the S_1 state of PtOEP is below that of PhPPV whereas the T_1 state of the sensitizer is above that of the PhPPV host, singlet excitons of the host will be transferred to the sensitizer and are converted to triplets that will subsequently return to the T_1 level of the host. The so increased population of the triplet state leads to a detectable number of photons that are emitted from the sample. Employing this technique phosphorescence of PhPPV has been observed and the T_1 level has been located at 1.63 eV (Fig. 24). Since the S_1 state is at 2.43 eV, the S_1 – T_1 gap is 0.8 eV. At 298 K phosphorescence decays non-exponentially with a $1/e$ decay time of about 40 μ s.

The spectral shape of fluorescence and phosphorescence differ slightly in vibrational intensity and linewidth, which reflects the differences in spin-dependent electronic structure. In general, the energetic spacing in the vibronic structure of phosphorescence spectra are identical to those of fluorescence spectra because the same molecular vibrations are involved, yet the intensity of the vibrational sidepeaks is different. A triplet excitation on a polymer chain is considered to be of a smaller extent than a singlet excitation since, for example, the bathochromic shift between polymer and short oligomers is smaller for phosphorescence spectra than for fluorescence spectra, and since the associated geometric distortion takes place over a smaller distance in the

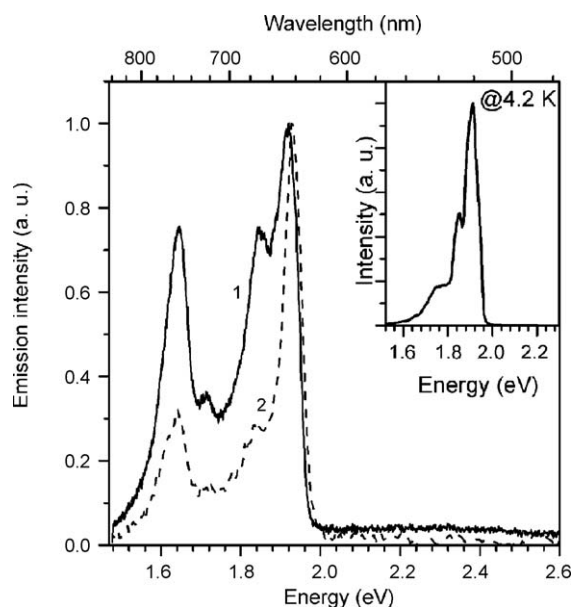


Fig. 24. The phosphorescence spectrum of the PPV-derivative PhPPV measured at 4 K (solid line, 1) and 80 K (dashed line, 2) using 2 wt% PtOEP as a sensitizer. The inset shows the 4 K emission from 1 wt% PtOEP in a MeLPPP matrix. For both spectra, excitation was at 2.32 eV. Reproduced from [211].

triplet state (see, for example, Ref. [78] for oligofluorenes, Ref. [35] for oligothiophenes or Ref. [33] for Pt-acetylide polymers). On this basis one expects a locally higher amplitude for the molecular distortion in the triplet state, and consequently a higher Huang Rhys factor. In other words, the intensity of the vibronic features should be enhanced in phosphorescence relative to fluorescence. While this may occasionally be observed, in many cases the opposite is found experimentally, as illustrated in Fig. 25. The

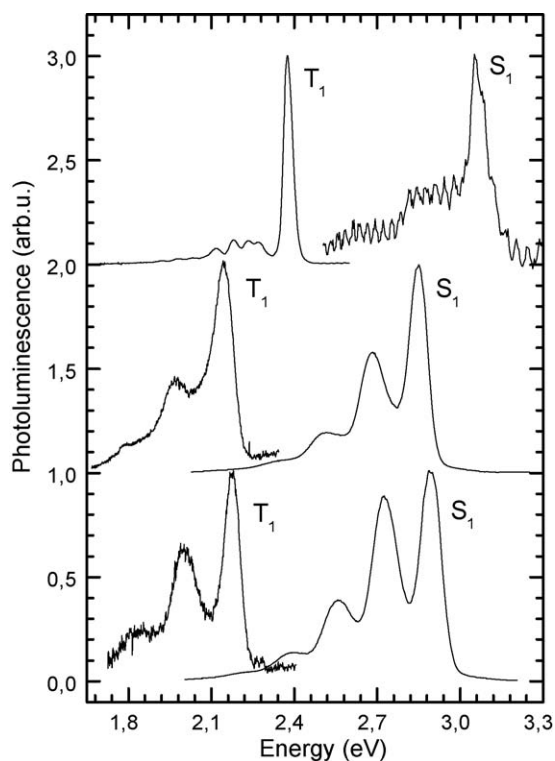


Fig. 25. The fluorescence spectra and phosphorescence spectra of a Pt-polymer with R = phenyl (top), PIF (middle) and PF2/6 (bottom) taken at 10 K with excitation at 3.5 eV. The spectra are normalized to unity and offset vertically for clarity.

reasons for this are not clear. All spectra shown in Fig. 25 can be modeled well with a Franck-Condon analysis, suggesting that each spectrum represents the true emission of a single state. The smaller extent of the triplet exciton also causes a smaller inhomogeneous line broadening of $T_1 \rightarrow S_0$ spectrum as compared to the $S_1 \rightarrow S_0$ spectrum (see Fig. 2 well above). As detailed in Section 2.2.1, there are two reasons for this. First, the smaller size of the triplet implies a smaller extent of the dipole moment in the excited state. As a result, the triplet is less susceptible to spatial fluctuations in the polarization of the environment. Second, based upon a particle in the box arguments the more confined triplet excitation is less effected to statistical variations of the effective conjugation length of the polymer.

Another, more practical difference in fluorescence and phosphorescence measurements are the high sensitivity of the triplet state to quenching by oxygen. Consequently, particular care needs to be taken to avoid oxygen, e.g. by freezing-out of solutions or film measurements taken in good vacuum or in thorough nitrogen-flow, when determining phosphorescence efficiencies and lifetimes. The high susceptibility of the triplet state to oxygen quenching can also be employed to identify the triplet nature of an emission. This has for example is used to distinguish the fluorescence and phosphorescence bands in benzophenone. In passing, we note that phosphorescence spectra of metal–ligand complexes can be rather broad and lack vibronic structure if significant metal-to-ligand charge-transfer (MLTC) occurs.

In π -bonded conjugated polymers the phosphorescence spectra are well separated from fluorescence and features a virtually identical vibronic structure. This is no longer true for σ -conjugated poly-silanes in which the phosphorescence band of $^3(\sigma, \sigma^*)$ character is structureless [212]. The superposition of an intra-chain $^1(\sigma, \pi^*)^{\text{CT}}$ charge-transfer band to the $^1(\sigma, \sigma^*)$ fluorescence demonstrates that the spectroscopy of σ -bonded poly-silanes is more complex than that of π -conjugated polymers.

6.1.2. Phosphorescence lifetime

The lifetime of any state is given by $\tau = (k_r + k_{nr})^{-1}$ where k_r and k_{nr} are the rate constants for radiative and non-radiative decay. In order to evaluate what controls the lifetime of a triplet state we therefore need to consider which parameters affect the associated radiative and non-radiative decay rates. For a pure triplet state, the radiative $T_1 \rightarrow S_0$ transition is forbidden by spin-selection rules, implying a radiative decay rate of zero. However, in any real molecule there is always some degree of spin–orbit coupling present that renders the $T_1 \rightarrow S_0$ transition partially allowed. For hydrocarbon systems, where spin–orbit interaction is mostly mediated by vibrations, it is weak, while the heavy metal in organometallic compounds results in strong spin–orbit coupling. As mentioned in Section 4.1.1, spin–orbit coupling may be treated as a perturbation that adds some singlet state wavefunctions to a nominal triplet state. As a result, the nominal $T_1 \rightarrow S_0$ transition acquires some oscillator strength from the singlet admixtures in the nominal triplet state [92]. The rate of radiative triplet state decay depends therefore first of all on the amount of spin–orbit coupling in the molecule. When this is very large and comparable, differences in wavefunction overlap may, in principle, become noticeable. For example, in organometallic complexes with the same T_1 energy and the same degree of spin–orbit coupling, $T_1 \rightarrow S_0$ transitions with a strong $\pi\pi^*$ character and concomitant high wavefunction overlap should have a higher radiative rate than those with a predominant MLCT character where wavefunction overlap is low. In practice, however, MLCT states have a larger spin–orbit coupling and consequently a larger singlet–triplet mixing due to the strong involvement of the metal centre, and this usually leads to higher decay rates for the MLCT states. Typical values for triplet state k_r range around 10^{-1} s^{-1} to 10^2 s^{-1} for

hydrocarbon molecules and polymers [27] and around 10^3 s^{-1} to 10^5 s^{-1} for organometallic compounds [59,66] (from the phosphorescence quantum yields and lifetimes given in [59], k_r can be estimated as outlined in [66]).

The intrinsic non-radiative decay, i.e. the decay in the absence of other processes such as energy transfer, quenching, excimer formation, *etcetera*, occurs via a process that chemists refer to as internal conversion and that physicists may regard as multiphonon emission. The energy of the excited state is dissipated through the simultaneous emission of quanta of the molecular vibrations. The photophysics of non-radiative transitions was studied intensively in the 1960s and 1970s of the past century [63–65,91,176,213]. Non-radiative transitions between two states consist first of a horizontal transition from the lowest vibrational level of the initial electronic state into higher energy vibrational levels of the final electronic state. This is followed by a vertical transition, i.e. an energetic relaxation that is the actual internal conversion or multiphonon emission process. The rate-limiting step is usually the horizontal transition, where the electronic energy of the initial state is converted to vibrational energy of the final state. It is governed by the overlap of vibrational wavefunctions, which is given by the Franck-Condon Factor, so that

$$k_{nr} = \left(\frac{2\pi}{\hbar}\right) \beta^2 F \rho \quad (13)$$

where β is the energy of interaction between the initial and final states (here the spin–orbit interaction), ρ is the number of states per unit energy, and F is the Franck-Condon factor of the appropriate energy [65]. On the basis of earlier works by Manneback and Siebrand calculated how the Franck-Condon factor changes as a function of energy [213,214]. He derived an exponential dependence, which yields the well-known energy gap law:

$$k_{nr} \propto \exp\left(\frac{-\gamma \Delta E}{\hbar \omega}\right) \quad (14)$$

for the dependence of the non-radiative decay rate on the energy difference between the two states involved in the transition. For the $T_1 \rightarrow S_0$ transition, ΔE is the energy of the T_1 state, γ is a term that can be expressed in terms of molecular parameters and ω is the maximum vibrational frequency available in the molecule that couples to the π -conjugated system. Due to the exponential dependence of k_{nr} on the phonon energy, it usually suffices to consider only the highest energy vibration, though for a system with several high-frequency modes a corresponding weighted term may be used [40].

This consideration regarding k_{nr} applies to singlet excited states as well as to triplet states. However, for any compound that emits in the visible spectral range, the S_1 – S_0 energy gap exceeds 1.5 eV, and the resulting non-radiative decay rate is therefore lower than the high radiative rate, so that the effect of internal conversion on the singlet lifetime is usually negligible. For example, for benzophenone and 1-chloronaphthalene at 77 K, the radiative and non-radiative decay rates differ by about 1–2 orders of magnitude [27]. For triplet excited states, however, the T_1 – S_0 energy gap is lower due to the exchange energy – about 0.7 eV for π -conjugated polymers – so that a high k_{nr} competes with a low radiative decay rate. The dependence of the non-radiative decay rates on energy is shown for a series of Pt-containing polymer in Fig. 26, along with the resulting quantum yields for phosphorescence. For these materials, k_{nr} is controlled by a carbon–carbon triple bond stretching mode with a frequency of about 260 meV. For materials where C=C double bond stretching modes with about 200 meV dominate, the energy dependence would be a little flatter. Also, the prefactor to the exponential varies according to

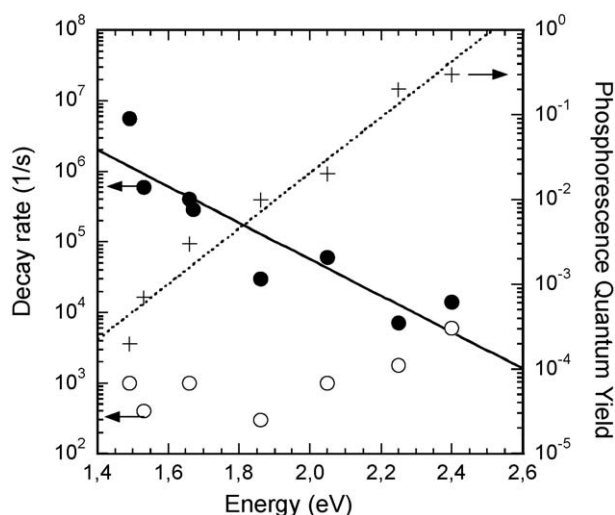


Fig. 26. Experimentally measured rates for the radiative decay (open dots) and non-radiative decay (filled dots) for a series of Pt-containing polymers at 20 K, along with an exponential fit to the non-radiative decay rates (solid line). The quantum yield of phosphorescence at 20 K (crosses) is also shown, along with an exponential fit to the data (dotted line). Data replotted with permission from Ref. [66], copyright 2001 American Chemical Society.

molecular structure, in particular with the strength of the spin-orbit coupling.

Keeping in mind, that typical values for the radiative rate of the triplet state are around 10^3 s^{-1} to 10^5 s^{-1} for organometallic complexes, and about 10^{-1} s^{-1} to 10^2 s^{-1} for hydrocarbon molecules, it is evident from this figure that for many hydrocarbon materials, the lifetime of the T_1 state is entirely controlled by the internal conversion. This also explains why the first reports of phosphorescence measurements in organic polymers were made for the blue emitting family of poly(*p*-phenylenes) with T_1 states around 2.3 eV. The range of many CCD detectors ends around 800 nm (1.55 eV). This, in combination with a very high k_{nr} at 1.55 eV, renders detection of triplets in this range extremely difficult. Assuming a S_1 – T_1 gap of 0.7 eV, this implies that for organic polymers with an optical gap below 2.25 eV (550 nm), phosphorescence is hard to detect and usually requires an enhancement of signal intensity through sensitization techniques. For organometallic compounds, k_r and k_{nr} can become comparable, although care still needs to be taken to ensure that, for the design of red emitting phosphorescent compounds, k_r is high enough to compete efficiently with non-radiative decay.

When considering modes that promote non-radiative decay, it is worth to bear in mind that in order for a mode to promote internal conversion it must not only be of high energy, but it must also couple to the π -conjugated system. For example, for anthracene, the high energy C–H stretching mode (about 370 meV) controls the non-radiative decay. In anthracene, the optical transition is along the short molecular axis, and so the π -system couples well to the C–H stretching mode. For a Pt-containing polymer, however, where the optical transition is polarized along the chain [107], the high energy C–H stretching mode was found not to contribute to the non-radiative decay. The latter was entirely dominated by the carbon–carbon triple bond stretching mode, which is well embedded in the π -conjugated system [66]. Similarly, for many transition metal diimine complexes the dominant acceptor vibration has been attributed to a ring-stretching mode of 160 meV that is observed from the progression in the structure of the 77 K emission profile [215–217]. One may conjecture, that the modes contributing to the non-radiative decay are the modes that dominate in the emission spectrum. For most conjugated polymers, this is the benzene ring-

stretching mode or related carbon–carbon double bond modes (around $1600 \text{ cm}^{-1} \approx 200 \text{ meV}$).

Experimentally determining the intrinsic lifetime of triplet states requires matrix isolation of the chromophore in frozen solution in order to suppress quenching by inadvertent impurities. Obviously, this effect plays a greater role in hydrocarbon conjugated polymers because intrinsic triplet lifetimes are on the order of 1 s [45,218].

6.1.3. Exploitation of phosphorescence in OLEDs

Since a large number of triplets can be formed under electrical excitation, phosphorescence may be utilized for the fabrication of efficient light-emitting diodes. The literature on phosphorescent OLEDs is proliferating, and a good introduction and synopsis to this topic can be found in the book “highly efficient OLEDs with phosphorescent materials” edited by Yersin [28] as well as in the recent feature article by Schwartz et al. [219]. In the context of this review article, we will restrain ourselves to outlining two main avenues that are commonly taken for the fabrication of phosphorescent OLEDs.

One approach yielding highly efficient OLEDs is a device design based on multiple layers that are deposited by thermal evaporation of small molecules [6,8,9,220–226]. The successive or simultaneous evaporation of the compounds allows for a high degree of sophistication and optimization of the device architecture. Typical device structures consist of sequences in the form anode/(hole transport layer)/(electron and exciton blocking layer)/(emissive layer)/(hole and exciton blocking layer)/(electron transport layer)/cathode. The hole transport layer and electron transport layer consist of organic molecules with HOMO and LUMO levels that ensure efficient charge injection and transport towards the emissive layer. Typical hole-transporter and electron-transporter are NPD and Alq3, respectively. The emissive layer may consist of a host material such as CBP and an organometallic emitter with a radiative decay rate that is high enough to compete efficiently with possible undesired non-radiative decay processes such as internal conversion to the ground state, triplet–triplet annihilation and triplet–charge annihilation. Usually, a transition metal complex fulfills the requirements such as Ir(ppy)₃ or PtOEP. The role of the host is to spatially separate the phosphorescent molecules in order to avoid triplet–triplet annihilation while maintaining charge transport to the phosphors. The blocking layers between the emissive layer and the charge transport layers are needed to prevent energy transfer between the triplet state formed on the emitter and possible lower energy triplet states on the charge transport materials. Furthermore, they inhibit for example an electron that has not yet recombined with a hole to migrate from the emissive layer into the hole transport layer, where it would be lost for the desired light emission.

The advantages of the multilayer approach are that each layer can be optimized for its own purpose, be it charge injection and transport or light emission. Furthermore, quenching processes can be reduced through the use of suitable interlayer such as the charge and exciton blocking layers. This device design can result in OLEDs with efficiencies close to the theoretical limit that are only reduced by the light outcoupling [6,227]. In addition, sophisticated structures can be built that allow for the simultaneous use of phosphorescence and fluorescence [9,224,228–230]. An example of such an efficient multilayer structure and its LED performance is given in Fig. 27. The disadvantages are mostly of a technical nature and include the time and expense required for the multiple evaporation process, uniformity issues of the deposition rate, compatibility challenges with flexible substrates and crystallization issues under long-term operation. Some of the latter issues can be dealt with through materials optimization while for the former, nitrogen-jet deposition seems to emerge as promising

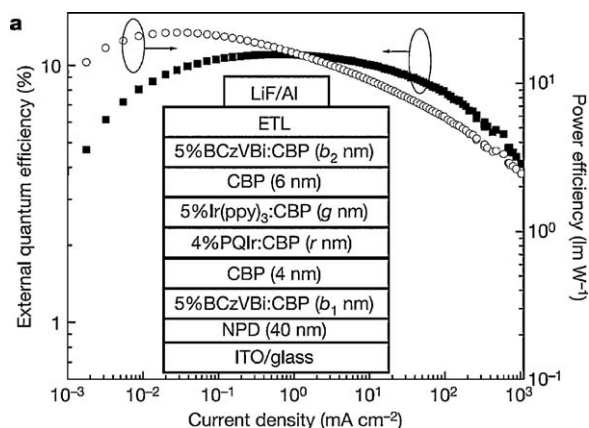


Fig. 27. Example of a multilayer WOLED structure along with the resulting forward viewing external quantum yield (filled squares) and power efficiency (open circles). Reprinted by permission from Macmillan publishers Ltd. from [9], copyright 2006.

alternatives. In this technique, a hot nitrogen carrier gas dissolves and transports the small molecules. This vapor passes through a nozzle onto a cold substrate where the molecules deposit. White organic light-emitting diodes (WOLEDs) have been demonstrated with peak forward view external quantum efficiencies around 11–16% and forward power efficiencies of 22–32 lm/W (total peak efficiencies around 38 lm/W) in 2006 and 2007 [8,9], though these values are continuously improving. In 2008, Kido and co-workers obtain device power efficiencies of 55 lm/W at 100 cd m⁻² rolling off to 44 lm/W at an illumination-relevant luminance of 1000 cd m⁻². At the time of writing this article, Leo and co-workers reported a WOLED structure yielding a device power efficiency of 90 lm/W at 1000 cd m⁻², based on all phosphorescent emitters in combination with a high outcoupling device structure [226].

Multilayer structures are far more difficult to realize when relying solely on soluble materials. One rather attractive approach is to use thermally induced or light-induced cross-linking of hole-transporting/electron-blocking layers on suitable anode materials. For example, a variety of triarylamine-based hole conducting materials have been used by Meerholz and co-workers as graded hole-injection layers to build highly efficient blue polymer light-emitting diodes [231]. By combining this approach with optimized layers embedding phosphorescent Ir-complexes, multilayer devices with almost 100% internal quantum efficiency could be prepared from solution [10]. An alternative approach to cross-linking is to insolubilize a thin layer of a suitable semiconducting polymer on a conducting polymer anode such as PEDOT:PSS. This so-called interlayer approach was published first by Kim et al. [232]. Choulis et al. could show that incorporating a suitable interfacial layer into a green emitting single-layer electrophosphorescent light-emitting diode leads to an improvement of more than 25% in their performance over comparable devices without the interfacial layer [233]. Yang et al. demonstrated that the electronic structures of the interlayer polymers has a significant effect on the device performance and the highest efficiency was obtained for a material selection which enabled efficient blocking of electrons in combination with the direct injection of holes from the interlayer to the phosphorescent dye [234].

An alternative to using multiple layers of insoluble molecules is to employ a single layer of a soluble polymer that comprises different functionalities, such as hole-transporting moieties, electron transporting moieties and phosphorescent emitters. Approaches include transporting and emitting units that are incorporated in the main chain backbone in a conjugated manner [171], polymers where the transporting units form the main chain backbone while the emitter is attached in a non-covalent manner

through a alkyl side-chain [170,189,235], conjugated polyfluorene backbones with hole-transporter and emitter attached through an alkyl side-chain [190,236], and finally non-conjugated main chains such polystyrene where emitter, hole-transporter and electron-transporter are all attached via the side-chain as shown in Fig. 28 [191,192]. The covalent attachment of the emitter to the polymer host in the main chain or side-chain avoids undesired phase separation during long-term device operation. The non-conjugated attachment via side-chains has proven superior to the conjugated inclusion, not only since it is synthetically less demanding but also because it prevents undesired triplet back transfer from the emissive guest to the non-emissive host [170]. In fact, triplet energy transfer in the film, be it from the emissive dye to the host

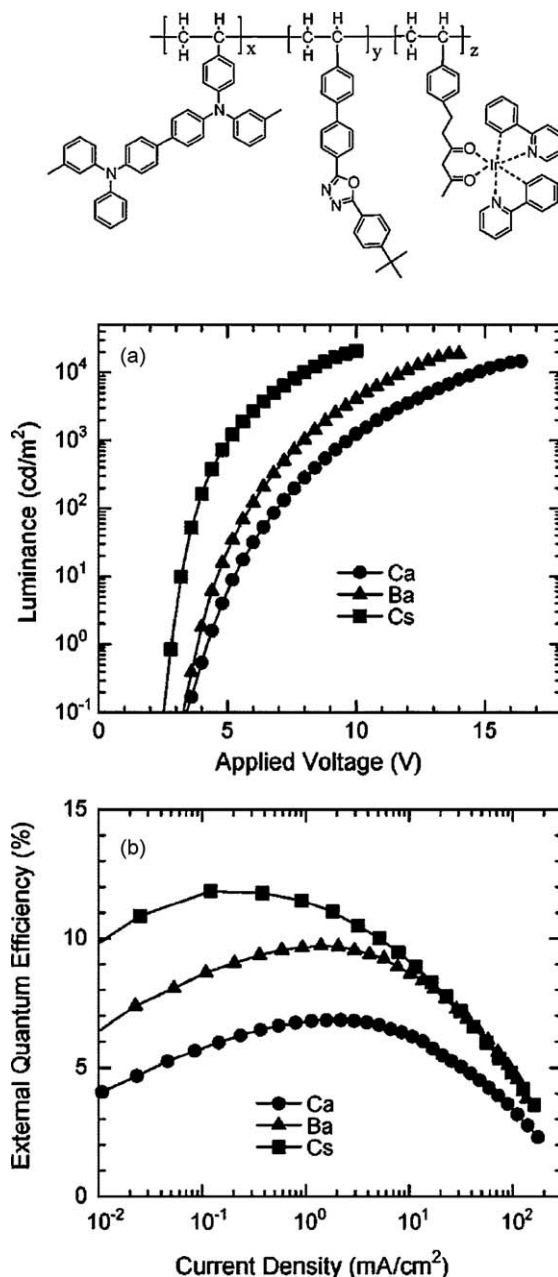


Fig. 28. (a) Example of a all-in-one polymer where the hole-transporting material TPD, the electron-transporting moiety PBD and the emitter Ir(ppy)₂acac are attached to a non-conjugated backbone. (b) The luminance-voltage curves obtained in a single-layer device with PEDT/PSS on ITO as anode and an Aluminum-capped metal as cathode. (c) The external quantum efficiency versus current density. Reprinted with permission from [191], copyright 2005 American Institute of Physics.

or to other phosphorescent dopants, can be suppressed through the use of long alkyl tethers [170,192,194]. At the same time, charge transport to the emitter is still sufficient, probably because of the much larger matrix element for charge transfer compared to triplet transfer (vide supra). External quantum efficiencies of about 12% and power efficiencies of 38.9 lm/W were reported by Suzuki and co-workers, who used the polystyrene backbone with functional side-chains. This approach seems a particularly promising avenue since it allows for a high degree of versatility in the choice of emitter, hole-transporter and electron-transporter. Furthermore, the composition of the organic semiconductor can be optimized in a blend prior to the more elaborate synthesis of the polymer, and color-stable compositions for white light emission are possible.

The attractiveness of the all-in-one-polymer approach lies in the technological ease of using just one single soluble processible polymer. It allows for solution-processing techniques including reel-to-reel coating or ink-jet deposition, and it is compatible with flexible substrates. This simplicity comes at the cost of a somewhat lower efficiency. A pure all-in-one-polymer approach does not allow for a separation into a charge injection zone near the electrodes and an emissive zone away from the electrodes. Such a graded structure is required for highest efficiencies, since it improves charge injection and to reduces exciton quenching. One may need to accept this limitation for the sake of simplicity or, alternatively, one could develop blends of two such polymers, one with a higher fraction of hole-transporting moieties, the other with a higher fraction of electron transporting moieties, that phase separate vertically and so ensure the necessary graded structure for high efficiencies.

When advancing both avenues – the all-in-one-polymer approach and the multiple layer scheme – towards higher efficiencies, one should also be aware of the significant improvement in light efficiency that can be archived through optimized outcoupling schemes [115,226,227].

6.2. Delayed fluorescence and triplet–triplet annihilation

Since in most cases the energy of a pair of triplet excitations exceeds the energy of the first excited singlet state, the encounter of two triplets with anti-parallel spin can generate a singlet excitation. This is a common, albeit not the only origin of delayed fluorescence (DF). In molecular crystals DF by triplet–triplet annihilation (TTA) was discovered earlier than phosphorescence because TTA usually dominates over monomolecular decay, at least in systems in which the rate of radiative decay is low. By the way, the excitation spectrum of DF has been used as a means to derive the triplet state $T_1 \leftarrow S_0$ absorption spectrum in an anthracene crystal [173].

6.2.1. The kinetics of delayed fluorescence via triplet–triplet annihilation

It seems to be appropriate to outline briefly kinetic aspects of DF, generated via TTA [237]. When triplets are populated by intersystem crossing via singlet states, they can decay either monomolecularly or bimolecularly. The corresponding rate equation of the concentration $[T]$ of triplet excitations is

$$\frac{d[T]}{dt} = G_T - \beta_0[T] - \gamma_{TTA}[T]^2 \quad (15)$$

with G_T being the generation rate of triplets, β_0 is the sum of the radiative k_r and non-radiative k_{nr} decay constant of the triplet states, and γ_{TTA} is the bimolecular annihilation constant. In case triplet quenching by charge carriers needs to be considered, an additional loss term $\gamma_{TP}[T][p]$ needs to be added. γ_{TP} is the bimolecular rate constant for triplet–charge annihilation, and $[p]$

denotes the concentration of charges carriers (see Section 6.3). γ_{TTA} is related to the triplet diffusion coefficient D via Smoluchowski's theory of bimolecular reactions:

$$\gamma_{TTA} = 8\pi f \langle R \rangle D \quad (16)$$

in which $\langle R \rangle$ is the distance between the reactants at which the reaction occurs, and f is the probability that the reaction complex has spin 0. Solving Eq. (15) for the concentration of triplet excitons $[T(t)]$, one obtains the time dependence of the phosphorescence intensity $I(t)_{ph} = k_r[T(t)]$ at low excitation densities:

$$I_{ph}(t) = k_r[T_0]e^{-\beta_0 t}, \quad \gamma_{TTA}[T]^2 \ll \beta_0[T] \quad (17a)$$

and at high excitation densities:

$$I_{ph}(t) = \frac{k_r[T_0]}{1 + \gamma_{TTA}[T_0]t}, \quad \gamma_{TTA}[T]^2 \gg \beta_0[T] \quad (17b)$$

The time dependence for the decay of the associated delayed fluorescence $I_{DF}(t)$ is given by

$$I_{DF}(t) = \frac{1}{2} \gamma_{TTA}[T(t)]^2 \quad (18)$$

Using the time dependence of the triplet concentration from 15, this gives:

$$I_{DF}(t) = \frac{1}{2} \gamma_{TTA}[T_0]^2 e^{-2\beta_0 t}, \quad \gamma_{TTA}[T]^2 \ll \beta_0[T] \quad (19a)$$

and

$$I_{DF}(t) = \frac{1}{2} \gamma_{TTA}[T_0]^2 (1 + \gamma_{TTA}[T_0]t)^{-2}, \quad \gamma_{TTA}[T]^2 \gg \beta_0[T] \quad (19b)$$

Eq. (19a) predicts that at low pump fluence the delayed fluorescence signal decays exponentially with time with a rate constant twice of that of the phosphorescence signal. From Eq. (19b) it follows that at high-pump intensity and moderately short times, defined as $\gamma_{TTA}[T_0]t \ll 1$, DF must be independent of pump intensity and approaches a t^{-2} law asymptotically:

$$I_{DF}(t) = \frac{1}{2} \gamma_{TTA}[T_0]^2, \quad \gamma_{TTA}[T_0]t \ll 1 \quad (20a)$$

and, for long times:

$$I_{DF}(t) = \frac{1}{2} \frac{f}{\gamma_{TTA}t^2}, \quad \gamma_{TTA}[T_0]t \gg 1 \quad (20b)$$

It is remarkable that according to Eqs. (20a) and (20b) the intensity of DF is independent of the pump intensity in the limit of long times and high pump intensities. A typical dependence of fluorescence, delayed fluorescence and phosphorescence on pump intensity versus time is shown in Fig. 29.

The situation becomes more complicated if the material is disordered as evidenced by inhomogeneous line broadening in absorption, fluorescence and phosphorescence spectra. If a singlet or triplet excitation has initially been generated at random within the density of states (DOSs), it will relax towards the tail states of the DOS distribution. An inevitable consequence of that type of electronic relaxation is spectral diffusion and, most importantly, dispersion of excitation transport. For a Gaussian DOS, the excitations tend to settle at an energy $-\sigma^2/kT$ below the centre of the DOS, where σ is the variance of the DOS, provided that the time required to reach dynamic equilibrium is less than the intrinsic lifetime of the excitations. The time dependence of the energetic relaxation process in the DOS features a logarithmic decay law. As a result, the bimolecular recombination constant γ_{TTA} is no longer constant, but also acquires a time dependence. This alters the time dependence of the DF signal. At short times, the DF signal is no longer constant but should reflect directly the time dependence of γ_{TTA} . At long times γ_{TTA} becomes constant again, and

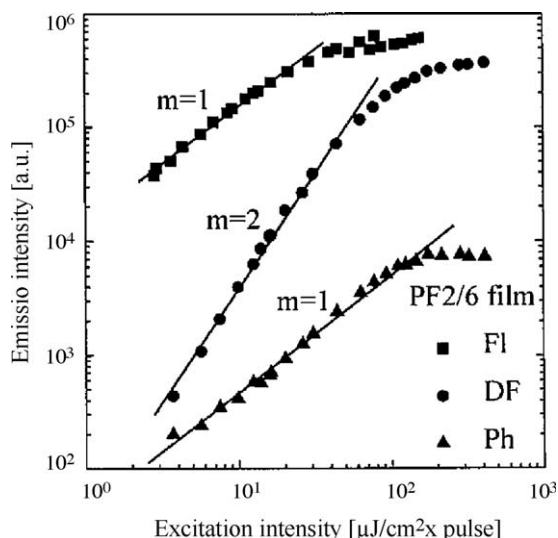


Fig. 29. The dependence of fluorescence (FI), phosphorescence (Ph) and delayed fluorescence (DF) on excitation intensity for a PF2/6 film at 80 K. Reprinted with permission from [169], copyright 2001 American Institute of Physics.

so the DF approaches a t^{-2} law again. This was verified in employing Monte Carlo simulations [238] and experimentally on polyfluorene [169] and is shown in Fig. 30.

A further complication is added when, at low temperatures, triplet diffusion becomes frustrated (see Section 5.1.3), i.e. thermally activated jumps are frozen out. In this case subsequent transport – and relaxation – can be accomplished only via longer ranged tunneling. Movaghar et al.'s has shown that in this case spectral relaxation is slowed down featuring a $\Delta\varepsilon \propto \ln(v_0 t)^{1/2}$ law (see [239]) while the time dependent diffusivity decays as $D \propto \ln(v_0 t)^{-1}$ which can be approximated by $D(t) \propto t^{-1.3}$ within a relevant time regime. The demarcation temperature T_d between normal and frustrated relaxation is set by $\sigma/kT_d \cong 5$.

6.2.2. The origin of delayed fluorescence—TTA versus polaron pair recombination

DF can also originate from the monomolecular recombination of a metastable pair of coulombically bound charges that have been generated by optical excitation. We refer to them as polaron pair

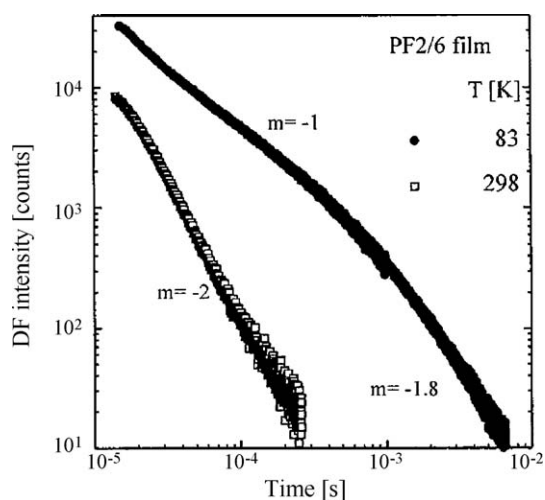


Fig. 30. The decay of the delayed fluorescence in a PF2/6 film at 83 K and at room temperature. The dispersity of the decay at short times at low temperature can be seen in the top curve. Reprinted with permission from [169], copyright 2001 American Institute of Physics.

(PP) or geminately bound electron hole pair (GP), where the latter term is used to emphasize the coulombic binding. In a single component organic system such as a homopolymer the energy of a polaron pair always exceeds the energy of the singlet state. To distinguish between DF caused by TTA and polaron pair recombination is notoriously difficult because the functional dependences regarding incident light intensity and temporal decay are quite similar. This initiated a lively debate culminating in the claim that in conjugated polymers a geminate pair is theoretical construct which is not based on solid experimental evidence [240]. The ambiguity is associated with the following facts:

- In a random system, such as a conjugated polymer, the delayed fluorescence resulting from the recombination of polaron pairs features an algebraic $t^{-\alpha}$ decay law with α being close 1. This is indistinguishable from the decay of DF via TTA at low temperatures when triplet diffusion is frustrated.
- The intensity dependence of DF generated via TTA or generated via the recombination of polaron pairs can be identical. TTA is caused by a bimolecular process, and hence its intensity dependence should be quadratic at low light intensities and linear at high intensities. If the geminate pairs are generated via a bimolecular recombination of two singlet states, the intensity dependence of DF would be indistinguishable from DF generated via TTA. Consequently, there is no way to distinguish whether or not DF is caused by TTA or by geminate polaron pair recombination unless both phosphorescence and prompt fluorescence as a function of light intensity are also measured.
- One way to distinguish between TTA and polaron pair recombination as the origin of DF is to apply a high electric field to the sample that is able to stabilize or dissociate geminate pairs in contrast to relaxed triplets. However, this method fails if the short lived vibrationally hot singlet state generated in the course of the TTA process has enough energy to undergo field-induced dissociation.

6.2.2.1. Delayed fluorescence by triplet–triplet annihilation. In films of polyfluorene (PF2/6) and on PF2/6 in frozen MTHF solution (10^{-6} mol of repeat units per mole solution, the molecular weight of the polymer being $M_n = 122,000$ g/mol) excited by periodic ns-laser pulses [169], DF could unambiguously be attributed to TTA, both in the PF2/6 film and in the matrix isolated polymer chains for the following reason:

- There is simultaneous phosphorescence (Ph) and DF following $I_{DF} \propto I_{Ph}^2$ within the entire range of pump intensities.
- At a critical pulse intensity of $60 \mu\text{J}/(\text{cm}^2 \text{ pulse})$, the intensity dependence changes from quadratic to linear at higher intensities (Fig. 29 above).
- At low I_{ex} , Ph decays exponentially with a triplet lifetime of 1.1 s, while the DF decays exponentially with a lifetime of about 0.55.
- At high light intensities $I_{DF}(t)$ follows a t^{-m} -law with $m = 1.0 \dots 1.3$ at short times and approaches a t^{-2} relation asymptotically (see Fig. 30 above).

By analyzing the transition from dispersive to non-dispersive triplet exciton motion in terms of random walk theory one can determine the width of the distribution of triplet states to be about 40 meV. This is consistent with the inhomogeneous broadening of the $T_1 \rightarrow S_0$ 0–0 transition. The fact that the light intensity at which triplet decay becomes TTA controlled is the same in film and frozen solution indicated that TTA is predominantly an intra-chain process. Rothe and Monkman [79] confirmed the above results and extended the experiments to lower temperatures where triplet

diffusion becomes frustrated in agreement with Movaghar et al.'s theory [241]. It is remarkable, though, that in PF2/6 film there is a long lasting tail of *DF* at $t > 1.5$ s that cannot be caused by *TTA*. It has to be attributed to slow polaron pair recombination.

6.2.2.2. Delayed fluorescence by geminate polaron pair recombination. Similar *DF*-experiments were performed on a member of the PPV family, namely the copolymer of phenyl-substituted PPV (PhPPV), the so-called superyellow of the former Covion company. For this compound, *DF* is caused by *TTA* in a frozen MTHF solution at 80 K, while it is attributed to geminate polaron pair formation in the film, although *DF* varies quadratically with prompt fluorescence within the entire intensity range explored. Evidence for polaron pair recombination is based upon field-quenching experiments on PhPPV. When applying a rectangular 2 MV/cm electric field pulse to a PhPPV film some 100–200 ns after optical excitation, *DF* decreases. It recovers after switching off the field [237]. This is demonstrated in Fig. 31. The field increases the distance between the charges in the polaron pair and so prevents their monomolecular recombination, yet only 10% of them are able to dissociate completely. Their majority can recombine when the field is switched off and contribute to *DF*. It was conjectured, however that field-quenching of *DF* could be due to the dissociation of electron–hole pairs generated as a result of *TTA* [240]. Evidence against this notion comes from a comparison of prompt and delayed fluorescence under an electric field of 2 MV/cm, recorded 200 ns after pulsed optical excitation. While prompt fluorescence decreases, *DF* increases (Fig. 32). Since formation of triplets via ISC is insensitive to the field, the increase of *DF* must originate from polaron pairs generated by incomplete dissociation of singlets into coulombically bound electron hole pairs. The fact

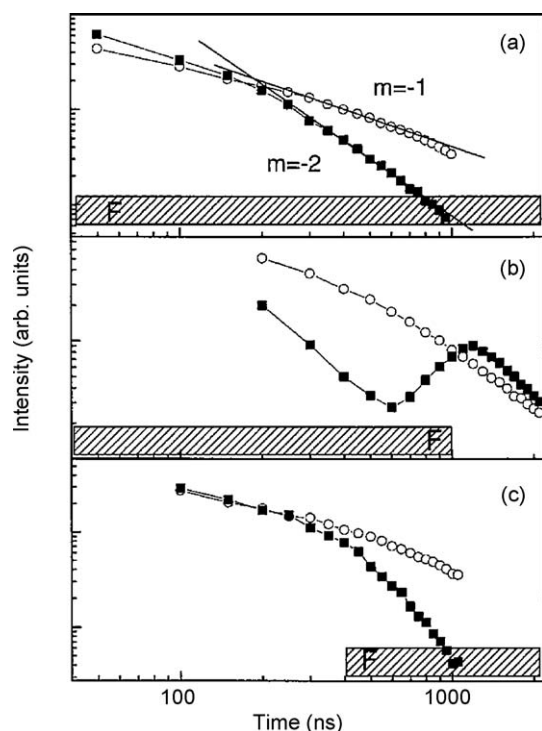


Fig. 31. The dependence of the delayed fluorescence versus time at room temperature taken with an integration time of 500 ns. The white circles represent the field free cases and the filled squares represent the case when an electric field of 2 MV/cm has been applied at the time indicated by the striped box. (a) A continuous field was applied. (b) The field was turned on during optical excitation and it was turned off after 1 μ s. (c) The electric field was off during optical excitation and it was turned on after 400 ns. Reprinted with permission from Ref. [237], copyright 2002 American Institute of Physics.

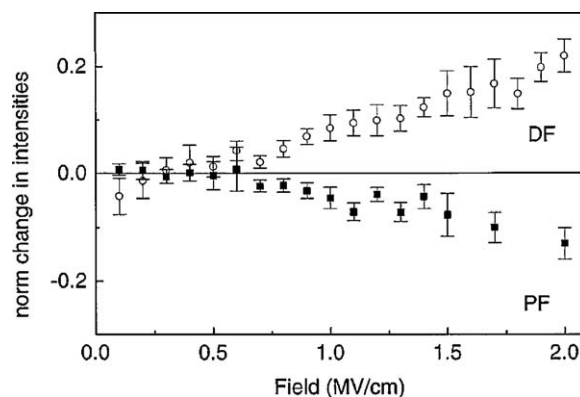


Fig. 32. The dependence of prompt fluorescence (PF) and delayed fluorescence (DF) intensities of PhPPV in a thin film at 295 K versus the electric field. Plotted is $\Delta I = [I(E) - I_0]/I_0$. Reprinted with permission from Ref. [237], copyright 2002 American Institute of Physics.

that the polaron pair mechanism can only operate in a bulk film rather than in dilute solution proves that metastable polaron pairs require inter-chain electron transfer. On-chain polaron pairs will recombine quickly and, consequently, *DF* is controlled by *TTA*.

One way to study delayed fluorescence by polaron pair recombination is to employ fast detection techniques on isolated PF2/6 chains in dilute liquid solution at 295 K. Xu et al. measured *DF* and photoinduced absorption upon excitation by high intensity 150 fs laser pulses within a time window ranging from sub-ps to 400 ps [242]. The photoinduced absorption signal is observed within a wavelength regime in which charges absorb rather than triplets. Furthermore, a *TTA* would occur in the ns to μ s range while the *DF* was detected on a ps timescale. Therefore the experiments prove unambiguously that delayed fluorescence is due to the recombination of eh-pairs generated via rapid dissociation of a higher energy excited state created by sequential two photon absorption [243].

6.2.2.3. The effect of electronic coupling on the polaron pair formation efficiency. Field-quenching experiments on films of MeLPPP support the notion that *DF* is dominated by polaron pairs rather than by *TTA* whereas in PF2/6 it is the opposite. The reason is likely to be related to the morphological difference that affects intra-chain triplet motion and inter-chain charge transfer. In this respect, it would be interesting to compare *DF* in the glassy and β -phases of PF2/6 in which chain packing effects are known to affect the efficiency of thermally stimulated recombination of polaron pairs to yield fluorescence [67,244].

Since the energy of a polaron pair exceeds the energy of a singlet excitation in a conjugated polymer, the excitation spectrum of *DF* can be used to distinguish whether or not it originates from *TTA* or polaron pair recombination. Such an experiment was performed on poly-phenylquinoxalines in frozen solution. The excitation spectrum of *DF* of the polymer in which the repeat units are linked together without a spacer bears out a 0.4 eV offset above the $T_1 \rightarrow S_0$ 0–0 transition while that of a polymer in which the repeat units are separated by an ether linkage is symbatic with absorption [245]. This demonstrates that in the former case *DF* originates from the recombination of on-chain polaron while in the latter it is caused by *TTA*. Obviously, it is the strength of electronic coupling among the repeat units that determines whether or not the dissociation of a vibrationally hot Franck-Condon state into a polaron pair is more efficient than ISC to the triplet state.

6.2.3. Delayed fluorescence by sensitization

Conventional *DF* is inefficient as compared to prompt fluorescence because – at least in purely organic polymers – the ISC yield

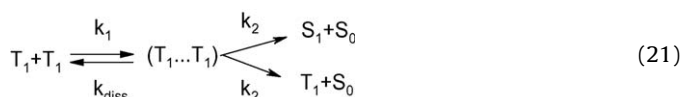
is only 1% or less. This disadvantage can be overcome by using triplet sensitizers. The idea is to select a combination of host (i.e. emitter) and sensitizer materials in which (i) the singlet energy of the host is above that of the sensitizer ($S_h > S_s$) while the triplet levels are reversed ($T_s > T_h$), and (ii) the ISC yield of the sensitizer is close to 100%. If one excites the sensitizer selectively, virtually all excitations are converted to triplets that are transferred rapidly to the triplet manifold of the host. Depending on light intensity the host triplets can annihilate bimolecularly (TTA) and DF of the host is emitted. This is illustrated in Fig. 33. This sensitization process has sometimes been referred to as a non-coherent way of generating “up-conversion” fluorescence [246]. Suitable sensitizers are metalized macrocycles such as Pt-, Pd-, Zn-, and Cu-porphyrines with highly efficient ISC and small $S_1 \rightarrow T_1$ gaps. As host materials a number of emitters were reported. Host-Sensitizer systems in the literature include diphenylanthracene doped with platinum porphyrine (PtOEP) in either benzene solution [246] or trichloroethane solution [247], MeLPPP films doped with platinum porphyrine (PtOEP) [248,249], a PF2/6 film doped with PtOEP [250], a polyspirobifluorene–anthracene copolymer film doped with PtOEP [251], and films of PtOEP doped end-capped poly-(pentaphenylene) [252]. A summary of relevant work is by Balushev et al. who report a maximal sensitization efficiency of 3.2% in an optimized system [253]. One achievement of the

technique is the energetically stepwise “up-conversion” of the terrestrial solar spectrum towards blue-green wavelengths. By using an enlarged porphyrine sensitizer the wavelength of the primary excitation could be extended to the near infrared [254].

6.2.4. Magnetic field effects on delayed fluorescence

Being excitations with spin, triplet excitons respond to a magnetic field. In 1967 Johnson et al. observed that the delayed fluorescence emitted from an anthracene crystal is sensitive to a magnetic field and to its orientation relative to the crystallographic directions [255]. For a fixed mutual field-crystal orientation there is a non-monotonic dependence of the intensity of DF on the magnetic field. DF increases with magnetic field up to 350 G, decreases at higher fields and finally saturates at about 80% of the zero field value at a field of about 2 kG. When rotating the crystal with the field being parallel to the ab-plane of the crystal, resonances appear. A similar phenomenon has been observed with other molecular crystals. The effect demonstrates that a magnetic field affects the annihilation of two triplet excitons. A phenomenological theory has been presented by Merrifield [256]. Suna developed a quantum mechanical model [257].

Merrifield's theory rests upon the notion that mobile excitons can collide and form an intermediate complex ($T_1 \dots T_1$):



where k_1 is the bimolecular rate constant for TT encounter and k_{diss} is the rate constant for dissociation of the complex without further reaction, i.e. back scattering. The field-sensitive parameter is the branching ratio between diffusion-controlled dissociation with a rate k_{diss} and annihilation with k_2 . The latter yields either a singlet or a triplet exciton. Merrifield assumes an identical rate for singlet and triplet exciton formation. Upon TT-interaction there are statistically nine possible collision pair states, i.e. one state with anti-parallel spins (total spin 0), three triplet states with total spin 1 and five quintet states with total spin 2. Since the quintet states require the simultaneous excitation of two electrons they are usually energetically inaccessible. The $(T_1 \dots T_1) \rightarrow S_1 + S_0$ route gives rise to delayed fluorescence while in the $(T_1 \dots T_1) \rightarrow T_1 + S_0$ route one of the triplets is quenched by non-radiative decay. The magnetic field effect on TTA is due to field dependent mixing of different multiplicities in the $(T_1 \dots T_1)$ pair wavefunction. This result in a fractional singlet contribution that controls the formation of the singlet state since only intermediate pair states with singlet spin character can make a transition to S_1 state. In order to describe the magnetic field effect quantitatively one has to consider the spin Hamiltonian of the intermediate pair state. It contains the Zeeman term that arises from the coupling of the external field with the triplet spins and the zero field splitting tensor (see Section 3.2). Because of the tensorial character of the zero field splitting term, field mixing of the different multiplicities of the pair state depends on the mutual orientation of the interacting pair and the external magnetic field. It turns out that, on average, at low fields the singlet character is enhanced whereas at high fields it is diminished. Since it is k_2 rather than k_{diss} that is field sensitive, the field effect is larger in systems in which triplet transport is slower because back scattering is reduced.

Very recently the method of magnetic field dependent TTA has been applied to a non-crystalline system. Mezyk et al. used a film of 9,10-diphenylanthracene doped with 2% PtOEP as a triplet sensitizer that increases the triplet concentration [258]. The results demonstrate that the magnetic field effect of TTA persists when going from a crystalline to a non-crystalline material. Data analysis of the experimental results in terms of Merrifield's theory

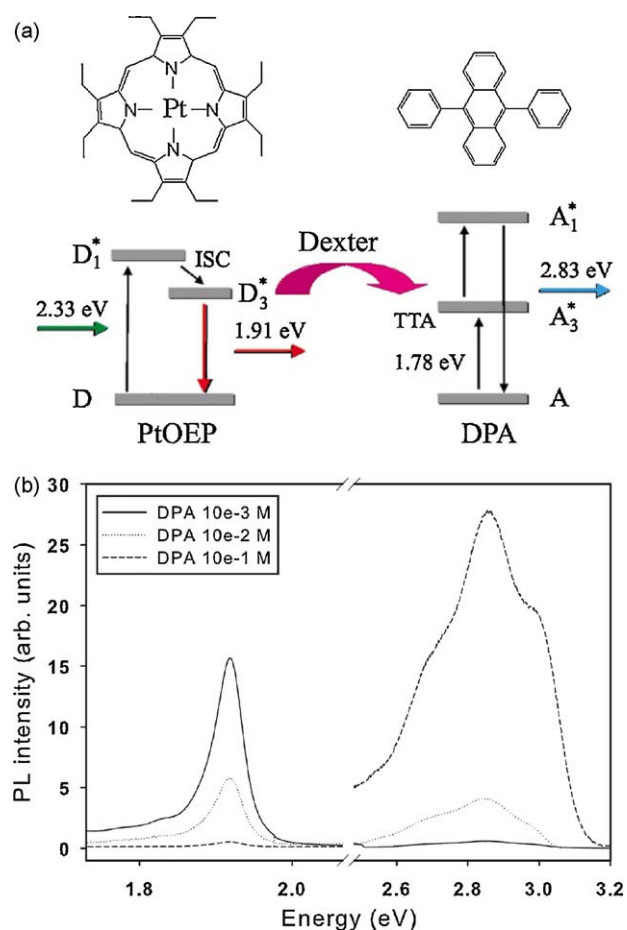


Fig. 33. Delayed fluorescence by sensitization-induced triplet–triplet annihilation. (a) Molecular structure of the sensitizer PtOEP and the emitter DPA, along with an outline of the energy transfer processes involved in the generation of delayed fluorescence. (b) Room temperature emission spectra of PtOEP and DPA in trichloroethane after excitation at 2.33 eV. The concentration of PtOEP was 1.4×10^{-4} M throughout and the concentration of DPA was varied as given in the figure. Reprinted with permission from [247], copyright 2008 American Physical Society.

indicates that in the test system *TTA* is an almost diffusion limited process because in a non-crystalline system triplet motion is much slower than in a crystal. Therefore back scattering of the *TT*-pair plays a minor role.

6.3. Non-radiative quenching of triplet states in OLED structures

When trying to harvest triplet excitons generated via electron–hole recombination in an OLED doped with phosphorescence emitters, one has to pay a prize since the triplets are more vulnerable towards non-radiative decay than singlets. This is caused by the long lifetime of the triplet state. Non-radiative triplet quenching results in a roll-off of the device efficiency at higher operating voltages and currents as exemplified in Fig. 34. Possible quenching mechanisms are (i) monomolecular field-induced dissociation, (ii) bimolecular triplet annihilation (*TTA*, see Section 6.2.2), and (iii) bimolecular reaction with charge carriers stored inside the device. In principle, all three processes can contribute to the roll-off of the device efficiency but the contribution of each of it depends on the kind of phosphorescence emitter and the operation conditions. An additional cause for the reduction of device efficiency at high driving currents is also an insufficient formation rate of the triplet state through saturation effects in the formation pathway [6].

We shall first consider the field-induced quenching process which is an ubiquitous phenomenon that is almost independent of the material under study [259–261]. In the course of experiments aimed at determining the binding energy of singlet excitations in conjugated polymers [262–264] it has been observed that singlet excitations are strongly bound with a binding energy of 0.5 eV or larger. They can dissociate intrinsically but this process requires an electric field in excess of 1 MV/cm in order to be significant. Since the binding strength of triplets exceeds that of singlets by the exchange energy, one might surmise that this process plays no role for triplets. However, in an OLED containing about 10% of phosphorescence emitters, triplets are formed via intermediate

geminately bound electron–hole pairs that can either recombine to form a triplet state or a singlet state followed by efficient intersystem crossing or they can dissociate again. Therefore the state on which the field acts is not the relaxed triplet state but, rather, an eh-pair with an appreciable excess energy relative to the T_1 state. Therefore dissociation should, to first order, be tractable in terms of Onsager's theory for recombination of geminate pairs [259,265]. Recent experiments on a model system, a film of Ir(III)(ppy)₃ excited by photons with an excess quantum energy of about 1 eV relative to the T_1 energy confirm this notion [261]. The observation is that the electric field reduces the amplitude of phosphorescence rather than its decay time. This proves that the field acts on the precursor state for triplets rather than the relaxed T_1 exciton itself. From an Onsager-type analysis, the separation of the precursor eh-pair was determined to be 1.4 nm in a pure Ir(III)(ppy)₃ system and 1.8 nm when the Ir(III)(ppy)₃ was dispersed in a TPD matrix. In summary, one may consider that field-induced phosphorescence quenching is only one manifestation of the general notion that an electric field affects the competition between recombination and dissociation of charge-transfer states that are a precursor for the final luminescent state. For singlet states, similar observations have for example been documented at polymer–polymer heterojunctions [266].

The results pertaining to monomolecular field quenching of triplet excitons [265] must not be generalized, though, because they depend crucially on the interplay between monomolecular and bimolecular quenching processes. At higher drive currents bimolecular effects, such as triplet–polaron quenching [267] and triplet–triplet annihilation become important and the field-quenching effects [265] can be excluded as the culprit for the roll-off in quantum efficiency. A strategy to reduce these effects is exciton confinement so that bimolecular effects are suppressed [268,269]. In this context it is worth noting that there is another detrimental effect regarding the device efficiency that acts before than excitons are generated. It is a field-sensitive imbalance of recombining electrons and holes. If charge injection is a field assisted process it is dependent of the field distribution inside the diode, yet the condition of perfect charge balance in an optimized device can be violated at higher drive currents/voltages [270]. The simplest means to maintain charge balance is to use ohmic electrodes for both hole and electron injection because they do not require a finite electric field at the electrodes.

Bimolecular *TTA* and triplet quenching by charge carriers can occur in addition to, or even instead of monomolecular field-induced field quenching [259,271]. Both effects, *TTA* and triplet–charge quenching, can be quantified in terms of the quenching rate constants γ_{TT} and γ_{TP} where $\gamma_{TT} = 8\pi\langle r_{TT} \rangle D_T$ and $\gamma_{TP} = 4\pi\langle r_{TP} \rangle (D_T + D_P)$ are the bimolecular rate constants for triplet–triplet annihilation and triplet–hole (or electron) interaction, and D_T and D_P are the diffusion constants of triplets or charge carriers, respectively. Under the premise that the interaction radii are comparable, one expects that $D_P \gg D_T$, i.e. $\gamma_{TP} \gg \gamma_{TT}$ unless charge transport is severely trap-limited while triplet diffusion is not. Quenching of triplets excitons by charge carriers is promoted by spin exchange between a charged molecules or polymer and a neighboring triplet excitation as outlined in Fig. 35, i.e. it is a short ranged process. A quantitative assessment of the process has been reported by Hertel and Meerholz [272]. They measured the reduction of phosphorescence of a polyspirofluorene doped with Pt-porphyrin as a triplet emitter in the presence of a space charge limited current. Fig. 36 shows how the phosphorescence lifetime decreases at increasing voltage, and concomitantly increasing current. Since the hole mobility was known, γ_{TP} could be determined to be $(4 \pm 1) \times 10^{-13} \text{ cm}^3 \text{ s}^{-1}$. It turns out that the interaction radius $\langle r_{TP} \rangle$ is about 0.2 nm, i.e. less than the intermolecular distance. This implies that not every encounter between a triplet exciton and a charge carrier

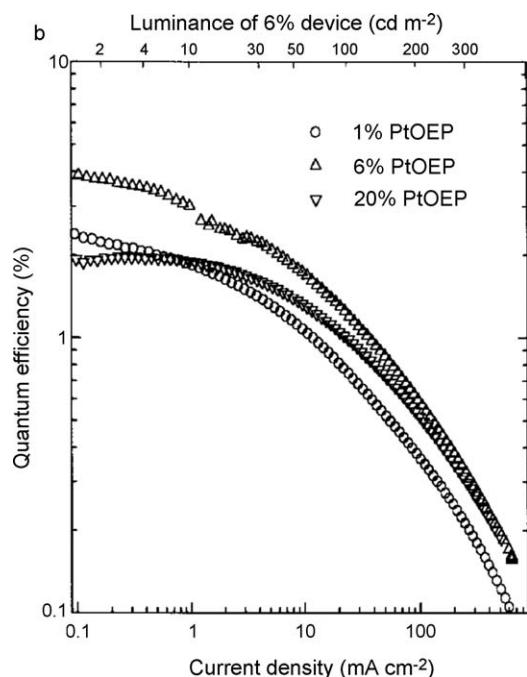


Fig. 34. Quantum efficiency of a multilayer LED with an emissive layer of PtOEP doped into a matrix of Alq₃ as a function of doping concentration and current density. The reduction of device efficiency at increasing current density is clearly visible. The top axis shows the luminance of the 6% PtOEP in Alq₃ device. Reprinted by permission from Macmillan Publishers Ltd. from [6], copyright 1998.

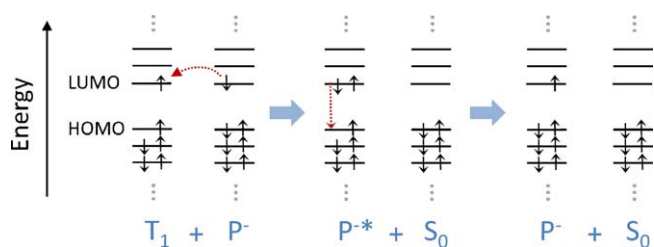


Fig. 35. Triplet polaron annihilation in an energy level scheme of molecular orbitals. P^- denotes a negative polaron, P^{*-} indicates a negative polaron with excess energy.

destroys the triplet. Similar experiments were done on MEH-PPV by Gesquiere et al. [271]. These authors also compared quenching of both triplets and singlets by holes. As expected, triplet quenching is more efficient than singlet quenching because of the much shorter singlet lifetime although the rate constant for singlet quenching exceeds that for triplets by several orders of magnitude. This is because first singlets diffuse faster and second quenching occurs via long ranged Förster energy transfer rather than by exchange interaction.

Using vapor-deposited five-layer OLED structures, Reineke et al. [267] were able to measure the rate constants for bimolecular quenching of triplet excitons by either electrons $k_{p,e}$ and holes $k_{p,h}$ inside the emission layer that was either TCTA:Ir(ppy)₃ or NPB:Ir(piq)₃. The values are $k_{p,e} = (2 \pm 1) \times 10^{-13} \text{ cm}^3 \text{ s}^{-1}$ and $k_{p,h} = (3 \pm 2) \times 10^{-13} \text{ cm}^3 \text{ s}^{-1}$ for TCTA:Ir(ppy)₃ and $k_{p,e} = (7 \pm 2) \times 10^{-13} \text{ cm}^3 \text{ s}^{-1}$ and $k_{p,h} = (2 \pm 1) \times 10^{-13} \text{ cm}^3 \text{ s}^{-1}$ for NPB:Ir(piq)₃. This is comparable to those that have been measured on a polymeric system doped with Pt-porphyrin [272]. It is remarkable that these values are about one order of magnitude smaller than the bimolecular rate constants for the annihilation of triplet excitons k_{TT} , i.e. $(3 \pm 2) \times 10^{-12} \text{ cm}^3 \text{ s}^{-1}$ for TCTA:Ir(ppy)₃ and $(1.4 \pm 0.6) \times 10^{-12} \text{ cm}^3 \text{ s}^{-1}$ for NPB:Ir(piq)₃, suggesting that in this case the triplet exciton is more mobile than either the electron or the hole.

6.4. Exploitation of triplet states in solar cells

Efficient organic solar cells are based on a bulk heterojunction architecture that can for example be realized by mixing two solutions of organic semiconductors with different electronegativity

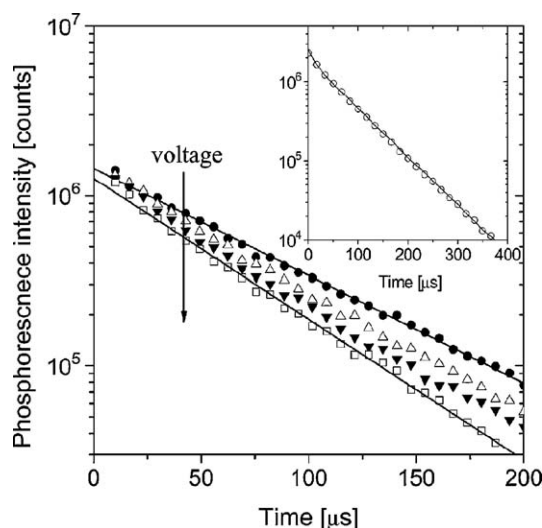


Fig. 36. Decay of the phosphorescence intensity with time as a function of drive voltage for PtOEP doped into a PSF-TAD unipolar device. Full dots, empty triangle, full triangle and empty squares correspond to data taken at 0 V, 5 V, 10 V and 16 V, respectively. Reprinted with permission from [272], copyright 2007 American Chemical Society. The inset shows the phosphorescence decay of PtOEP for a reference device.

ities and subsequently spinning a film [273]. Their operation requires the photoexcited state in one material to diffuse until it reaches the interface to the other material, where dissociation takes place—provided the energy gained exceeds the exciton binding energy [274]. This necessitates that the size of the phase separation between the two materials be on the same length scale than the exciton diffusion length. Furthermore, a percolation path for the separated charges to reach the respective electrodes needs to exist. The morphology of the film can be optimized through careful control of the processing procedures such as the annealing conditions or the choice of solvents. For example, by spin-coating a (low bandgap polymer)/(fullerene derivative) blend from a solvent mixture containing a small fraction of the high boiling point solvent alkane dithiol in the majority solvent chlorobenzene, solar cells with power conversion efficiencies of up to 5.5% have been achieved [275].

It has been conjectured that a possibly larger diffusion length of triplet excitons compared to singlets may be of advantage for solar cells. This allows for a larger scale of the phase separation, which is also of benefit to the percolation path. A longer diffusion length for triplets is often argued on the basis of the longer triplet lifetime, though one should consider that the diffusion length depends on both, lifetime and mean velocity, so that the slow Dexter transfer rate needs to be overcompensated by the lifetime. In amorphous films, singlet diffusion lengths are typically in the range of 10–20 nm [184,276] (though larger values may be obtained in systems with high oscillator strength and optimum spatial arrangement), while values ranging from 20 nm to 140 nm have been reported for triplet diffusion lengths (see Section 5.1.3).

The possible benefit of a larger scale for phase separation needs to be considered against the larger exciton binding energy of the triplet. For a triplet state, the exchange energy adds to the binding energy of a singlet exciton. This raises the barrier for exciton dissociation – which can be overcome by suitable energy level matching – and, more to the point; it wastes a fraction of the collected solar energy. The maximum possible power conversion efficiency η , predicted to be about 11% for some solar cells using singlets [277–279] is therefore likely to be somewhat lower for triplet solar cells. From thermodynamic considerations it is obvious that compounds with a small exchange energy are to be favored.

Solar cells that make use of the triplet exciton for the generation of charge carriers were first reported in 1994 [14], shortly after the first accounts of polymer solar cells based on singlets [280]. The material used was a conjugated platinum containing polymer of the form *trans*-[Pt(PBu₃)₂C≡CRC≡C]_n (R = phenylene) that shows an intersystem crossing efficiency near unity. Through variation of the conjugated spacer R a whole class of related compounds can be synthesized [13,29,82,182,281], that are interchangeably referred to as Pt-polymers, Pt-acetylides, Pt-polyynes or Pt-ethynyls. The efficiencies of single-layer single-material solar cells based on such Pt-polymers [14,282] are comparable to that of analogously built singlet-based solar cells. They increase accordingly when the triplet state is dissociated a bulk heterojunction architecture with C₆₀ [15] or PCBM [16] to give power conversion efficiencies up to 0.3% [16]. Pt-polymers with a phenylene or thiophene spacer have a high exchange energy of 0.7 eV, and they absorb in the blue spectral range while the solar emission spectrum peaks in the red spectral range. While they are suitable for proof-of-principle devices, application-oriented materials require a lower energy absorption. Alternative materials are Pt-polymers with a spacer that has either strong electron-accepting character such as to cause a donor–acceptor interaction with the platinum or that has a donor–acceptor interaction by itself. This results in Pt-polymers where the first absorption band has some charge-transfer character, as evidenced by the low absorption energy in the red spectral range and the reduced

intensity of the first absorption band [29,30,283,284]. With such low-energy Pt-polymers in combination with PCBM, higher power conversion efficiencies have been reported [13,285,286]. Wong et al. suggest the power conversion efficiency to be of almost 5%, though Janssen and co-workers point out that the optical properties of the new polymer presented in the paper are incompatible with such high efficiency data, and that – based on the optical data – the efficiency is unlikely to exceed 2% [287]. Even with a power conversion efficiency of 2%, this presents an interesting step forward. This higher efficiency is likely to be assisted by the charge-transfer character of the excited state, and this aspect may warrant further investigation [288]. Details on the dynamics of photoinduced electron transfer from the triplet state are studied carefully in triads consisting of two fullerenes bridged by a Pt-acetylide oligomer [102].

Efficient triplet state dissociation is also reported by Arif and co-workers for bulk heterojunction devices based on a ladder-type poly(para-phenylene) polymer PhLPPP that contains trace quantities of covalently bound Pd atoms in combination with PCBM [18]. Power conversion efficiencies around 0.2% are obtained. The involvement of the triplet state in the charge generation process is inferred from the eightfold enhancement of the photocurrent compared to the analogous MeLPPP that does not contain the trace amounts of Pd. The role of the Pd in the charge generation process is to enhance the intersystem crossing and thus to increase the number of triplet excitons on the PhLPPP.

Yang and co-workers blended PFO with Ir(mppy)₃ to increase the number of triplets formed in the PFO. In organic/inorganic hybrid solar cells made with the Ir-complex doped PFO and CdSe they observed an enhanced photovoltaic response. To prevent phase separation in such systems, Schulz and Holdcroft synthesized a polyfluorene with a Ir(ppy)₃-complex covalently included in the chain backbone [289]. For comparison, a copolymer with polyfluorene and phenylpyridine without Iridium was also prepared. In a blend with PCBM, the Ir-containing PFO gives a 10 times higher EQE than the PFO copolymer without Ir. The authors argue that electron transfer occurs directly from the Ir(ppy)₃-complex, though the photocurrent enhancement would suggest that triplet diffusion via back transfer to the PFO chain might also contribute.

A different concept to employ triplet states for solar cells is presented by Shao and Yang [17]. They employ the long triplet diffusion length to build a multilayer heterojunction cell with PtEOP and C60. This design yields good charge transport properties while still collecting enough excitons, resulting in power conversion efficiencies of 2%.

7. Concluding remarks

Over the past decade our understanding of the triplet state photophysics developed strongly. This evolution was fostered by

several factors. The development of phosphorescent light-emitting diodes required a solid foundation, and this prompted research activity on triplet state properties. In addition, technical advances made intensified CCD cameras more widely available. This enabled phosphorescence measurements also on purely organic compounds and so facilitated investigations into the triplet state energetics and dynamics.

Today, the formation of triplet states by optical excitation and its intrinsic non-radiative decay seem well understood. Issues that still require further work concern the formation of triplets by electrical excitation, such as the details of the formation mechanism with a view to the role of charge-transfer states in the electron–hole recombination process. A new emerging area is spintronics, where the charge carrier spin and possibly also the spin of the state that results from the charge carrier recombination may be controlled by injection from suitable electrodes. While we seem to comprehend what controls the energy levels of triplets for the first excited intra-chain state, we may still need to get a fuller picture for charge-transfer states and higher-lying states that have a triplet spin. Concerning the triplet state dynamics, more quantitative studies on triplet diffusion rates and lengths in amorphous films would be beneficial for the systematic design of devices. Details on the kinetics of triplet state back transfer processes and their relation to host–guest morphologies, as well as the relative contributions of Förster and Dexter-type transfer in organometallic materials are also of practical relevance. From a more fundamental perspective, a comparison between the mechanism of triplet state transfer and charge transfer may be illuminating since both processes require wavefunction overlap yet differ in the width of the associated density of states. The exploitation of the triplet state decay in OLED structures is advancing well and has reached the market, while the investigation of their usage in solar cells is gathering momentum. Processes that warrant further studies are the interaction of triplet excitons with each other, with charge carriers and with defects, since such processes are known to affect device efficiencies.

In this review we aimed to introduce some of the intriguing issues associated with the spin triplet excited state, and we hope to have stimulated the reader to take up some of the remaining challenges, thereby undoubtedly producing new ones.

Acknowledgments

We thank S.T. Hoffman for the unpublished data presented in Figs. 2 and 25 as well as for assistance with several of the schematics.

Appendix A

See Tables 1 and 2.

Table 1
Abbreviations used in the text for the compounds.

Abbreviation	Chemical name or description
<i>Polymers</i>	
PIF	Poly-2,8-indenofluorene
PF2/6	Poly(2,7-(9,9-bis(2-ethylhexyl))fluorene)
PFO or PF8	Poly(2,7-(9,9-dioctylfluorene))
DDO-PPP	Dodecyloxy-poly(<i>p</i> -phenylene)
MeLPPP	Methyl-substituted ladder-type poly(<i>p</i> -phenylene)
PhLPPP	Diphenyl-substituted ladder-type poly(<i>p</i> -phenylene)
PPP	Poly(<i>p</i> -phenylene)
PPV	Poly(1,4-phenylene vinylene)
MEH-PPV	Poly(2-methoxy-5-(2-ethylhexyloxy)-1,4-phenylenevinylene)
MDMO-PPV	Poly(2-methoxy-5-(3',7'-dimethyloctyloxy)-1,4-phenylenevinylene)
PPE	Poly(<i>p</i> -phenylene ethynylene)

Table 1 (Continued)

Abbreviation	Chemical name or description
F8BT	Poly(9,9'-dioctylfluorene-co-benzothiadiazole)
PFB	Poly(9,9'-dioctylfluorene-co-bis- <i>N,N'</i> -(4-butylphenyl)-bis- <i>N,N'</i> -phenyl-1,4-phenylene-diamine)
PNP	Poly(4-(<i>N</i> -4-vinylbenzyloxyethyl, <i>N</i> -methylamino- <i>N</i> -(2,5-di- <i>tert</i> -butylphenyl)naphthalimide))
Pt-polymers, Pt-acetylides, Pt-polyynes, Pt-ethynylenes	Polymer of the form <i>trans</i> -[Pt(PBu ₃) ₂ -C≡C-R-C≡C-] _n ; R = phenylene, (oligo)thiophene, pyridine, or any other conjugated chromophore. The most common type is R = phenylene.
<i>Small molecules</i>	
HBC	Hexa- <i>peri</i> -hexabenzocoronene
CBP	4,4'-bis(<i>N</i> -carbazolyl)-2,2'-biphenyl
Alq ₃	Tris(8-hydroxyquinoline)aluminium
PDI	Perylenediimide
DCM ₂	A red fluorophore (see [69] for structure)
BCP	2,9-dimethyl-4,7-diphenyl-1,10-phenanthroline
OEP	Octaethylporphyrin
TPD	<i>N,N'</i> -bis(3-methylphenyl)- <i>N,N'</i> -biphenyl-4,4'-diamine
mCP	<i>m</i> -bis(<i>N</i> -carbazolyl)benzene
BCzVBi	4,4'-Bis(9-ethyl-3-carbazovinylenes)-1,1'-biphenyl
COT	Cyclooctatetraene
PCBM	[6,6]-phenyl C ₆₁ -butyric acid methyl ester
TCTA	4,4',4'-tris(<i>N</i> -carbazolyl)-triphenylamine
NPB	<i>N,N'</i> -di(naphthalen-2-yl)- <i>N,N'</i> -diphenyl-benzidine
<i>Organometallic complexes</i>	
Ir(ppy) ₃	<i>fac</i> -tris(2-phenylpyridyl)iridium(III)
Ir(mppy) ₃	Iridium(III)tris[2-(4-tolyl)pyridinato- <i>N,C</i> 2]
Ir(<i>t</i> Bu-ppy) ₃	<i>fac</i> -tris[2-(4'- <i>tert</i> -butylphenyl)pyridinato-]iridium
Ir(piq) ₃	tris(1-phenylisoquinoline) iridium
ppy) ₂ Ir(acac)	bis(2-phenylpyridinato- <i>N,C</i> ^{2'})iridium(III)(acetylacetonate)
(btp) ₂ Ir(acac)	Bis(2-(2'-benzothienyl)-pyridinato- <i>N,C</i> _{3'})iridium(III)(acetylacetonate)
(tpy) ₂ Ir(acac)	Bis(2-(4-tolyl)pyridinato- <i>N,C</i> ^{2'})iridium(III)acetylacetonate)
Flrpic	Bis[(4,6-difluorophenyl)pyridinato- <i>N,C</i> ^{2'}] (picolinato) iridium(III)
PQIr	Bis(2-phenyl quinolyl- <i>N,C</i> ^{2'})Iridium(III)acetylacetonate
FPt ₁	Platinum(II) (2-(4,6'-difluorophenyl) pyridinato- <i>N,C</i> ^{2'}) acetyl acetate
PtOEP	2,3,7,8,12,13,17,18-octaethyl-21H,23H-porphine platinum(II)

The compounds are listed in order of first appearance in the text, though related compounds are grouped together.

Table 2

The energies for the $\pi\pi^* S_1 \rightarrow S_0$ transition (at room temperature) and $T_1 \rightarrow T_n$ transitions (at 10 K or 77 K) displayed in Fig. 11 for thin films of various conjugated polymers, along with references to the original work.

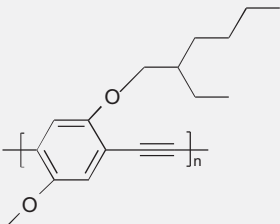
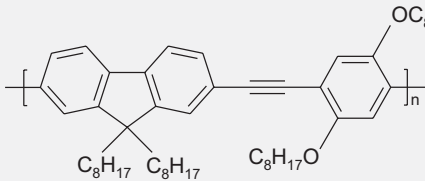
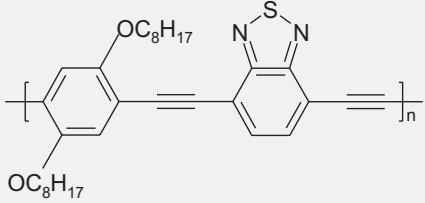
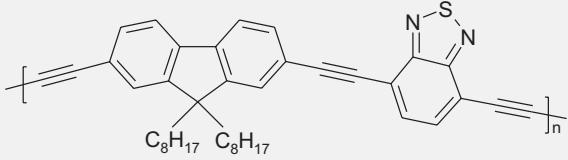
Compound	$S_1 \rightarrow S_0$ (eV)	$T_1 \rightarrow T_n$ (eV)	Ref
<i>PPPs</i>			
PF2/6	2.97	1.50	[48]
PFO (glassy phase)	2.93	1.51	[244]
PFO (β -phase)	2.82	1.43	[244]
PIF	2.89	1.40	[48]
PIFTO (PIF with R = n-octyl)	2.81	1.44	[290]
PIFTTEH (PIF with R = 2-ethylhexyl)	2.88	1.48	[290]
Poly(ladder-type tetraphenylene)	2.81	1.37	[48]
Poly(ladder-type tetraphenylene)	2.78	1.37	[48]
MeLPPP	2.6	1.3	[291]
<i>Other</i>			
PPV	2.4	1.45	[292,293]
F8BT	2.3	1.42	[86,135] ([294] for $S_1 \rightarrow S_0$)
PFB	2.8	1.35	[86] ([294] for $S_1 \rightarrow S_0$)
Pt-acetylides (i.e. <i>trans</i> -[Pt(PBu ₃) ₂ -C≡C-R-C≡C-] _n)			
R = phenylene	3.06	1.48	[295]
R = thiophene	2.86	1.73	[295]
R = pyridine	3.2	1.47	[295]
R = thieno[3,2- <i>b</i>]thiophene	2.76	1.6	[296]
R = dithieno[3,2- <i>b</i> :2'- <i>d'</i>]thiophene	2.67	1.7	[296]
<i>PPEs</i>			
	2.54	1.34	[297]

Table 2 (Continued)

Compound	$S_1 \rightarrow S_0$ (eV)	$T_1 \rightarrow T_n$ (eV)	Ref
	2.73	1.53	[298]
	2.11	1.38	[298]
	2.32	1.48	[298]

References

- [1] M. Pope, P. Magnante, H.P. Kallmann, J. Chem. Phys. 38 (1963) 2042.
- [2] W. Helfrich, W.G. Schneider, Phys. Rev. Lett. 14 (1965) 229.
- [3] C.W. Tang, S.A. van Slyke, Appl. Phys. Lett. 51 (1987) 913.
- [4] J.H. Burroughes, D.D.C. Bradley, A.R. Brown, R.N. Marks, K. Mackay, R.H. Friend, P.L. Burn, A.B. Holmes, Nature 347 (1990) 539.
- [5] Y.V. Romanovskii, A. Gerhard, B. Schweitzer, U. Scherf, R.I. Personov, H. Bässler, Phys. Rev. Lett. 84 (2000) 1027.
- [6] M.A. Baldo, D.F. O'Brien, Y. You, A. Shoustikov, S. Sibley, M.E. Thompson, S.R. Forrest, Nature 395 (1998) 151.
- [7] R.H. Friend, R.W. Gymer, A.B. Holmes, J.H. Burroughes, R.N. Marks, C. Taliani, D.D.C. Bradley, D.A. Dos Santos, J.L. Brédas, M. Logdlund, W.R. Salaneck, Nature 397 (1999) 121.
- [8] Y.R. Sun, S.R. Forrest, Appl. Phys. Lett. 91 (2007) 263503.
- [9] Y.R. Sun, N.C. Giebink, H. Kanno, B.W. Ma, M.E. Thompson, S.R. Forrest, Nature 440 (2006) 908.
- [10] X.H. Yang, D.C. Müller, D. Neher, K. Meerholz, Adv. Mater. 18 (2006) 948.
- [11] X. Gong, M.R. Robinson, J.C. Ostrowski, D. Moses, G.C. Bazan, A.J. Heeger, Advanced Materials 14 (2002) 581.
- [12] E. Holder, B.M.W. Langeveld, U.S. Schubert, Adv. Mater. 17 (2005) 1109.
- [13] W.Y. Wong, Macromol. Chem. Phys. 209 (2008) 14.
- [14] A. Köhler, H.F. Wittmann, R.H. Friend, M.S. Khan, J. Lewis, Synth. Met. 67 (1994) 245.
- [15] A. Köhler, H.F. Wittmann, R.H. Friend, M.S. Khan, J. Lewis, Synth. Met. 77 (1996) 147.
- [16] F.Q. Guo, Y.G. Kim, J.R. Reynolds, K.S. Schanze, Chem. Commun. (2006) 1887.
- [17] Y. Shao, Y. Yang, Adv. Mater. 17 (2005) 2841.
- [18] M. Arif, K. Yang, L. Li, P. Yu, S. Guha, S. Gangopadhyay, M. Forster, U. Scherf, Appl. Phys. Lett. 94 (2009) 063307.
- [19] J.B. Birks, Photophysics of Aromatic Molecules, Wiley-Interscience, London, 1970.
- [20] F. Wilkinson, D.J. McGarvey, A.F. Olea, J. Phys. Chem. 98 (1994) 3762.
- [21] F. Schindler, J.M. Lupton, J. Feldmann, U. Scherf, Adv. Mater. 16 (2004) 653.
- [22] P.M. Borsenberger, D.S. Weiss, Organic Photoreceptors for Xerography, Marcel-Dekker, New York, 1998.
- [23] M. Sano, M. Pope, H. Kallmann, J. Chem. Phys. 43 (1965) 2920.
- [24] J.E. Anthony, Angew. Chem.-Int. Ed. 47 (2008) 452.
- [25] L. Jiang, W. Hu, Z. Wei, W. Xu, H. Meng, Adv. Mater. 21 (2009) 1.
- [26] P.W. Atkins, Molecular Quantum Mechanics, Oxford University Press, 1983.
- [27] N.J. Turro, Modern Molecular Photochemistry, University Science Books, Sausalito, 1991.
- [28] H. Yersin (Ed.), Highly Efficient OLEDs with Phosphorescent Materials, Wiley-VCH, Weinheim, 2008.
- [29] A. Köhler, J.S. Wilson, R.H. Friend, M.K. Al-Suti, M.S. Khan, A. Gerhard, H. Bässler, J. Chem. Phys. 116 (2002) 9457.
- [30] A. Köhler, D. Beljonne, Adv. Funct. Mater. 14 (2004) 11.
- [31] A.P. Monkman, H.D. Burrows, I. Hamblett, S. Navarathnam, M. Svensson, M.R. Andersson, J. Chem. Phys. 115 (2001) 9046.
- [32] L. Kador, J. Chem. Phys. 95 (1991) 5574.
- [33] D. Beljonne, H.F. Wittmann, A. Köhler, S. Graham, M. Younus, J. Lewis, P.R. Raithby, M.S. Khan, R.H. Friend, J.L. Brédas, J. Chem. Phys. 105 (1996) 3868.
- [34] D. Beljonne, Z. Suhai, R.H. Friend, J.L. Brédas, J. Chem. Phys. 102 (1995) 2042.
- [35] D. Beljonne, J. Cornil, R.H. Friend, R.A.J. Janssen, J.L. Brédas, J. Am. Chem. Soc. 118 (1996) 6453.
- [36] J.W. van der Horst, P.A. Bobbert, M.A.J. Michels, H. Bässler, J. Chem. Phys. 114 (2001) 6950.
- [37] J. Rissler, H. Bässler, F. Gebhard, P. Schwerdtfeger, Phys. Rev. B 64 (2001) 045122.
- [38] M.G. Harrison, S. Möller, G. Weiser, G. Urbasch, R.F. Mahrt, H. Bässler, Phys. Rev. B 60 (1999) 8650.
- [39] H. Ibach, H. Lüth, Solid-state Physics, Springer-Verlag, Heidelberg, 1993.
- [40] M. Pope, C.E. Swenberg, Electronic Processes in Organic Crystals and Polymers, Oxford University Press, Oxford, 1999.
- [41] A.D. Yoffe, Adv. Phys. 50 (2001) 1.
- [42] G.D. Scholes, G. Rumbles, Nat. Mater. 5 (2006) 683.
- [43] V. Coropceanu, J. Cornil, D.A. da Silva, Y. Olivier, R. Silbey, J.L. Brédas, Chem. Rev. 107 (2007) 926.
- [44] W.T. Stacy, C.E. Swenberg, J. Chem. Phys. 52 (1970) 1962.
- [45] D. Hertel, S. Setayesh, H.G. Nothofer, U. Scherf, K. Müllen, H. Bässler, Adv. Mater. 13 (2001) 65.
- [46] D. Wasserberg, P. Marsal, S.C.J. Meskers, R.A.J. Janssen, D. Beljonne, J. Phys. Chem. B 109 (2005) 4410.
- [47] E. Jansson, P.C. Jha, H. Aren, Chem. Phys. 336 (2007) 91.
- [48] F. Laquai, A.K. Mishra, M.R. Ribas, A. Petrozza, J. Jacob, L. Akcelrud, K. Müllen, R.H. Friend, G. Wegner, Adv. Funct. Mater. 17 (2007) 3231.
- [49] W. Kuhn, Helv. Chim. Acta 31 (1948) 1780.
- [50] J. Gierschner, J. Cornil, H.J. Egelhaaf, Adv. Mater. 19 (2007) 173.
- [51] B. El Hamaoui, F. Laquai, S. Balushev, J.S. Wu, K. Müllen, Synth. Met. 156 (2006) 1182.
- [52] K. Ohno, H. Inokuchi, Chem. Phys. Lett. 23 (1973) 561.
- [53] K.Y. Kim, S.X. Liu, M.E. Kose, K.S. Schanze, Inorg. Chem. 45 (2006) 2509.
- [54] A. van Dijken, J.J.A.M. Bastiaansen, N.M.M. Kiggen, B.M.W. Langeveld, C. Rothe, A. Monkman, I. Bach, P. Stossel, K. Brunner, J. Am. Chem. Soc. 126 (2004) 7718.
- [55] K. Brunner, A. van Dijken, H. Börner, J.J.A.M. Bastiaansen, N.M.M. Kiggen, B.M.W. Langeveld, J. Am. Chem. Soc. 126 (2004) 6035.
- [56] N. Zhang, A. Hayer, M.K. Al-Suti, R.A. Al-Belushi, M.S. Khan, A. Köhler, J. Chem. Phys. 124 (2006) 244701.
- [57] I. Avilov, P. Marsal, J.-L. Brédas, D. Beljonne, Adv. Mater. 16 (2004) 1624.
- [58] S. Lamansky, P. Djurovich, D. Murphy, F. Abdel-Razzaq, R. Kwong, I. Tsyba, M. Bortz, B. Mui, R. Bau, M.E. Thompson, Inorg. Chem. 40 (2001) 1704.
- [59] S. Lamansky, P. Djurovich, D. Murphy, F. Abdel-Razzaq, H.E. Lee, C. Adachi, P.E. Burrows, S.R. Forrest, M.E. Thompson, J. Am. Chem. Soc. 123 (2001) 4304.
- [60] S. Haneder, E. Da Como, J. Feldmann, J.M. Lupton, C. Lennartz, P. Erk, E. Fuchs, O. Molt, I. Munster, C. Schildknecht, G. Wagenblast, Adv. Mater. 20 (2008) 3325.
- [61] M.A. Baldo, M.E. Thompson, S.R. Forrest, Nature 403 (2000) 750.
- [62] C. Adachi, M.A. Baldo, M.E. Thompson, S.R. Forrest, J. Appl. Phys. 90 (2001) 5048.
- [63] R. Englman, J. Jortner, Mol. Phys. 18 (1970) 145.
- [64] W. Siebrand, J. Chem. Phys. 47 (1967) 2411.
- [65] G.W. Robinson, R.P. Frosch, J. Chem. Phys. 38 (1963) 1187.
- [66] J.S. Wilson, N. Chawdhury, M.R.A. Al-Mandhary, M. Younus, M.S. Khan, P.R. Raithby, A. Köhler, R.H. Friend, J. Am. Chem. Soc. 123 (2001) 9412.
- [67] A. Kadashchuk, A. Vakhnin, I. Blonski, D. Beljonne, Z. Suhai, J.L. Brédas, V.I. Arkhipov, P. Heremans, E.V. Emelianova, H. Bässler, Phys. Rev. Lett. 93 (2004) 066803.

- [68] S. Difley, D. Beljonne, T. Van Voorhis, *J. Am. Chem. Soc.* 130 (2008) 3420.
- [69] M. Segal, M. Singh, K. Rivoire, S. Difley, T. Van Voorhis, M.A. Baldo, *Nat. Mater.* 6 (2007) 374.
- [70] H. Port, D. Rund, *Chem. Phys. Lett.* 69 (1980) 406.
- [71] J. Schmidt, J.H.D. Van Der Waals, *Chem. Phys. Lett.* 2 (1968) 640.
- [72] M. Schwoerer, H. Sixl, *Chem. Phys. Lett.* 2 (1968) 14.
- [73] H. Sternlicht, H.M. McConnell, *J. Chem. Phys.* 35 (1961) 1793.
- [74] W.J. Finkenzeller, T. Hofbeck, M.E. Thompson, H. Yersin, *Inorg. Chem.* 46 (2007) 5076.
- [75] J.C. Ribierre, A. Ruseckas, I.D.W. Samuel, S.V. Staton, P.L. Burn, *Phys. Rev. B* 77 (2008) 085211.
- [76] A.F. Rausch, M.E. Thompson, H. Yersin, *Inorg. Chem.* 48 (2009) 1928.
- [77] E. Peeters, A.M. Ramos, S.C.J. Meskers, R.A.J. Janssen, *J. Chem. Phys.* 112 (2000) 9445.
- [78] D. Wasserberg, S.P. Dudek, S.C.J. Meskers, R.A.J. Janssen, *Chem. Phys. Lett.* 411 (2005) 273.
- [79] C. Rothe, A.P. Monkman, *Phys. Rev. B* 68 (2003) 075208.
- [80] I. Carmichael, G.L. Hug, *J. Phys. Chem. Ref. Data* 15 (1986) 250.
- [81] I. Carmichael, W.P. Helman, G.L. Hug, *J. Phys. Chem. Ref. Data* 16 (1987) 239.
- [82] J.E. Rogers, T.M. Cooper, P.A. Fleitz, D.J. Glass, D.G. McLean, *J. Phys. Chem. A* 106 (2002) 10108.
- [83] T.J. McKay, J. Staromlynska, T.R. Davy, J.A. Bolger, *J. Opt. Soc. B-Opt. Phys.* 18 (2001) 358.
- [84] K. Glusac, M.E. Kose, H. Jiang, K.S. Schanze, *J. Phys. Chem. B* 111 (2007) 929.
- [85] X.D. Yang, C.L. Lee, S. Westenhoff, X.P. Zhang, N.C. Greenham, *Adv. Mater.* 21 (2009) 916.
- [86] T.A. Ford, I. Avilov, D. Beljonne, N.C. Greenham, *Phys. Rev. B* 71 (2005) 125212.
- [87] N.E. Geacintov, M. Pope, *J. Chem. Phys.* 47 (1967) 1194.
- [88] F.Q. Guo, W.F. Sun, Y. Liu, K. Schanze, *Inorg. Chem.* 44 (2005) 4055.
- [89] G.J. Zhou, W.Y. Wong, S.Y. Poon, C. Ye, Z.Y. Lin, *Adv. Funct. Mater.* 19 (2009) 531.
- [90] D. Beljonne, Z. Shuai, G. Pourtois, J.L. Brédas, *J. Phys. Chem. A* 105 (2001) 3899.
- [91] W. Siebrand, D.F. Williams, *J. Chem. Phys.* 46 (1967) 403.
- [92] S.P. McGlynn, T. Azumi, M. Kinoshita, *Molecular Spectroscopy of the Triplet State*, Prentice-Hall, New Jersey, 1969.
- [93] R. Jankowiak, H. Bässler, *Chem. Phys. Lett.* 108 (1984) 209.
- [94] S.M. King, R. Matheson, F.B. Dias, A.P. Monkman, *J. Phys. Chem. B* 112 (2008) 8010.
- [95] J.E. Rogers, B.C. Hall, D.C. Hufnagel, J.E. Slagle, A.P. Ault, D.G. McLean, P.A. Fleitz, T.M. Cooper, *J. Chem. Phys.* 122 (2005) 214708.
- [96] B.F. Minaev, S. Knuts, H. Agren, *Chem. Phys.* 181 (1994) 15.
- [97] J. Lupton, A. Pogantsch, T. Piok, E. List, S. Patil, U. Scherf, *Phys. Rev. Lett.* 89 (2002) 167401.
- [98] C. Rothe, S. King, A. Monkman, *Nat. Mater.* 5 (2006) 463.
- [99] T. Piok, C. Gadermaier, F.P. Wenzl, S. Patil, R. Montenegro, K. Landfester, G. Lanzani, G. Cerullo, U. Scherf, E.J.W. List, *Chem. Phys. Lett.* 389 (2004) 7.
- [100] R. Richert, H. Bässler, B. Ries, B. Movaghar, M. Grunewald, *Phil. Mag. Lett.* 59 (1989) 95.
- [101] R. Richert, *Chem. Phys. Lett.* 171 (1990) 222.
- [102] F.Q. Guo, K. Ogawa, Y.G. Kim, E.O. Danilov, F.N. Castellano, J.R. Reynolds, K.S. Schanze, *Phys. Chem. Chem. Phys.* 9 (2007) 2724.
- [103] T.A. Ford, H. Ohkita, S. Cook, J.R. Durrant, N.C. Greenham, *Chem. Phys. Lett.* 454 (2008) 237.
- [104] D. Veldmann, T. Offermans, J. Sweelssen, M.M. Koetse, S.C.J. Meskers, R.A.J. Janssen, *Thin Solid Films* 333 (2006) 511.
- [105] S. King, C. Rothe, A. Monkman, *J. Chem. Phys.* 121 (2004) 10803.
- [106] G.J. Hedley, A. Ruseckas, I.D.W. Samuel, *J. Phys. Chem. A* 113 (2009) 2.
- [107] J.S. Wilson, R.J. Wilson, R.H. Friend, A. Köhler, M.K. Al-Suti, M.R.A. Al-Mandhary, M.S. Khan, *Phys. Rev. B* 67 (2003) 125206.
- [108] S.M. King, H.L. Vaughan, A.P. Monkman, *Chem. Phys. Lett.* 440 (2007) 268.
- [109] A.N. Terenin, V. Ermolaev, *Trans. Faraday Soc.* 52 (1956) 1042.
- [110] S.A. Bagnich, H. Bässler, D. Neher, *J. Chem. Phys.* 121 (2004) 9178.
- [111] A.P. Monkman, H.D. Burrows, L.J. Hartwell, L.E. Horsburgh, I. Hamblett, S. Navaratnam, *Phys. Rev. Lett.* 86 (2001) 1358.
- [112] N. Geacintov, M. Pope, F. Vogel, *Phys. Rev. Lett.* 22 (1969) 593.
- [113] A.M. Müller, Y.S. Avlasevich, K. Müllen, C.J. Bardeen, *Chem. Phys. Lett.* 421 (2006) 518.
- [114] A.M. Müller, Y.S. Avlasevich, W.W. Schoeller, K. Müllen, C.J. Bardeen, *J. Am. Chem. Soc.* 129 (2007) 14240.
- [115] A. Köhler, J.S. Wilson, R.H. Friend, *Adv. Mater.* 14 (2002) 701.
- [116] M. Wohlgenannt, Z. Vardeny, *J. Phys.: Condens. Matter* 15 (2003) R83.
- [117] A. Köhler, J. Wilson, *Org. Electron.* 4 (2003) 179.
- [118] Y. Cao, I.D. Parker, G. Yu, C. Zhang, A.J. Heeger, *Nature* 397 (1999) 414.
- [119] J.S. Kim, P.K.H. Ho, N.C. Greenham, R.H. Friend, *J. Appl. Phys.* 88 (2000) 1073.
- [120] P.K.H. Ho, J.S. Kim, J.H. Burroughes, H. Becker, S.F.Y. Li, T.M. Brown, F. Cacialli, R.H. Friend, *Nature* 404 (2000) 481.
- [121] K. Okumoto, H. Kanno, Y. Hamaa, H. Takahashi, K. Shibata, *Appl. Phys. Lett.* 89 (2006) 063504.
- [122] J.S. Wilson, A.S. Dhoot, A.J.A.B. Seeley, M.S. Khan, A. Köhler, R.H. Friend, *Nature* 413 (2001) 828.
- [123] M.A. Baldo, D.F. O'Brien, M.E. Thompson, S.R. Forrest, *Phys. Rev. B* 60 (1999) 14422.
- [124] C. Rothe, S.M. King, A.P. Monkman, *Phys. Rev. Lett.* 97 (2006) 076602.
- [125] M. Wohlgenannt, K. Tandon, S. Mazumdar, S. Ramasesha, Z.V. Vardeny, *Nature* 409 (2001) 494.
- [126] M. Wohlgenannt, X. Jiang, Z. Vardeny, R. Janssen, *Phys. Rev. Lett.* 88 (2002) 197401.
- [127] C. Yang, Z.V. Vardeny, A. Köhler, M. Wohlgenannt, M.K. Al-Suti, M.S. Khan, *Phys. Rev. B* 70 (2004) 241202.
- [128] M.-K. Lee, M. Segal, Z.G. Soos, J. Shinar, M.A. Baldo, *Phys. Rev. Lett.* 94 (2005) 137403.
- [129] M. Segal, M.A. Baldo, M.K. Lee, J. Shinar, Z.G. Soos, *Phys. Rev. B* 71 (2005) 245201.
- [130] C.G. Yang, E. Ehrenfreund, Z.V. Vardeny, *Phys. Rev. Lett.* 96 (2006) 089701.
- [131] M.K. Lee, M. Segal, Z.G. Soos, J. Shinar, M.A. Baldo, *Phys. Rev. Lett.* 96 (2006) 089702.
- [132] C.G. Yang, E. Ehrenfreund, M. Wohlgenannt, Z.V. Vardeny, *Phys. Rev. B* 75 (2007) 246201.
- [133] M.A. Baldo, M. Segal, J. Shinar, Z.G. Soos, *Phys. Rev. B* 75 (2007) 246202.
- [134] A.S. Dhoot, D.S. Ginger, D. Beljonne, Z. Shuai, N.C. Greenham, *Chem. Phys. Lett.* 360 (2002) 195.
- [135] A.S. Dhoot, N.C. Greenham, *Adv. Mater.* 14 (2002) 1834.
- [136] C.L. Lee, X. Yang, N.C. Greenham, *Phys. Rev. B* 76 (2007) 245201.
- [137] M. Segal, M.A. Baldo, R.J. Holmes, S.R. Forrest, Z.G. Soos, *Phys. Rev. B* 68 (2003) 075211.
- [138] M. Reufer, M.J. Walter, P.G. Lagoudakis, A.B. Hummel, J.S. Kolb, H.T.G. Rosokos, U. Scherf, *J.M. Lupton, Nat. Mater.* 4 (2005) 340.
- [139] A.L. Burin, M.A. Ratner, *J. Chem. Phys.* 109 (1998) 6092.
- [140] M.N. Kobrak, E.R. Bittner, *Phys. Rev. B* 62 (2000) 11473.
- [141] S. Karabunarliev, E.R. Bittner, *Phys. Rev. Lett.* 90 (2003) 057402.
- [142] M. Wohlgenannt, O. Mermer, *Phys. Rev. B* 71 (2005) 165111.
- [143] T. Hong, H. Meng, *Phys. Rev. B* 63 (2001) 1.
- [144] Z. Shuai, D. Beljonne, R.J. Silbey, J.L. Brédas, *Phys. Rev. Lett.* 84 (2000) 131.
- [145] K. Tandon, S. Ramasesha, S. Mazumdar, *Phys. Rev. B* 67 (2003) 045109.
- [146] A. Ye, Z. Shuai, J.L. Brédas, *Phys. Rev. B* 65 (2002) 045208.
- [147] D. Beljonne, A.J. Ye, Z. Shuai, J.L. Brédas, *Adv. Funct. Mater.* 14 (2004) 684.
- [148] W. Barford, *Phys. Rev. B* 70 (2004) 205204.
- [149] S. Westenhoff, I.A. Howard, J.M. Hodgkiss, K.R. Kirov, H.A. Bronstein, C.K. Williams, N.C. Greenham, R.H. Friend, *J. Am. Chem. Soc.* 130 (2008) 13653.
- [150] Y. Wu, H. Bu, J. Howe, A. Li, J. Shen, *Phys. Rev. B* 75 (2007) 075413.
- [151] A. Hayer, A. Köhler, E. Arisi, I. Bergenti, A. Dediu, C. Taliani, M. Al-Suti, M.S. Khan, *Synth. Met.* 147 (2004) 155.
- [152] T. Förster, *Ann. Phys.* 2 (1948) 55.
- [153] D.L. Dexter, *J. Chem. Phys.* 21 (1953) 836.
- [154] M. Klessinger, J. Michl, *Excited States and Photochemistry of Organic Molecules*, VCH Publishers, New York, 1995.
- [155] J.R. Lakowicz, *Principles of Fluorescence Spectroscopy*, Kluwer, Academic/Plenum Publishers, New York, 1999.
- [156] L. Poulsen, M. Jazdzzyk, J.-E. Communal, J.C. Sancho-Garcia, A. Mura, G. Bongiovanni, D. Beljonne, J. Cornil, M. Hanack, H.-J. Egelhaaf, J. Gierschner, *J. Am. Chem. Soc.* 129 (2007) 8585.
- [157] G.D. Scholes, *Annu. Rev. Phys. Chem.* 54 (2003) 57.
- [158] R.D. Harcourt, G.D. Scholes, K.P. Ghiggino, *J. Chem. Phys.* 101 (1994) 10521.
- [159] A.H.A. Clayton, G.D. Scholes, K.P. Ghiggino, M.N. Paddon-Row, *J. Phys. Chem.* 100 (1996) 10912.
- [160] Y. Kawamura, J. Brooks, J.J. Brown, H. Sasabe, C. Adachi, *Phys. Rev. Lett.* 96 (2006) 017404.
- [161] V. Cleave, G. Yahioglu, P. Le Barny, R.H. Friend, N. Tessler, *Adv. Mater.* 11 (1999) 285.
- [162] D. Wasserberg, S.C.J. Meskers, R.A.J. Janssen, *J. Phys. Chem. A* 111 (2007) 1381.
- [163] N.C. Giebink, Y. Sun, S.R. Forrest, *Org. Electron.* 7 (2006) 375.
- [164] N. Matsusue, S. Ikame, Y. Suzuki, H. Naito, *Appl. Phys. Lett.* 85 (2004) 4046.
- [165] D. Beljonne, J. Cornil, R. Silbey, P. Millie, J.L. Brédas, *J. Chem. Phys.* 112 (2000) 4749.
- [166] D. Beljonne, G. Pourtois, C. Silva, E. Hennebicq, L.M. Herz, R.H. Friend, G.D. Scholes, S. Setayesh, K. Müllen, J.L. Brédas, *Proc. Natl. Acad. Sci.* 99 (2002) 10982.
- [167] T.Q. Nguyen, J.J. Wu, V. Doan, B.J. Schwartz, S.H. Tolbert, *Science* 288 (2000) 652.
- [168] L. Sudha Devi, M.K. Al-Suti, C. Dosche, M.S. Khan, R.H. Friend, A. Köhler, *Phys. Rev. B* 78 (2008) 045210.
- [169] D. Hertel, H. Bässler, R. Guentner, U. Scherf, *J. Chem. Phys.* 115 (2001) 10007.
- [170] N.R. Evans, L.S. Devi, C.S.K. Mak, S.E. Watkins, S.I. Pascu, A. Köhler, R.H. Friend, C.K. Williams, A.B. Holmes, *J. Am. Chem. Soc.* 128 (2006) 6647.
- [171] A.J. Sandee, C.K. Williams, N.R. Evans, J.E. Davies, C.E. Boothby, A. Köhler, R.H. Friend, A.B. Holmes, *J. Am. Chem. Soc.* 126 (2004) 7041.
- [172] V. Ern, P. Avakian, R.E. Merrifield, *Phys. Rev.* 148 (1966) 862.
- [173] P. Avakian, R.E. Merrifield, *Mol. Cryst.* 5 (1968) 37.
- [174] B. Nickel, H. Maxdorf, *Chem. Phys. Lett.* 9 (1971) 555.
- [175] N. Karl, *J. Cryst. Growth* 51 (1981) 509.
- [176] R.W. Munn, W. Siebrand, *J. Chem. Phys.* 52 (1970) 47.
- [177] S.C.J. Meskers, J. Hubner, M. Oestreich, H. Bässler, *J. Phys. Chem. B* 105 (2001) 9139.
- [178] H. Bässler, *Phys. Status Solidi B-Basic Res.* 175 (1993) 15.
- [179] V.I. Arkhipov, I.I. Fishchuk, A. Kadashchuk, H. Bässler, in: G. Hadzioannou, G.G. Malliaras (Eds.), *Semiconducting Polymers*, vol. 1, Wiley-VCH, Weinheim, Germany, 2007, p. 275.
- [180] H. Bässler, G. Hadzioannou, in: P.F.V. Hutten (Ed.), *Semiconducting Polymers. Chemistry, Physics and Engineering*, Wiley-VCH, Weinheim, 1999, p. 365.
- [181] C. Rothe, A. Monkman, *Phys. Rev. B* 65 (2002) 073201.
- [182] K.S. Schanze, E.E. Silverman, X.M. Zhao, *J. Phys. Chem. B* 109 (2005) 18451.
- [183] I.I. Fishchuk, A. Kadashchuk, L. Sudha Devi, P. Heremans, H. Bässler, A. Köhler, *Phys. Rev. B* 78 (2008) 045211.
- [184] R.R. Lunt, N.C. Giebink, A.A. Belak, J.B. Benziger, S.R. Forrest, *J. Appl. Phys.* 105 (2009) 053711.
- [185] B.J. Mulder, *Philips Res. Rep.* 22 (1967) 142.
- [186] J.L. Sessler, B. Wang, A. Harriman, *J. Am. Chem. Soc.* 117 (1995) 704.
- [187] A.M. Brun, A. Harriman, *J. Am. Chem. Soc.* 116 (1994) 10383.
- [188] M.S. Arnold, G.J. McGraw, S.R. Forrest, R.R. Lunt, *Appl. Phys. Lett.* 92 (2008) 053301.
- [189] J.X. Jiang, C.Y. Jiang, W. Yang, H.G. Zhen, F. Huang, Y. Cao, *Macromolecules* 38 (2005) 4072.

- [190] X.W. Chen, J.L. Liao, Y.M. Liang, M.O. Ahmed, H.E. Tseng, S.A. Chen, *J. Am. Chem. Soc.* 125 (2003) 636.
- [191] M. Suzuki, S. Tokito, F. Sato, T. Igarashi, K. Kondo, T. Koyama, T. Yamaguchi, *Appl. Phys. Lett.* 86 (2005) 103507.
- [192] C. Schütz, B. Höfer, F. Jaiser, H. Krueger, M. Thesen, S. Janietz, A. Köhler, *Phys. Status Solidi B-Basic Solid State Phys.* 245 (2008) 810.
- [193] M. Sudhakar, P.I. Djurovich, T.E. Hogen-Esch, M.E. Thompson, *J. Am. Chem. Soc.* 125 (2003) 7796.
- [194] S.P. Huang, T.H. Jen, Y.C. Chen, A.E. Hsiao, S.H. Yin, H.Y. Chen, S.A. Chen, *J. Am. Chem. Soc.* 130 (2008) 4699.
- [195] S.C. Lo, R.N. Bera, R.E. Harding, P.L. Burn, I.D.W. Samuel, *Adv. Funct. Mater.* 18 (2008) 3080.
- [196] K.M. Jung, T.W. Lee, K.H. Kim, M.J. Cho, J.I. Jin, D.H. Choi, *Chem. Lett.* 38 (2009) 314.
- [197] S. Schols, A. Kadashchuk, P. Heremans, A. Helfet, U. Scherf, *Chemphyschem* 10 (2009) 1071.
- [198] P.C. Subudhi, E.C. Lim, *J. Chem. Phys.* 63 (1975) 5491.
- [199] B.T. Lim, E.C. Lim, *J. Chem. Phys.* 78 (1983) 5262.
- [200] B. Nickel, M.F.R. Prieto, *Chem. Phys. Lett.* 146 (1988) 125.
- [201] T. Offermans, P.A. van Hal, S.C.J. Meskers, M.M. Koetse, R.A.J. Janssen, *Phys. Rev. B* 72 (2005) 045213.
- [202] B. D'Andrade, S.R. Forrest, *Chem. Phys.* 286 (2003) 321.
- [203] F. Uckert, Y.H. Tak, K. Müllen, H. Bässler, *Adv. Mater.* 12 (2000) 905.
- [204] B.W. D'Andrade, J. Brooks, V. Adamovich, M.E. Thompson, S.R. Forrest, *Adv. Mater.* 14 (2002) 1032.
- [205] M. Cocchi, J. Kalinowski, D. Virgili, V. Fattori, S. Develay, J.A.G. Williams, *Appl. Phys. Lett.* 90 (2007) 163508.
- [206] E.L. Williams, K. Haavisto, J. Li, G.E. Jabbour, *Adv. Mater.* 19 (2007) 197.
- [207] H.F. Wittmann, R.H. Friend, M.S. Khan, J. Lewis, *J. Chem. Phys.* 101 (1994) 2693.
- [208] J.E. Slagle, T.M. Cooper, D.M. Krein, J.E. Rogers, D.G. McLean, A.M. Urbas, *Chem. Phys. Lett.* 447 (2007) 65.
- [209] Y.V. Romanovskii, H. Bässler, *Chem. Phys. Lett.* 326 (2000) 51.
- [210] M. Reuter, F. Schindler, S. Patil, U. Scherf, J.M. Lupton, *Chem. Phys. Lett.* 381 (2003) 60.
- [211] F. Laquai, C. Im, A. Kadashchuk, H. Bässler, *Chem. Phys. Lett.* 375 (2003) 286.
- [212] Y. Skryshevski, Y. Piryatinski, A. Vakhnin, I. Blonsky, A. Kadashchuk, S. Nespurek, *Opt. Mater.* 30 (2007) 384.
- [213] W. Siebrand, *J. Chem. Phys.* 46 (1967) 440.
- [214] C. Manneback, *Physica* 17 (1951) 1001.
- [215] J.V. Caspar, E.M. Kober, B.P. Sullivan, T.J. Meyer, *J. Am. Chem. Soc.* 104 (1982) 630.
- [216] E.M. Kober, J.V. Caspar, R.S. Lumpkin, T.J. Meyer, *J. Phys. Chem.* 90 (1986) 3722.
- [217] J.V. Caspar, T.J. Meyer, *J. Am. Chem. Soc.* 105 (1983) 5583.
- [218] C.Y. Chi, C. Im, G. Wegner, *J. Chem. Phys.* 124 (2006) 024907.
- [219] G. Schwartz, S. Reineke, T.C. Rosenow, K. Walzer, K. Leo, *Adv. Funct. Mater.* 19 (2009) 1319.
- [220] S.R. Forrest, *Nature* 428 (2004) 911.
- [221] X.F. Qi, M. Sloatsky, S. Forrest, *Appl. Phys. Lett.* 93 (2008) 193306.
- [222] S. Tokito, T. Iijima, T. Tsuzuki, F. Sato, *Appl. Phys. Lett.* 83 (2003) 2459.
- [223] S. Tokito, T. Iijima, Y. Suzuri, H. Kita, T. Tsuzuki, F. Sato, *Appl. Phys. Lett.* 83 (2003) 569.
- [224] D.S. Qin, Y. Tao, *Appl. Phys. Lett.* 86 (2005) 113507.
- [225] D.S. Qin, Y. Tao, *J. Appl. Phys.* 97 (2005) 044505.
- [226] S. Reineke, F. Lindner, G. Schwartz, N. Seidler, K. Walzer, B. Lussem, K. Leo, *Nature* 459 (2009) 234.
- [227] B.W. D'Andrade, R.J. Holmes, S.R. Forrest, *Adv. Mater.* 16 (2004) 624.
- [228] G. Schwartz, K. Fehse, M. Pfeiffer, K. Walzer, K. Leo, *Appl. Phys. Lett.* 89 (2006) 083509.
- [229] G. Schwartz, M. Pfeiffer, S. Reineke, K. Walzer, K. Leo, *Adv. Mater.* 19 (2007) 3672.
- [230] G. Cheng, F. Li, Y. Duan, J. Feng, S.Y. Liu, S. Qiu, D. Lin, Y.G. Ma, S.T. Lee, *Appl. Phys. Lett.* 82 (2003) 4224.
- [231] D.C. Müller, T. Braig, H.G. Nothofer, M. Arnoldi, M. Gross, U. Scherf, O. Nuyken, K. Meerholz, *Chemphyschem* 1 (2000) 207.
- [232] J.S. Kim, R.H. Friend, I. Grizzi, J.H. Burroughes, *Appl. Phys. Lett.* 87 (2005) 023506.
- [233] S.A. Choulis, V.E. Choong, M.K. Mathai, F. So, *Appl. Phys. Lett.* 87 (2005) 113503.
- [234] X.H. Yang, F. Jaiser, B. Stiller, D. Neher, F. Galbrecht, U. Scherf, *Adv. Funct. Mater.* 16 (2006) 2156.
- [235] B. Du, L. Wang, H.B. Wu, W. Yang, Y. Zhang, R.S. Liu, M.L. Sun, J.B. Peng, Y. Cao, *Chem. Eur. J.* 13 (2007) 7432.
- [236] F.I. Wu, X.H. Yang, D. Neher, R. Dodda, Y.H. Tseng, C.F. Shu, *Adv. Funct. Mater.* 17 (2007) 1085.
- [237] A. Gerhard, H. Bässler, *J. Chem. Phys.* 117 (2002) 7350.
- [238] M. Scheidler, B. Cleve, H. Bässler, P. Thomas, *Phys. Lett.* 225 (1994) 431.
- [239] B. Movaghar, B. Ries, M. Grunewald, *Phys. Rev. B* 34 (1986) 5574.
- [240] C. Rothe, A. Monkman, *J. Chem. Phys.* 123 (2005) 244904.
- [241] B. Movaghar, M. Grunewald, B. Ries, H. Bässler, D. Wurtz, *Phys. Rev. B* 33 (1986) 5545.
- [242] Q.H. Xu, D. Moses, A.J. Heeger, *Phys. Rev. B* 69 (2004) 113314.
- [243] C. Silva, A.S. Dhoot, D.M. Russell, M.A. Stevens, A.C. Arias, J.D. MacKenzie, N.C. Greenham, R.H. Friend, S. Setayesh, K. Müllen, *Phys. Rev. B* 6412 (2001) 125211.
- [244] A. Hayer, A.L.T. Khan, R.H. Friend, A. Köhler, *Phys. Rev. B* 71 (2005) 241302(R).
- [245] A. Hayer, H. Bässler, B. Falk, S. Schrader, *J. Phys. Chem. A* 106 (2002) 11045.
- [246] S. Balushev, T. Miteva, V. Yakutkin, G. Nelles, A. Yasuda, G. Wegner, *Phys. Rev. Lett.* 97 (2006) 143903.
- [247] A. Monguzzi, R. Tubino, F. Meinardi, *Phys. Rev. B* 77 (2008) 155122.
- [248] S.A. Bagnich, H. Bässler, *Chem. Phys. Lett.* 381 (2003) 464.
- [249] S. Balushev, P.E. Keivanidis, G. Wegner, J. Jacob, A.C. Grimsdale, K. Müllen, T. Miteva, A. Yasuda, G. Nelles, *Appl. Phys. Lett.* 86 (2005) 061904.
- [250] P.E. Keivanidis, S. Balushev, T. Miteva, G. Nelles, U. Scherf, A. Yasuda, G. Wegner, *Adv. Mater.* 15 (2003) 2095.
- [251] F. Laquai, G. Wegner, C. Im, A. Busing, S. Heun, *J. Chem. Phys.* 123 (2005) 074902.
- [252] S. Balushev, J. Jacob, Y.S. Avlasevich, P.E. Keivanidis, T. Miteva, A. Yasuda, G. Nelles, A.C. Grimsdale, K. Müllen, G. Wegner, *Chemphyschem* 6 (2005) 1250.
- [253] S. Balushev, V. Yakutkin, T. Miteva, G. Wegner, T. Roberts, G. Nelles, A. Yasuda, S. Chernov, S. Aleshchenkov, A. Cheprakov, *New J. Phys.* 10 (2008) 013007.
- [254] S. Balushev, V. Yakutkin, T. Miteva, Y. Avlasevich, S. Chernov, S. Aleshchenkov, G. Nelles, A. Cheprakov, A. Yasuda, K. Müllen, G. Wegner, *Angew. Chem.-Int. Ed.* 46 (2007) 7693.
- [255] R.C. Johnson, R.E. Merrifield, P. Avakian, R.B. Flippin, *Phys. Rev. Lett.* 19 (1967) 285.
- [256] R.E. Merrifield, *J. Chem. Phys.* 48 (1968) 4318.
- [257] A. Suna, *Phys. Rev. B* 1 (1970) 1716.
- [258] J. Mezyk, R. Tubino, A. Monguzzi, A. Mech, F. Meinardi, *Phys. Rev. Lett.* 102 (2009) 087404.
- [259] J. Kalinowski, W. Stampor, J. Szymkowski, D. Virgili, M. Cocchi, V. Fattori, C. Sabatini, *Phys. Rev. B* 74 (2006) 085316.
- [260] R.J. Holmes, S.R. Forrest, T. Sajoto, A. Tamayo, P.I. Djurovich, M.E. Thompson, *Org. Electron.* 7 (2006) 163.
- [261] J. Mezyk, F. Meinardi, R. Tubino, M. Cocchi, *Appl. Phys. Lett.* 93 (2008) 093301.
- [262] R. Kersting, U. Lemmer, M. Deussen, H.J. Bakker, R.F. Mahrt, H. Kurz, V.I. Arkhipov, H. Bässler, E.O. Gobel, *Phys. Rev. Lett.* 73 (1994) 1440.
- [263] W. Graupner, G. Cerullo, G. Lanzani, M. Nisoli, E.J.W. List, G. Leising, S. De Silvestri, *Phys. Rev. Lett.* 81 (1998) 3259.
- [264] V. Gulbinas, Y. Zaushitsyn, V. Sundstrom, D. Hertel, H. Bässler, A. Yartsev, *Phys. Rev. Lett.* 89 (2002) 107401.
- [265] L. Onsager, *Phys. Rev.* 54 (1938) 554.
- [266] A.C. Morteani, P. Sreearunthai, L.M. Herz, R.H. Friend, C. Silva, *Phys. Rev. Lett.* 92 (2004) 247402.
- [267] S. Reineke, K. Walzer, K. Leo, *Phys. Rev. B* 75 (2007) 125328.
- [268] S.J. Su, E. Gonmori, H. Sasabe, J. Kido, *Adv. Mater.* 20 (2008) 4189.
- [269] S. Reineke, G. Schwartz, K. Walzer, K. Leo, *Appl. Phys. Lett.* 91 (2007) 123508.
- [270] N.C. Giebink, S.R. Forrest, *Phys. Rev. B* 77 (2008) 235215.
- [271] A.J. Gesquiere, S.J. Park, P.F. Barbara, *J. Am. Chem. Soc.* 127 (2005) 9556.
- [272] D. Hertel, K. Meerholz, *J. Phys. Chem. B* 111 (2007) 12075.
- [273] J.J.M. Halls, C.A. Walsh, N.C. Greenham, E.A. Marseglia, R.H. Friend, S.C. Moratti, A.B. Holmes, *Nature* 376 (1995) 498.
- [274] J.J.M. Halls, J. Cornil, D.A.D. Santos, R. Silbey, D.-H. Hwang, A.B. Holmes, J.L. Brédas, R.H. Friend, *Phys. Rev. B* 60 (1999) 5721.
- [275] J. Peet, J.Y. Kim, N.E. Coates, W.L. Ma, D. Moses, A.J. Heeger, G.C. Bazan, *Nat. Mater.* 6 (2007) 497.
- [276] J.J.M. Halls, K. Pichler, R.H. Friend, S.C. Moratti, A.B. Holmes, *Appl. Phys. Lett.* 68 (1995) 3120.
- [277] L.J.A. Koster, V.D. Mihailetschi, P.W.M. Blom, *Appl. Phys. Lett.* 88 (2006) 093511.
- [278] D. Veldman, S.C.J. Meskers, R.A.J. Janssen, *Adv. Funct. Mater.* 19 (2009) 1.
- [279] M.C. Scharber, D. Mühlbacher, M. Koppe, P. Denk, C. Waldauf, A.J. Heeger, C.J. Brabec, *Adv. Mater.* 18 (2006) 789.
- [280] R.N. Marks, J.J.M. Halls, D.D.C. Bradley, R.H. Friend, A.B. Holmes, *J. Phys.-Condens. Matter* 6 (1994) 1379.
- [281] G.R. Whittell, I. Mannes, *Adv. Mater.* 19 (2007) 3439.
- [282] N. Chawdhury, A. Köhler, R.H. Friend, W.Y. Wong, J. Lewis, M. Younus, P.R. Raithby, T.C. Corcoran, M.R.A. Al-Mandhary, M.S. Khan, *J. Chem. Phys.* 110 (1999) 4963.
- [283] M. Younus, A. Köhler, S. Cron, N. Chawdhury, M. Al-Mandhary, M. Khan, J. Lewis, N. Long, R. Friend, P. Raithby, *Angew. Chem.-Int. Ed.* 37 (1998) 3036.
- [284] J.S. Wilson, A. Köhler, R.H. Friend, M.K. Al-Suti, M.R.A. Al-Mandhary, M.S. Khan, P.R. Raithby, *J. Chem. Phys.* 113 (2000) 7627.
- [285] W.-Y. Wong, X.-Z. Wang, Z. He, A.B. Djurisic, C.-T. Yip, K.-Y. Cheung, H. Wang, C.S.K. Mak, W.-K. Chan, *Nat. Mater.* 6 (2007) 521.
- [286] W.Y. Wong, X.Z. Wang, Z. He, K.K. Chan, A.B. Djurisic, K.Y. Cheung, C.T. Yip, A.M.C. Ng, Y.Y. Xi, C.S.K. Mak, W.K. Chan, *J. Am. Chem. Soc.* 129 (2007) 14372.
- [287] J. Gilot, M.M. Wienk, R.A.J. Janssen, *Nat. Mater.* 6 (2007) 704.
- [288] A. Köhler, M. Younus, M.R.A. Al-Mandhary, P.R. Raithby, M.S. Khan, R.H. Friend, *Synth. Met.* 101 (1999) 246.
- [289] G.L. Schulz, S. Holdcroft, *Chem. Mater.* 20 (2008) 5351.
- [290] C. Silva, D.M. Russell, A.S. Dhoot, L.M. Herz, C. Daniel, N.C. Greenham, A.C. Arias, S. Setayesh, K. Müllen, R.H. Friend, *J. Phys.-Condens. Matter* 14 (2002) 9803.
- [291] M. Wohlgenannt, W. Graupner, G. Leising, Z.V. Vardeny, *Phys. Rev. B* 60 (1999) 5321.
- [292] R. Österbacka, M. Wohlgenannt, M. Shkunov, D. Chinn, Z.V. Vardeny, *J. Chem. Phys.* 118 (2003) 8905.
- [293] N.F. Colaneri, D.D.C. Bradley, R.H. Friend, P.L. Burn, A.B. Holmes, C.W. Sprangler, *Phys. Rev. B* 42 (1990) 11670.
- [294] A.C. Morteani, P.K.H. Ho, R.H. Friend, C. Silva, *Appl. Phys. Lett.* 86 (2005) 163501.
- [295] N. Chawdhury, A. Köhler, R.H. Friend, M. Younus, N.J. Long, P.R. Raithby, J. Lewis, *Macromolecules* 31 (1998) 722.
- [296] L. Sudha Devi, M.K. Al-Suti, N. Zhang, S.J. Teat, L. Male, H.A. Sparkes, P.R. Raithby, M.S. Khan, A. Köhler, *Macromolecules* 42 (2009) 1131.
- [297] A. Köhler, Unpublished data.
- [298] N. Zhang, Properties of triplet and charged excited states in conjugated polymers, PhD, Department of Physics, Cambridge, Cambridge (2006).